UNITED NATIONS EDUCATIONAL, SCIENTIFIC AND CULTURAL ORGANIZATION
INTERNATIONAL ATOMIC ENERGY AGENCY
INTERNATIONAL CENTRE FOR THEORETICAL PHYSICS
I.C.T.P., P.O. BOX 586, 34100 TRIESTE, ITALY, CABLE: CENTRATOM TRIESTE

SMR.998c - 4

Research Workshop on Condensed Matter Physics
30 June - 22 August 1997
MINIWORKSHOP ON
PATTERN FORMATION AND SPATIO-TEMPORAL CHAOS
28 JULY - 8 AUGUST 1997

"Spatio-temporal dynamics of the d-1 complex Ginzburg Landau Equation (CGLE)"

M. SAN MIGUEL
Universitat de les Illes Balears
IMEDEA CSIC/UIB
Instituto Mediterraneo de Estudios Avanzados
07071 Palma de Mallorca
Spain

These are preliminary lecture notes, intended only for distribution to participants.

[25] L.-H. Tang, B.M. Forrest and D.E. Wolf, Kinetic surface roughening. Part II. Hypercube-stacking models, Phys. Rev. A 45 (1992) 7162.
[26] S.F. Edwards and D.R. Wilkinson, The surface statistics of a granular aggregate, Proc. Roy. Soc. London Ser. A 381 (1982) 17.
[27] Y.-C. Zhang, Non-universal roughening of kinetic self-affine interfaces, J. Phys. France 51 (1990) 2129; M.H. Jensen and I. Procaccia, Unusual exponents in interface roughening: The effects of pinning, J. Phys. II France 1 (1991) 1139.
[28] V. Yakhot, Large scale properties of unstable systems governed by the Kuramoto–Sivashinsky equation, Phys. Rev. A 24 (1981) 642.
[29] S. Zaleski, A stochastic model for the large scale dynamics of some fluctuating interfaces, Physica D 34 (1989) 427.
[30] K. Sneppen, J. Krug, M.H. Jensen, C. Jayaprakash and T. Bohr, Dynamic scaling and crossover analysis for the Kuramoto–Sivashinsky equation, Phys. Rev. A 46 (1992) 7351.
[31] F. Hayot, C. Jayaprakash and Ch. Josserand, Long-wavelength properties of the Kuramoto–Sivashinsky equation, Phys. Rev. E 47 (1993) 911.
[32] V.S. L'vov, V.V. Lebedev, M. Paton and I. Procaccia, Proof of scale invariant solutions in the Kardar–Parisi–Zhang and Kuramoto–Sivashinsky equations in 1 + 1 dimensions: Analytical and numerical results, Nonlinearity 6 (1993) 25.
[33] C.C. Chow and T. Hwa, Defect-mediated stability: An effective hydrodynamic theory of spatiotemporal chaos, Physica D 84 (1995) 494.
[34] H. Chaté, in preparation.
[35] I. Procaccia, M.H. Jensen, V.S. L'vov, K. Sneppen and R. Zeitak, Surface roughening and the long-wavelength properties of the Kuramoto–Sivashinsky equation, Phys. Rev. A 46 (1992) 3220.
[36] V.S. L'vov and I. Procaccia, Comparison of the scale invariant solutions of the Kuramoto–Sivashinsky and Kardar–Parisi–Zhang equations in d dimensions, Phys. Rev. Lett. 69 (1992) 3543.
[37] C. Jayaprakash, F. Hayot and R. Pandit, Universal properties of the two-dimensional Kuramoto–Sivashinsky equation, Phys. Rev. Lett. 71 (1993) 12.
[38] V. L'vov and I. Procaccia, Comment on Universal properties of the two-dimensional Kuramoto–Sivashinsky equation, and reply by C. Jayaprakash, F. Hayot and R. Pandit, Phys. Rev. Lett. 72 (1994) 307, 308.
[39] G. Grinstein, C. Jayaprakash and R. Pandit, Conjectures about phase turbulence in the complex Ginzburg–Landau equation, Physica D 90 (1996) 96.
[40] L.-H. Tang and T. Natterman, Kinetic Surface Roughening. Part I. The Kardar–Parisi–Zhang equation in the weak coupling regime, Phys. Rev. A 45 (1992) 7156.

ELSEVIER

PHYSICA D

Physica D 96 (1996) 47–65

Numerical study of a Lyapunov functional for the complex Ginzburg–Landau equation

R. Montagne *,[1], E. Hernández-García [2], M. San Miguel [3]

Departament de Física, Universitat de les Illes Balears, and Institut Mediterrani d'Estudis Avançats, IMEDEA (CSIC-UIB), E-07071 Palma de Mallorca, Spain

Abstract

We numerically study in the one-dimensional case the validity of the functional calculated by Graham and coworkers (Graham and Tel, 1990; Descalzi and Graham, 1994) as a Lyapunov potential for the Complex Ginzburg–Landau equation. In non-chaotic regions of parameter space the functional decreases monotonically in time towards the plane wave attractors, as expected for a Lyapunov functional, provided that no phase singularities are encountered. In the phase turbulence region the potential relaxes towards a value characteristic of the phase turbulent attractor, and the dynamics there approximately preserves a constant value. However, there are very small but systematic deviations from the theoretical predictions, that increase when going deeper in the phase turbulence region. In more disordered chaotic regimes characterized by the presence of phase singularities the functional is ill-defined and then not a correct Lyapunov potential.

PACS: 05.45.+b; 05.70.Ln
Keywords: Complex Ginzburg–Landau equation; Non-equilibrium potential; Lyapunov potential; Spatio-temporal chaos

1. Introduction

The Complex Ginzburg–Landau Equation (CGLE) is the amplitude equation describing universal features of the dynamics of extended systems near a Hopf bifurcation [1,2].

$$\partial_t A = aA + (D_r + iD_i)\nabla^2 A - (b_r + ib_i)\,|A|^2 A. \tag{1.1}$$

Examples of this situation include binary fluid convection [3], transversally extended lasers [4] and chemical turbulence [5]. We will consider here only the one-dimensional case, $A = A(x,t)$, with $x \in [0, L]$. Suitable scaling of the complex amplitude A, space, and time shows that for fixed sign of a there are only three independent parameters in (1.1) (with D_r and $b_r > 0$ that we assume henceforth). They can be chosen to be L, $c_1 \equiv D_i/D_r$, and $c_2 \equiv b_i/b_r$.

The CGLE for $a > 0$ displays a rich variety of complex spatio-temporal dynamical regimes that have been recently classified in a phase diagram in the parameter space $\{c_1, c_2\}$ [6–8]. It is commonly stated that such non-trivial dynamical behavior, occurring also in other non-equilibrium systems, originates from the non-potential or non-variational character of the dynamics [9]. This general statement needs to be qualified because it involves some confusion in the

* Corresponding author. E-mail: montagne@hp1.uib.es.
[1] on leave from Universidad de la República (Uruguay).
[2] E-mail: dfsehg4@ps.uib.es.
[3] E-mail: dfsmsm0@ps.uib.es.

PII S0167-2789(96)00013-9

terminology. For example the term "non-variational" is often used meaning that there is no Lyapunov functional for the dynamics. But Graham and coworkers, in a series of papers [10–14], have shown that a Lyapunov functional does exist for the CGLE, and they have constructed it approximately in a small-gradient approximation. The correct statement for the CGLE is that it is not a gradient flow. This means that there is no real functional of A from which the right-hand side of (1.1) could be obtained by functional derivation.

Part of the confusion associated with the qualification of "non-variational" dynamics comes from the idea that the dynamics of systems having non-trivial attractors, such as limit cycles or strange chaotic attractors, cannot be deduced from the minimization of a potential which plays the role of the free energy of equilibrium systems. However, such idea does not preclude the existence of a Lyapunov functional for the dynamics. The Lyapunov functional can have local minima which identify the attractors. Once the system has reached an attractor which is not a fixed point, dynamics can proceed on the attractor due to "non-variational" contributions to the dynamical flow which do not change the value of the Lyapunov functional. This just means that the dynamical flow is not entirely determined once the Lyapunov functional is known. This situation is very common and well known in the study of dynamical properties within the framework of conventional statistical mechanics: The equilibrium free energy of the system is a Lyapunov functional for the dynamics, but equilibrium critical dynamics [15] usually involves contributions, such as mode–mode coupling terms, which are not determined just by the free energy. The fact that the dynamical evolution is not simply given by the minimization of the free energy is also true when studying the non-equilibrium dynamics of a phase transition in which the system evolves between an initial and a final equilibrium state after, for example, a jump in temperature across the critical point [16].

A Lyapunov functional plays the role of a potential which is useful in characterizing global properties of the dynamics, such as attractors, relative or nonlinear stability of these attractors, etc. In fact, finding such potentials is one of the long-sought goals of non-equilibrium physics [17,18], the hope being that they should be instrumental in the characterization of non-equilibrium phenomena through phase transition analogies. The use of powerful and very general methods based on these analogies has been advocated by a number of authors [6–8,19,20]. In this context, it is a little surprising that the finding of a Lyapunov functional for the CGLE [12–14] has not received much attention in the literature. A possible reason for this is that the construction of non-equilibrium potentials has been historically associated with the study of stochastic processes, in particular in the search of stationary probability distributions for systems driven by random noise [17,18,21]. We want to make clear that the finding of the Lyapunov functional for the CGLE [12–14] as well as the whole approach and discussion in the present paper is completely within a purely deterministic framework and it does not rely on any noise considerations. A second possible reason for the relative little attention paid to the Lyapunov functional for the CGLE is the lack of any numerical check of the uncontrolled approximations made on its derivation. The main purpose of this paper is precisely to report such numerical check of the results of Graham and collaborators, thus delimiting the range of validity of the approximations involved. We also provide a characterization of the time evolution of the Lyapunov functional in different regions of the phase diagram of the CGLE [6–8], which illustrates the use of such potential.

Our main findings are that the expressions by Graham and coworkers behave to a good approximation as a proper Lyapunov potential when phase singularities (vanishing of the modulus of A) are not present. This includes non-chaotic regimes as well as states of phase turbulence. In this last case some small but systematic discrepancies with the predictions are found. In the presence of phase singularities the potential is ill-defined and then it is not a correct Lyapunov functional.

The paper is organized as follows. For pedagogical purposes, we first discuss in Section 2 a classification of dynamical flows in which notions like relaxational or potential flows are considered. The idea of a potential for the CGLE is clearer in this context.

In Section 3 we review basic phenomenology of the CGLE and the main analytical results for the Lyapunov functional of the CGLE. Sections 4 and 5 contain our numerical analyses. Section 4 is devoted to the Benjamin–Feir stable regime of the CGLE and Section 5 to the phase turbulent regime. Our main conclusions are summarized in Section 6.

2. A classification of dynamical flows

In the following we review a classification of dynamical systems that, although rather well established in other contexts [17,18], it is often overlooked in general discussions of deterministic spatio-temporal dynamics. Non-potential dynamical systems are often defined as those for which there is no Lyapunov potential. Unfortunately, this definition is also applied to cases in which there is no *known* Lyapunov potential. To be more precise, let us consider dynamical systems of the general form

$$\partial_t A_i = V_i[A], \tag{2.1}$$

where A_i represents a set of, generally complex, dynamical variables which are spatially dependent fields: $A_i = A_i(\mathbf{x}, t)$. $V_i[A]$ is a functional of them. The notation A_i^* represents the complex conjugate of A_i and for simplicity we will keep the index i implicit. Let us now split V into two contributions:

$$V[A] = G[A] + N[A]\,, \tag{2.2}$$

where G, the *relaxational* part, will have the form

$$G[A] = -\frac{\Gamma}{2}\frac{\delta F[A]}{\delta A^*} \tag{2.3}$$

with F a real and scalar functional of A. Γ is an arbitrary hermitic and positive-definite operator (possibly depending on A). In the particular case of real variables there is no need of taking the complex conjugate, and hermitic operators reduce to symmetric ones. The functional $N[A]$ in (2.2) is the remaining part of $V[A]$. The important point is that, if the splitting (2.2) can be done in such a way that the following orthogonality condition is satisfied (c.c. denotes the complex conjugate expression):

$$\int \mathrm{d}\mathbf{x}\left(\frac{\delta F[A]}{\delta A(\mathbf{x})} N[A(\mathbf{x})] + \text{c.c.}\right) = 0\,, \tag{2.4}$$

then the terms in N neither increase nor decrease the value of F, which due to the terms in G becomes a decreasing function of time:

$$\frac{\mathrm{d}F[A(\mathbf{x},t)]}{\mathrm{d}t} \le 0\,. \tag{2.5}$$

If F is bounded from below then it is a Lyapunov potential for the dynamics (2.1). Eq. (2.6) with $N = V - G$, that is

$$\int \mathrm{d}\mathbf{x}\left(\frac{\delta F[A]}{\delta A(\mathbf{x})}\left(V[A(\mathbf{x})] + \frac{\Gamma}{2}\frac{\delta F[A]}{\delta A^*(\mathbf{x})}\right) + \text{c.c.}\right) = 0, \tag{2.6}$$

can be interpreted as an equation for the Lyapunov potential F associated to a given dynamical system (2.1). It has a Hamilton–Jacobi structure. When dealing with systems perturbed by random noise, Γ is fixed by statistical requirements, but in deterministic contexts such as the present paper, it can be arbitrarily chosen in order to simplify (2.6).

Solving (2.6) is in general a difficult task, but a number of non-trivial examples of the splitting (2.2)–(2.5) exist in the literature. Some of these examples correspond to solutions of (2.6) found in the search of potentials for dynamical systems [10–12]. Other examples just correspond to a natural splitting of dissipative and non-dissipative contributions in the dynamics of systems with well established equilibrium thermodynamics, as for example models of critical dynamics [15] or the equations of nematodynamics in liquid crystals [22].

Once the notation above has been set up, we can call relaxational systems those for which there is a solution F of (2.6) such that $N = 0$, that is all the terms in V contribute to decrease F. Potential systems can be defined as those for which there is a non-trivial (i.e. a non-constant) solution F to (2.6). In relaxational systems there is no long-time dynamics, since there is no time evolution of A once a minimum of F is reached. On the contrary, for potential systems for which $N \neq 0$, the minima of F define the attractors of the dynamical flow, but once one of these attractors is reached, non-trivial sustained dynamics might exist

on the attractor. Such dynamics is determined by N and maintains a constant value for the functional F.

A possible more detailed classification of the dynamical flows is the following:

(1) *Relaxational gradient flows*: Those dynamical systems for which $N = 0$ with Γ proportional to the identity operator. In this case the time evolution of the system follows the lines of steepest descent of F. A well-known example is the so-called Fisher–Kolmogorov equation, also known as model A of critical dynamics [15], or (real) Ginzburg–Landau equation for a real field $A(\mathbf{x}, t)$

$$\dot{A} = \alpha A + \gamma \nabla^2 A - \beta \mid A \mid^2 A \,, \tag{2.7}$$

where α, γ and β are real coefficients. This equation is of the form of Eqs. (2.1)–(2.3) with $N = 0$, $\Gamma = 1$, and $F = F_{GL}[A]$, the Ginzburg–Landau free energy:

$$F_{GL}[A] = \int \mathrm{d}\mathbf{x} \left(-\alpha \mid A \mid^2 + \gamma \mid \nabla A \mid^2 + \frac{\beta}{2} \mid A \mid^4 \right). \tag{2.8}$$

(2) *Relaxational non-gradient flows*: Still $N = 0$ but with Γ not proportional to the identity, so that the relaxation to the minimum of F does not follow the lines of steepest descent of F. The matrix operator Γ might depend on A or involve spatial derivatives. A well-known example of this type is the Cahn–Hilliard equation of spinodal decomposition, or model B of critical dynamics for a real variable A. [15]:

$$\dot{A} = \left(-\frac{1}{2} \nabla^2 \right) \left(-\frac{\delta F_{GL}[A]}{\delta A} \right). \tag{2.9}$$

The symmetric and positive-definite operator $(-\nabla^2)$ has its origin in a conservation law for A.

(3) *Non-relaxational potential flows*: N does not vanish, but the potential F, solution of (2.6) exists and is non-trivial. Most models used in equilibrium critical dynamics [15] include non-relaxational contributions, and therefore belong to this category. A particularly simple example is

$$\dot{A} = -(1 + \mathrm{i}) \frac{\delta F_{GL}[A]}{\delta A^*}, \tag{2.10}$$

where now A is a complex field. Notice that we can not interpret this equation as being of type 1, because $(1 + \mathrm{i})$ is not a hermitic operator, but still F_{GL} is a Lyapunov functional for the dynamics. Eq. (2.10) is a special case of the CGLE, in which $V[A]$ is the sum of a relaxational gradient flow and a non-linear-Schrödinger-type term $N[A] = -i(\delta F_{GL}[A]/\delta A^*)$.

The general CGLE [2] is of the form (2.7) but A is complex and α, γ and β are arbitrary complex numbers. For the special case in which $\mathrm{Re}[\Gamma]/\mathrm{Im}[\Gamma] = \mathrm{Re}[\beta]/\mathrm{Im}[\beta]$, as for example in (2.10), the Lyapunov functional for the CGLE is known exactly [23]. Such choice of parameters has important dynamical consequences [24]. Beyond such special cases, the calculations by Graham and coworkers indicate [13,14] that the CGLE, a paradigm of complex spatio-temporal dynamics, might be classified within this class of non-relaxational potential flows because a solution of (2.6) is found. The difficulty is that the explicit form of the potential is, so far, only known as an uncontrolled small-gradient expansion.

(4) *Non-potential flows*: Those for which the only solutions F of (2.6) are the trivial ones (that is $F =$ constant). Hamiltonian systems as for example the non-linear Schrödinger equation are of this type.

3. A Lyapunov functional for the CGLE

It is well known that for $a < 0$ the one-dimensional CGLE (1.1) has $A = 0$ as a stable solution, whereas for $a > 0$ there are Travelling Wave (TW) solutions of the form

$$A_k = A_0 \mathrm{e}^{\mathrm{i}(kx + \omega t) + \varphi_0} \tag{3.1}$$

with $A_0 = \sqrt{(a - D_r k^2)/b_r}$, $|k| < \sqrt{a/b_r}$, and $\omega = (b_i a + D_- k^2)/b_r$. We have introduced

$$D_- \equiv D_r b_i - D_i b_r \,. \tag{3.2}$$

φ_0 is any arbitrary constant phase.

The linear stability of the homogeneous solution ((3.1) with $k = 0$) with respect to long wavelength fluctuations divides the parameter space $\{c_1, c_2\}$ in two regions: the Benjamin–Feir (BF) stable and the BF unstable zone. This line is given by [25,26]

$$D_+ \equiv D_r b_r + D_i b_i = 0. \tag{3.3}$$

In the BF unstable region ($D_+ < 0$) there are no stable TW solutions, while in the BF stable region ($D_+ > 0$) TW's with a wave number $k < k_E$ are linearly stable. For $k > k_E$, TW's become unstable through the long wavelength instability known as the Eckhaus instability [27,28]. The Eckhaus wave number k_E is given by

$$k_E^2 = \frac{a b_r D_+}{D_r (3 D_+ b_r + 2 D_- b_i)}. \tag{3.4}$$

Recent numerical work for $a > 0$ and L large [6–8,29] has identified regions of the parameter space displaying different kinds of regular and spatio-temporal chaotic behavior (obtained at long times from random initial conditions and periodic boundary conditions), leading to a "phase diagram" for the CGLE. The five different regions, each leading to a different asymptotic phase, are shown in Fig. 1 as a function of the parameters c_1 and c_2 ($a > 0$, L large). Two of these regions are in the BF stable zone and the other three in the BF unstable one. One of the main distinctions between the different asymptotic phases is in the behavior of the modulus of A at long times. In some regions it never vanishes, whereas in others it vanishes from time to time at different points. A more detailed description of the asymptotic behavior in the different regions is as follows:

(i) *Non-chaotic region*. The evolution here ends in one of the Eckhaus-stable TW solutions for almost all the initial conditions.

(ii) *Spatio-temporal intermittency region*. Despite the fact that there exist stable TW, the evolution from random initial conditions is not attracted by them but by a chaotic attractor in which typical configurations of the field A consist of patches of TW interrupted by turbulent bursts. The modulus of A in such bursts typically touches zero quite often.

(iii) *Defect turbulence*. This is a strongly disordered phase in which the modulus of A has a finite density of space–time zeros. In addition the space and time correlation functions have a quasi-exponential decay [6,7].

(iv) *Phase turbulence*. This is a weakly disordered phase in which $|A(x, t)|$ remains away from zero. The temporal correlations decay slower than exponentially [6,7].

(v) *Bi-chaos region*. Depending on the particular initial condition, the system ends on attractors similar to the ones in regions 3, 4, or in a new attractor in which the configurations of A consist of patches of phase and defect turbulence.

An approximate Lyapunov functional for the CGLE was calculated by Graham and collaborators [13,14,30]. Earlier attempts to find a Lyapunov functional were based on polynomial expansions [23,31–33], while more recent and successful approaches focused in solving the Hamilton–Jacobi equation (2.6) with $\Gamma = 1$ in different ways. This was done first by a minimization procedure involving an action integral [10–12], and more recently by a more direct expansion method [13,14,30]. This last method provides also expressions in higher dimensions, but we will restrict here to the one-dimensional case. In any case, the solution involves an uncontrolled gradient expansion around space-independent solutions of the CGLE. Such expansion obviously limits the validity of the result to regions in the phase diagram in which there are not strong gradients. This excludes the regions in which zeros in the modulus of A are typical, since the phase of A becomes singular there. In particular spatio-temporal intermittency regimes, bi-chaos and defect turbulence are out of the range of validity of Graham's expansion. The meaningfulness of the potential in the other regions of parameter space remains still an open question because of the uncontrolled small gradient approximations used to calculate it, and calls for some numerical check.

In their solution of the Hamilton–Jacobi equation, Graham and collaborators find different branches of the Lyapunov functional with expressions valid for different values of the parameters. In particular they identify the BF line (3.3) as separating two branches of the solution to (2.6).

The explicit expressions (obtained with $\Gamma = 1$) are given in polar coordinates:

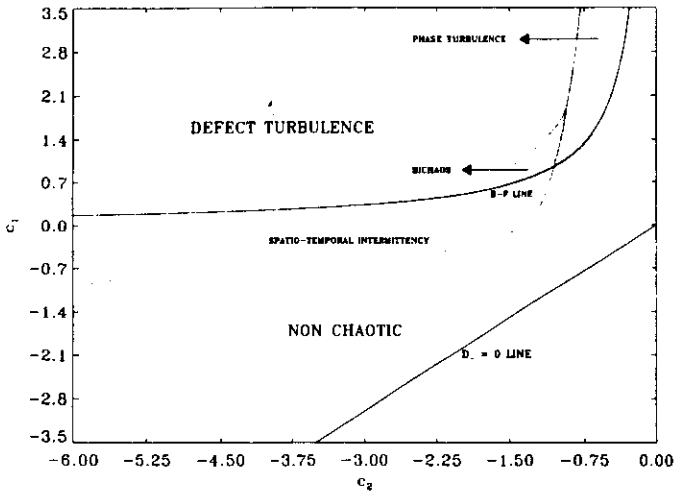

Fig. 1. Regions of the parameter $[c_1 - c_2]$-space ($a = 1$) for the $d = 1$ CGLE displaying different kinds of regular and chaotic behavior. Two analytically obtained lines, the Benjamin–Feir line (B–F line) and the D_- line, are also shown.

$$A(x,t) = r(x,t)e^{i\varphi(x,t)}. \tag{3.5}$$

In terms of the amplitude r, the phase φ, and their spatial derivates (denoted as $r_x, \varphi_x, \varphi_{xx}$, etc.) the Lyapunov functional per unit of length $\Phi \equiv F/L$ was found [13,14] for $a < 0$:

$$\Phi = \int \left\{ b_r r^4 - 2ar^2 + 2\left[D_r + \frac{D_- b_i r^4}{3(a - b_r r^2)^2} \right] r_x^2 - \frac{2D_- r^3}{3(a - b_r r^2)} r_x \varphi_x + 2D_r r^2 \varphi_x^2 \right\} dx. \tag{3.6}$$

We note that even in this relatively simple case $a < 0$, the result for Φ is only approximate and its structure reveals a highly non-trivial dynamics.

For $a > 0$, in the BF stable region ($D_+ > 0$) the expression for Φ results:

$$\Phi = \int \left\{ b_r r^4 - 2ar^2 + \left[(A_1 r + B_1/r^2) r_x^2 + (A_2 r + B_2/r) r_x \varphi_x + 2(D_r r^2 - D_- b_i a / |b|^2 b_r) \varphi_x^2 \right] + \left[\frac{D_- D_r b_i}{3 b_r |b|^2} \varphi_x^4 + \left(-\frac{D_-^2 a}{2 b_r^4 r^2} - \frac{D_-}{b_r^2}(D_-/b_r + 2D_i) \ln r + C_1 \right) \varphi_{xx}^2 + \frac{2D_- D_r}{3 b_r^2 |b|^2}(b_i^2 - b_r^2) \frac{\varphi_x^3 r_x}{r} + \frac{2D_- D_r b_i}{3 b_r^3 |b|^2}(b_i^2 - 2b_r^2) \frac{\varphi_x^2 r_x^2}{r^2} - \frac{4 D_r b_i D_-}{3 b_r^3 r} \left(1 + \frac{\ln(b_r r^2/a)}{1 - b_r r^2/a} \right) r_x \varphi_x \varphi_{xx} \right] \right\} dx, \tag{3.7}$$

where:

$$A_1 = 2(D_r + b_i D_-/3b_r^2),$$
$$A_2 = 2D_-/b_r,$$
$$B_1 = \frac{2D_- b_i a}{3 b_r^3 |b|^2}(2b_r^2 - b_i^2),$$
$$B_2 = \frac{2D_- a}{b_r^2 |b|^2}(b_r^2 - b_i^2). \tag{3.8}$$

Clearly, Φ is ill-defined when $r = 0$.

By writing-out the Euler–Lagrange equations associated to the minimization of Φ the TW solutions (3.1) are identified as local extrema of Φ. Since they occur in families parametrized by the arbitrary phase φ_0, the minima associated to the TW of a given k are not isolated points but lay on a one-dimensional closed manifold. The non-variational part of the dynamics (N in (2.2)) can be explicitly written-down by subtracting $G = -(1/2)(\delta F/\delta A^*)$ with $F = L\Phi$ to the right-hand-side of (1.1). It is seen to produce, when evaluated on the manifold of minima of Φ with a given k, constant motion along it. This produces the periodic time dependence in (3.1) and identifies the TW attractors as limit cycles.

The value of k for which the corresponding extrema change character from local minima to saddle points is precisely the Eckhaus wave number k_E. It is remarkable that, although expression (3.7) was obtained in a gradient expansion around the homogeneous TW, their minima identify exactly all the TW's of Eq. (1.1), and their frequencies and points of instability are also exactly reproduced. This gives confidence on the validity of Graham's approximations. However, it should be stressed that they are not exact and can lead to unphysical consequences. For instance, the value of the potential Φ evaluated on a TW of wave-number k ($|k| < \sqrt{a/b_r}$) is [12]

$$\Phi_k \equiv \Phi[A_k] = \frac{2D_+ a}{|b|^2} k^2 \left(1 - \frac{k^2}{6k_E^2} \right) + \Phi_{k=0}, \tag{3.9}$$

where $\Phi_{k=0} = -a^2/b_r$. For a range of parameter values this expression gives mathematical sense to the intuitive fact that the closer to zero k is the more stable is the associated TW (because its potential is lower). But for some parameter values the minimal potential corresponds to large wave numbers close to $\pm\sqrt{a/b_r}$. This is counterintuitive and calls for some numerical test. The test will be described below and it will be shown that the wave numbers close to $\pm\sqrt{a/b_r}$ are out of the range of validity of the small gradient approximations leading to (3.7).

We already mentioned in Section 2 that the Lyapunov functional for the CGLE is exactly known for special values of the parameters [12,13,24]. This happens for $D_- \equiv D_r b_i - D_i b_r = 0$, which lies in the BF-stable region as indicated in Fig. 1. In this case it is clear that (1.1) can be written as

$$\dot{A} = -\frac{1}{2}\frac{\delta F_{GL}[A]}{\delta A^*} + ib_i \left(-|A|^2 + \frac{D_r}{b_r}\nabla^2 \right) A, \tag{3.10}$$

where $F_{GL}[A]$ is (2.8) for complex A and with $\alpha = 2a$, $\beta = 2b_r$, and $\gamma = 2D_r$. It is readily shown that the term proportional to b_i is orthogonal to the gradient part, so that F_{GL} is an exact solution of (2.6) for these values of the parameters, and (3.10) is a relaxational non-gradient flow (see classification in Section 2). It is seen that the approximate expressions (3.6) and (3.7) greatly simplify when $D_- = 0$ leading both to the same expression:

$$L\Phi = \int \left\{ -2ar^2 + b_r r^4 + 2D_r r r_x^2 + 2D_r r^2 \varphi_x^2 \right\} dx. \tag{3.11}$$

When expressed in terms of A and A^* it reproduces F_{GL} in (3.10). Thus the gradient expansion turns out to be exact on the line $D_- = 0$.

In the Benjamin–Feir unstable region ($a > 0$, $D_+ < 0$) the gradient expansion for Φ becomes [14, 30]:

$$\Phi = \int \left\{ b_r r^4 - 2ar^2 + \left[(A_1 r + \tilde{B}_1/r^2) r_x^2 + (A_2 r + \tilde{B}_2/r) r_x \varphi_x + 2D_r \left(r^2 - \frac{a}{b_r} \right) \varphi_x^2 \right] + \left[\frac{D_r^2}{b_r} \varphi_x^4 + \left(\frac{b_r}{2a^2 r^2} \left(\frac{\tilde{B}_2^2}{4} + \frac{4D_r^2 a^2}{b_r^2} \right) \left(r^2 - \frac{a}{b_r} \right) - \frac{A_2}{2b_r} \left(\frac{A_2}{4} + D_i \right) \ln \left(\frac{r^2 b_r}{a} \right) + \frac{D_i^2}{b_r} \right) \varphi_{xx}^2 - \frac{4D_r b_i D_-}{b_r^3 r} \left(1 + \frac{D_r |b|^2 + 2b_r D_+}{b_i D_- \left(1 - \frac{b_r r^2}{a} \right)} \times \ln \left(\frac{r^2 b_r}{a} \right) \right) \varphi_x r_x \varphi_{xx} \right] \right\}$$

$$+\frac{2D_r}{3b_r^2 r}(5b_i D_r + D_i b_r)\varphi_x^3 r_x + \frac{2b_i D_r}{3b_r^3 r^2}(7b_i D_r + D_i b_r)\varphi_x^2 r_x^2\Big]\Big]\,\mathrm{d}x, \qquad (3.12)$$

where in addition to the previous definitions

$$\tilde{B}_1 = -\frac{2ab_i}{3b_r^3}(D_r b_i + 2D_i b_r),$$
$$\tilde{B}_2 = -\frac{2a}{b_r^2}(D_r b_i + D_i b_r). \qquad (3.13)$$

It was noted before that this expression can be adequate, at most, for the phase turbulent regime, since in the other BF unstable regimes $|A|$ vanishes at some points and instants, so that (3.12) is ill-defined.

The long time dynamics occurs in the attractor defined by the minima of Φ. The Euler–Lagrange equations associated to the minimization of (3.12) lead to a relationship between amplitude and phase of A which implies the well-known adiabatic following of the amplitude to the phase dynamics commonly used to describe the phase turbulence regime by a non-linear phase equation. The explicit form of this relationship is

$$\omega_r = \frac{a}{br} - \frac{D_r}{b_r}(\nabla\varphi)^2 - \frac{D_i}{b_r}\nabla^2\varphi + \frac{b_i D_i^2}{2ab_r^2}\nabla^4\varphi + 2\frac{D_r D_i b_i}{ab_r^2}\nabla\varphi\nabla^3\varphi + 2\frac{b_i D_r^2}{ab_r^2}\nabla\varphi\nabla\nabla^2\varphi + \left[\frac{D_r D_i b_i}{ab_r^2} - \frac{|D|^2}{ab_r}\right](\nabla^2\varphi)^2. \qquad (3.14)$$

It defines the attractor characterizing the phase turbulent regime. Dynamics in this attractor follows from the non-relaxational part N in (2.2). When (3.14) is imposed in such non-relaxational part of the dynamics the generalized Kuramoto–Shivashinsky equation containing terms up to fourth order in the gradients [34] is obtained [14,30].

We finally note that in the phase turbulent regime the Lyapunov functional Φ gives the same value [14,30] when evaluated for any configuration satisfying (3.14), at least within the small gradient approximation. This corresponds to the evolution on a chaotic attractor (associated to the Kuramoto–Sivashinsky dynamics coming from N) which is itself embedded in a region of constant Φ (the potential plateau [18]). This plateau consists of the functional minima of Φ (3.14). All the (unstable) TW are also contained in the same plateau, since they satisfy (3.14).

4. Numerical studies of the Lyapunov functional in the Benjamin–Feir stable regime

We numerically investigate the validity of $\Phi[A]$ in (3.6), (3.7), and (3.12) as an approximate Lyapunov functional for the CGLE. When evaluated on solutions $A(x,t)$ of (1.1) it should behave as a monotonously decreasing function of time, until $A(x,t)$ reaches the asymptotic attractor. After then, Φ should maintain in time a constant value characteristic of the particular attractor.

All the results reported here were obtained using a pseudo-spectral code with periodic boundary conditions and second-order accuracy in time. Spatial resolution was typically 512 modes, with runs of up to 4096 modes to confirm the results. Time step was typically $\Delta t = 0.1$ except when differently stated in the figure captions. Since very small effects have been explored, care has been taken of confirming the invariance of the results with decreasing time step and increasing number of modes. System size was always taken as $L = 512$, and always $D_r = 1$ and $b_i = -1$, so that $c_1 = D_i$ and $c_2 = -1/b_r$. When a random noise of amplitude ϵ is said to be used as or added to an initial condition it means that a set of uncorrelated Gaussian numbers of zero mean and variance ϵ^2 was generated, one for each collocation point in the numerical lattice.

4.1. Negative a

The uniform state $A = 0$ is stable for $a < 0$. We start our numerical simulation with a plane wave $A = A_0 e^{ikx}$ of arbitrary wave number $k = 0.295$ and arbitrary amplitude $A_0 = 1$ (note that the TW's (3.1) do not exist for $a < 0$), and calculate Φ for the evolving configurations. In order to have relevant non-linear effects during the relaxation towards $A = 0$ we have chosen a small value for the coefficient of the linear term ($a = -0.01$). The remaining parameters were $D_i = 1$ and $b_r = 1.25$ ($c_1 = 1$, $c_2 = -0.8$). Despite the presence of non-relaxational terms in (1.1), Φ decreases monotonously (see Fig. 2) to the final value $\Phi(t = \infty) = \Phi[A = 0] = 0$ confirming its adequacy as a Lyapunov potential.

4.2. Positive a: Benjamin–Feir stable regime

We take in this section always $a = 1$. Non-chaotic (TW) states and spatio-temporal intermittency are the two phases found below the BF line in Fig. 1. We first perform several numerical experiments in the non-chaotic region.

A first important case is the one on the line $D_- = 0$, for which (3.11) is an exact Lyapunov functional F_{GL}. We take $D_i = -1$ and $b_r = 1$ ($c_1 = c_2 = -1$), on the $D_- = 0$ line, and compute the evolution of $\Phi = F_{GL}/L$ along a solution of (1.1), taking as initial condition for A a Gaussian noise of amplitude $\epsilon = 0.01$. Despite of the strong phase gradients present specially in the initial stages of the evolution, and of the presence of non-relaxational terms, Φ decays monotonously in time (Fig. 3). The system evolved towards a TW attractor of wave number $k = 0.0245$. The value of Φ in such state is, from Eq. (3.9), $\Phi_{k=0.0245} = -0.998796$. It is important to notice that our numerical solution for A and numerical evaluation of the derivatives in Φ reproduce this value within a 0.3% in the last time showed in Fig. 3, and continues to approach the theoretical value for the asymptotic attractor at longer times.[4]

We continue testing the Lyapunov functional for $D_i = 1$, $b_r = 1.25$ ($c_1 = 1$, $c_2 = -0.8$). This is still in the non-chaotic region but, since $D_- \neq 0$, Φ is not expected to be exact, but only a small gradient approximation. We check now the relaxation back to a stable state after a small perturbation. As initial condition we slightly perturb a TW of Eckhaus-stable wave number ($k = 0.13 < k_E$) by adding random noise of amplitude $\epsilon = 0.09$. Φ decays monotonously (Fig. 4) from its perturbed value to the value $\Phi_{k=0.13} = -0.796632$ as the perturbation is being washed out, as expected for a good Lyapunov functional.

A more demanding situation was investigated for $D_i = -1$ and $b_r = 0.5$ (again in the non-chaotic region, $c_1 = -1$ and $c_2 = -2$, and $D_- \neq 0$). Two TW of different wave numbers ($k_1 = 0.4$, $k_2 = 0.08$, both Eckhaus-stable) were joined (at two points because of the periodic boundary conditions) and the resulting state (see inset in Fig. 5) was used as initial condition. The interfaces between the two TW's contain initially discontinuities in the gradient of the phase which are washed out in a few integration steps. The two interfaces move at constant velocity but one of them remains sharp, whereas the other widens in time, progressively replacing the two initial waves. An important observation is that during the whole process the modulus of $A(x,t)$ never vanishes and then the winding number, defined as

$$\nu \equiv \frac{1}{2\pi}\int_0^L \nabla\varphi\,\mathrm{d}x, \qquad (4.1)$$

remains constant ($\nu = 20$) (with periodic boundary conditions ν is constant except at the instants in which the phase becomes singular, that is when $r = 0$). The state (limit cycle) finally reached is a TW of $k = 2\pi\nu/L = 0.245$. Despite of the complicated and non-relaxational processes occurring Φ behaves as a good Lyapunov functional monotonously decreasing from the value $\Phi(t = 0) = -1.825$ corresponding to the two-wave configuration to the value $\Phi = -1.863$ of the final attractor (Fig. 5). The dynamics of the moving fronts is more complicated than in some relaxational models [35]. For this particular set of parameters and initial wave numbers, the center of the diffuse front moves invading the region of longest wave number, while the sharp one moves towards the small wave number region.

The good behavior of Φ will be obviously lost if the field $A(x,t)$ vanishes somewhere during the evolution. As the next numerical experiment (for $D_i = 1$ and $b_r = 1.25$, that is $c_1 = 1$, $c_2 = -0.8$) we used

[4] If a smaller time step is used greater accuracy is obtained. For example, if the time step is reduced to 0.05 the value of Φ is reproduced within 10^{-7}%. But this takes quite a long computing time.

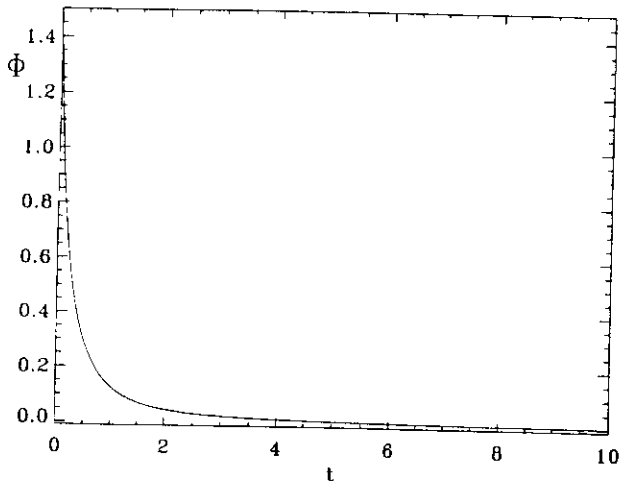

Fig. 2. Relaxation to the simple attractor for $a < 0$. The parameter values are $a = -0.01, c_1 = 1$ and $c_2 = -0.8$. The initial condition is a TW of arbitrary wave number $k = 0.295$ and arbitrary amplitude $A_0 = 1.0$.

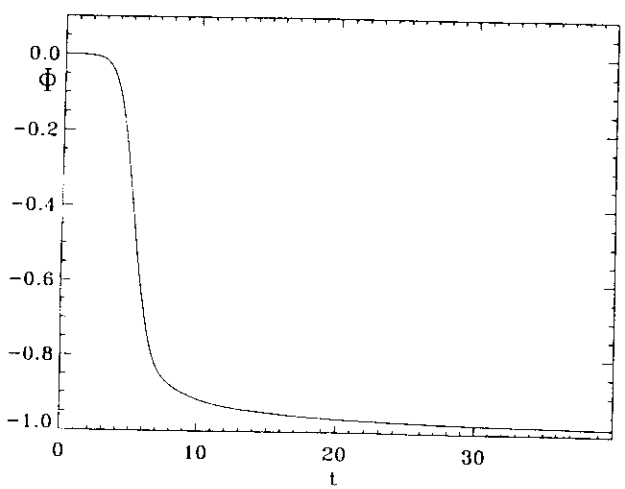

Fig. 3. Time evolution of Φ on the D_- line. The parameter values are $a = 1, c_1 = -1$ and $c_2 = -1$. The initial condition is a Gaussian noise of amplitude $\epsilon = 0.01$. The system evolved towards a TW attractor of wave number $k = 0.0245$.

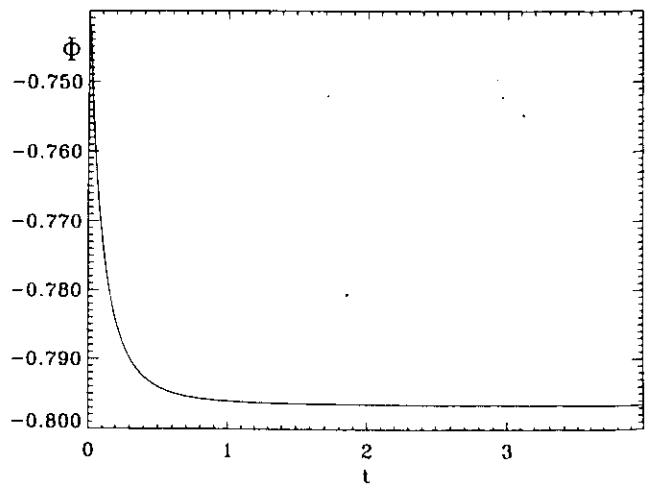

Fig. 4. Time evolution of Φ in the non-chaotic region for $c_1 = -1$ and $c_2 = -0.8$. The initial condition is an Eckhaus stable TW of wave number $k = 0.13$ perturbed by random noise of small amplitude $\epsilon = 0.09$.

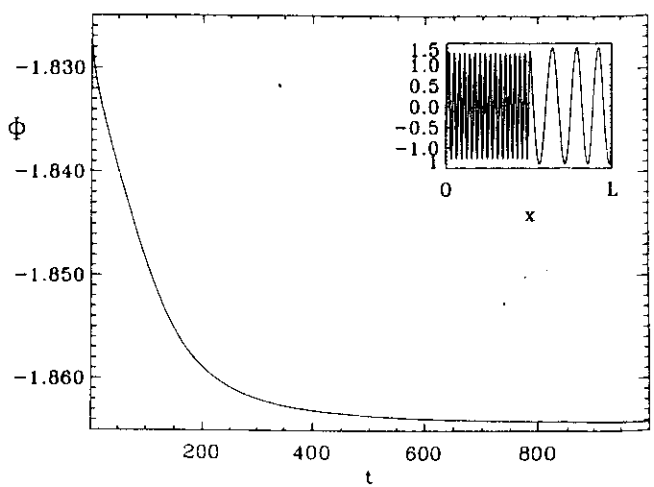

Fig. 5. Same as Fig. 4 but for $c_1 = -1$ and $c_2 = -2$. The initial condition for A consists of two Eckhaus stable TW of different wave numbers ($k_1 = 0.4, k_2 = 0.08$) joined together. The inset shows the real part of this initial configuration.

as initial condition a small ($\epsilon = 0.01$) random Gaussian noise. The system was left to evolve towards its asymptotic state (a TW). Fig. 6 shows that after a transient Φ monotonously decreases. During the initial transient it widely fluctuates, increasing and decreasing and loosing then its validity as a Lyapunov functional. This incorrect behavior occurs because during the initial stages $A(x,t)$ is small and often vanishes, changing ν. When A (and then r) vanishes the phase and (3.7) are ill-defined and out of the range of validity of a small gradient approximation. Note the contrast with the case $D_- = 0$ in which the potential is exact and well behaved even when ν is strongly changing. The particular values of the maxima and minima during the transient in which ν is changing depend on the spatial and temporal discretization, since it is clear from (3.7) that Φ is ill-defined or divergent when r vanishes. Note that this incorrect behavior of Φ for $D_- \neq 0$ is not a problem for the existence of a Lyapunov functional, but comes rather from the limited validity of the hypothesis used for its approximate construction. Nevertheless, as soon as the strong gradients disappear Φ relaxes monotonously to the value $\Phi = -0.79997$, corresponding to the final state, a TW of wave number $k = -0.0123$.

As another test in the non-chaotic region, for $D_i = -1$ and $b_r = 0.5$ ($c_1 = -1, c_2 = -2$) we use as initial condition an Eckhaus-unstable TW ($k = 0.54 > k_E = 0.48$) slightly perturbed by noise. The system evolves to an Eckhaus-stable TW ($k = 0.31$) by decreasing its winding number (initially $\nu = 44$ and finally $\nu = 26$). Fig. 7 shows the evolution of Φ from its initial value $\Phi(0) = -1.485$ the final one $\Phi = -1.77$. Although there is a monotonously decreasing baseline, sharp peaks are observed corresponding to the vanishing of r associated with the changes in ν. When ν finally stops changing, so that A is close enough to the final TW, Φ relaxes monotonously as in Fig. 4.

It was explained in Section 3 that there are parameter ranges in which Φ is smaller near the boundaries for existence of TW, that is near $k = \pm\sqrt{a/b_r}$, than for the homogeneous TW: $k = 0$. This happens for example for $D_i = 1$, $b_r = 1.25$ ($c_1 = 1, c_2 = -0.8$). The corresponding function Φ_k is shown in Fig. 8. If this prediction is true, and if Φ is a correct Lyapunov functional, evolution starting with one of these extreme and Eckhaus-unstable TW would not lead to any final TW, since this would increase the value of the Lyapunov functional. This would imply the existence for this value of the parameters of an attractor different from the TW's perhaps related to the spatio-temporal intermittency phenomenon. We use as initial condition at the parameter values of Fig. 8 an unstable TW of wave number $k = 0.64$ ($\Phi \approx -0.81$), slightly perturbed by noise. From Fig. 8, the system should evolve to a state with a value of Φ value even lower than that. What really happens can be seen in Fig. 9. The system changes its winding number from the initial value $\nu = 52$, a process during which Φ widely fluctuates and is not a correct Lyapunov functional, and ends-up in a state of $\nu = 5$, with a value of Φ larger than the initial one. After this the system relaxes to the associated stable TW of $k = 2\pi\nu/L = 0.061 < k_E = 0.23$. As clearly stated by Graham and coworkers, the expressions for the potential are only valid for small gradients. Since k is a phase gradient, results such as Fig. 8 can only be trusted for k small enough.

Finally, we show the behavior of Φ in the spatio-temporal intermittency regime. Since ν is constantly changing in this regime it is clear that (3.7) will not be a good Lyapunov functional and this simulation is included only for completeness. We take $D_i = 0$ and $b_r = 0.5$ ($c_1 = 0, c_2 = -2$) and choose as initial condition a TW with $k = 0.44 > k_E = 0.30$ ($\Phi = -1.89814$), with a small amount of noise added. The TW decreases its winding number and the system reaches soon the disordered regime called spatio-temporal intermittency. Fig. 10 shows that the time evolution of Φ is plagued with divergences, reflecting the fact that ν is constantly changing (see inset). It is interesting to observe, however, that during the initial escape from the unstable TW Φ shows a decreasing tendency, and that its average value in the chaotic regime, excluding the divergences, seems smaller than the initial one.

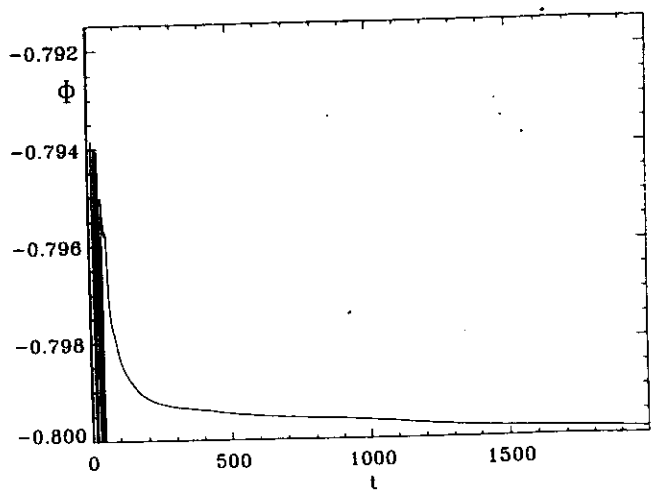

Fig. 6. Same as Fig. 4 but for $c_1 = 1$ and $c_2 = -0.8$. The initial condition is a random noise of amplitude $\epsilon = 0.01$.

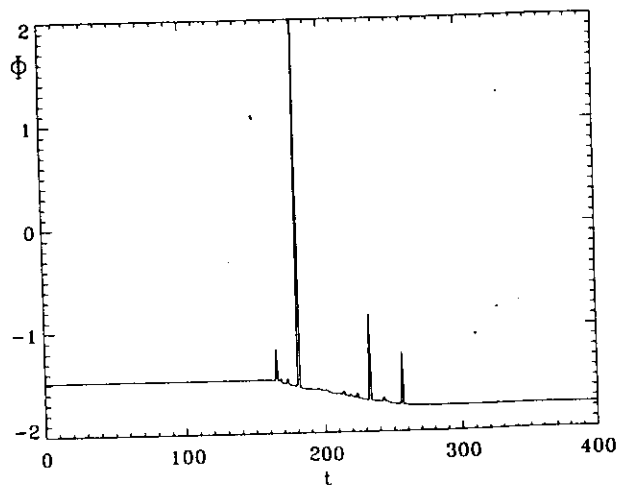

Fig. 7. Same as Fig. 4 but for $c_1 = -1$ and $c_2 = -2$. The initial condition is an Eckhaus-unstable TW ($k = 0.54 > k_E = 0.48$ slightly perturbed by noise.

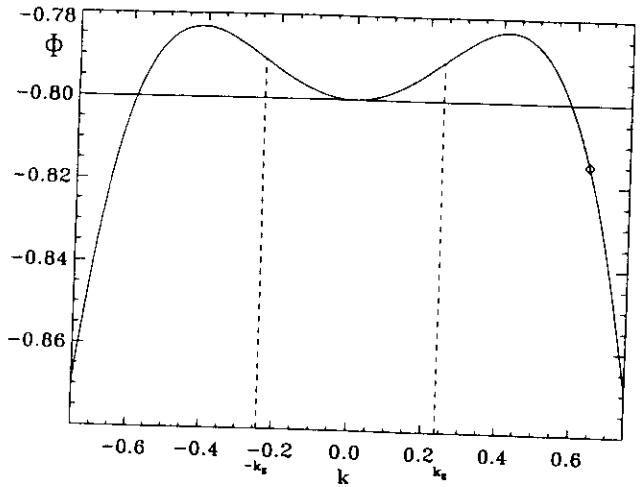

Fig. 8. The function $\Phi_k \equiv \Phi[A_k]$ as a function of k. The parameter values are $a = 1$, $c_1 = 1$ and $c_2 = -0.8$. The values of k_E are indicated by dashed lines. The diamond indicates the point $\Phi_{k=0.64}$ taken as initial condition for the simulation in Fig. 9.

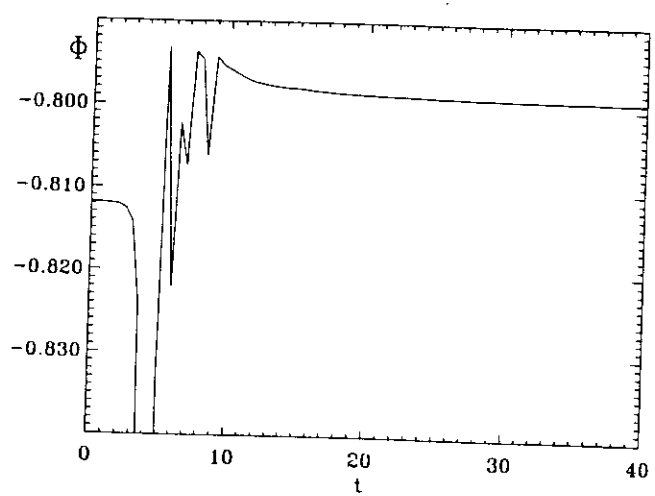

Fig. 9. Time evolution of Φ for $c_1 = 1$ and $c_2 = -0.8$. The initial condition is an Eckhaus-unstable TW ($k = 0.64 > k_E = 0.48$) slightly perturbed by noise.

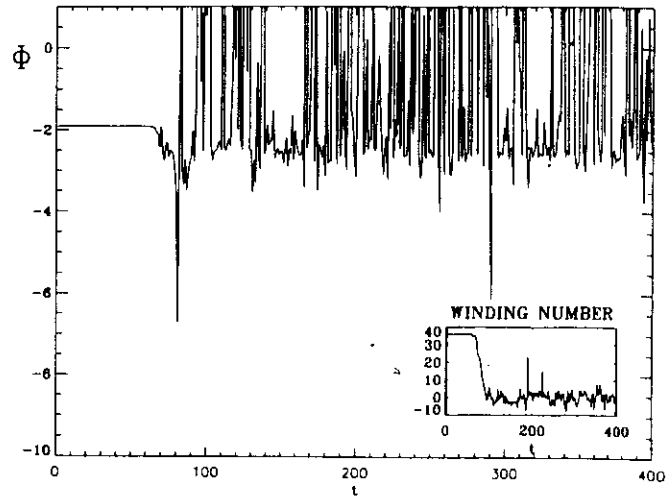

Fig. 10. Time evolution of Φ in the STI region ($c_1 = 0.0$ and $c_2 = -2$). The initial condition is an Eckhaus-unstable TW ($k = 0.45 > k_E = 0.30$) slightly perturbed by noise. The winding number evolution is plotted in the inset.

5. Numerical studies of the Lyapunov functional in the phase turbulence regime

The phase turbulence regime is characterized by the absence of phase singularities (thus ν is constant). This distinguishes it as the only chaotic regime for which Φ would be well defined. Graham and co-workers [14,30] derived especially for this region an expression proposed as Lyapunov functional in the small gradient approximation (3.12).

We recall that the calculations in [14,30] predict that the phase turbulent attractor lies on a potential plateau, consisting of all the complex functions satisfying (3.14), in which all the unstable TW cycles are also embedded. The value of the potential on such plateau can be easily calculated by substituting in (3.12) an arbitrary TW, and the result is

$$\Phi_{\rm pl} = -\frac{a^2}{b_r}. \tag{5.1}$$

We note that this value does not depend on D_i or D_r and then it is independent of c_1, the vertical position in the diagram of Fig. 1, within the phase turbulence region.

In this section we take also $a = 1$. We perform different simulations for $D_i = 1.75$ and $b_r = 1.25$ ($c_1 = 1.75$, $c_2 = -0.8$). In the first one, we start the evolution with the homogeneous oscillation solution (TW of $k = 0$). This solution is linearly unstable, but since no perturbation is added, the system does not escape from it. The potential value predicted by (5.1) is $\Phi_{\rm pl} = -0.8$. This value is reproduced by the numerical simulation up to the sixth significant figure for all times (Fig. 11, solid line). This agreement, and the fact that the unstable TW is maintained, gives confidence in our numerical procedure.

In a second simulation, a smooth perturbation (of the form μe^{iqx} with $q = 0.049$ and $\mu = 0.09$) is added to the unstable TW and the result used as initial condition. This choice of perturbation was taken to remain as much as possible within the range of validity of the small gradient hypothesis. After a transient the perturbation grows and the TW is replaced by the phase turbulence state (the winding number remains fixed to 0). The corresponding evolution of Φ

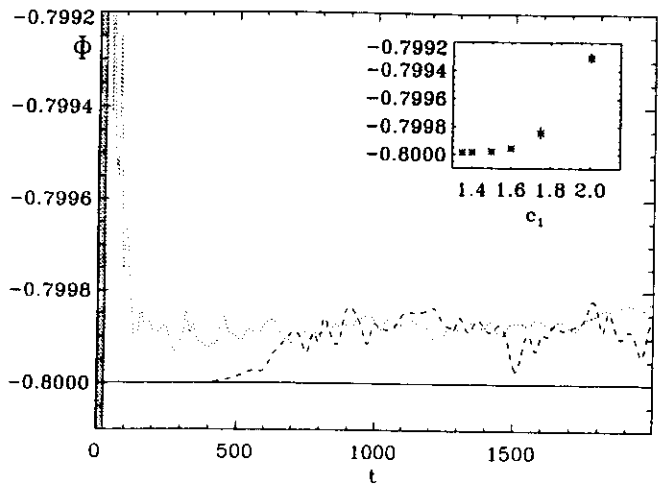

Fig. 11. Time evolution of Φ in the phase turbulence region ($c_1 = 1.75$ and $c_2 = -0.8$). Solid line: evolution of an unperturbed unstable traveling wave. Dotted line: evolution from noise. Dashed line: evolution from a slightly perturbed traveling wave. The inset shows final average values of Φ as a function of the c_1 parameter ($c_2 = -0.8$). The error bars indicate the standard deviation of the fluctuations around the average value.

is shown in Fig. 11 (long-dashed line). The value of the potential increases from Φ_{pl} to a higher value, and then irregularly oscillates around it. Both the departure and the fluctuation are very small, of the order of 10^{-4} times the value of Φ. Simulations with higher precisions confirm that these small discrepancies from the theoretical predictions are not an artifact of our numerics, but should be attributed to the terms with higher gradients which are not included in (3.12). As a conclusion, the prediction that the phase turbulence dynamics, driven by non-relaxational terms, maintains constant Φ in a value equal to the one for TW is confirmed within a great accuracy.

However, it is interesting to study how systematic are the small deviations from the theory. To this end we repeat the launching of the TW with a small perturbation for several values of $D_i = c_1$, for the same value of b_r as before. The prediction is that Φ should be independent of c_1. The inset in Fig. 11 shows that the theoretical value $\Phi_{pl} = -0.8$ is attained near the BF line, and that as c_1 is increased away from the BF line there are very small but systematic discrepancies. The values shown for the potential are time averages of its instantaneous values, and the error bars denote the standard deviation of the fluctuations around the average.

Again for $c_1 = 1.75$, $c_2 = -0.8$, we perform another simulation (Fig. 11, short-dashed line) consisting in starting the system in a random Gaussian noise configuration, of amplitude 0.01, and letting it to evolve towards the phase turbulence attractor. As in other cases, there is a transient in which Φ is ill-defined since the winding number is constantly changing. After this Φ decreases. This decreasing is not monotonous but presents small fluctuations around a decreasing trend. The decreasing finally stops and Φ remains oscillating around approximately the same value as obtained from the perturbed TW initial condition. The final state has $\nu = -1$, so that in fact the attractor reached is different from the one in the previous runs ($\nu = 0$) but the difference is the smallest possible and the difference in value of the associated

potential cannot be distinguished within the fluctuations of Fig. 11. These observations confirm the idea of a potential which decreases as the system advances towards an attractor, and remains constant there, but at variance with the cases in the non-chaotic region here the decreasing is not perfectly monotonous, and the final value is only approximately constant.

Since the small discrepancies with the theory increase far from the BF line, and since it is known that condition (3.14) can be obtained from an adiabatic-following of the modulus to the phase that looses accuracy far from the BF line, one is lead to consider the role of adiabatic following on the validity of Φ as a potential. To this end we evaluated Φ along trajectories $A(x, t)$ constructed with the phase obtained from solutions of (1.1), but with modulus replaced by (3.14), so enforcing the adiabatic following of the modulus to the phase. No significant improvement was obtained with respect to the cases in which the adiabatic following was not enforced since that, in fact, adiabatic following was quite well accomplished by the solution of (1.1). Then it is not the fact that the solutions of (1.1) do not fulfill (3.14) exactly, but the absence of higher gradient terms in both (3.14) and (3.12) the responsible for the small failures in the behavior of Φ.

Finally, it is interesting to show that the Lyapunov potential Φ can be used as a diagnostic tool for detecting changes in behavior that would be difficult to monitor by observing the complete state of the system. For example the time at which the phase turbulence attractor is reached can be readily identified from the time-behavior of Φ in Fig. 11. More interestingly it can be used to detect the escape from metastable states. For example, Fig. 12 shows Φ for evolution from a Gaussian noise initial condition ($\epsilon = 0.01$). $D_i = 2$ and $b_r = 1.25$ ($c_1 = 2$, $c_2 = -0.8$). The system reaches first a long lived state with $\nu = 2$ not too different from the usual phase turbulent state of $\nu = 2$. After a long time, however, the system leaves this metastable state and approaches a more ordered state that can be described [36] as phase turbulent fluctuations around quasi-periodic configurations related to those of [28]. More details about this state will be described elsewhere [36]. What is of interest here is that from Fig. 12 one can easily identify the changes between the different dynamical regimes. In particular the decrease in the fluctuations of Φ near $t \approx 1000$ identifies the jump from the first to the second turbulence regimes.

6. Conclusions and outlook

The validity of the expressions for the Lyapunov functional of the CGLE found by Graham and coworkers has been numerically tested. The most important limitation is that they were explicitly constructed in an approximation limited to small gradients of modulus and phase. This precludes its use for evolution on attractors such that zeros of r and thus phase singularities appear (defect turbulence, bi-chaos, spatio-temporal intermittency). The same problem applies to transient states of evolution towards more regular attractors, if phase singularities appear in this transient (for instance decay of an Eckhaus unstable TW, evolution from random states close to $A = 0$, etc.). It would be interesting to have the expansion of the Lyapunov potential for small gradients of the real and imaginary components of A, instead of using polar coordinates. This would eliminate the problem of the ill-definition of the phase, and clarify further the stability of the gradient expansion.

Apart from this, if changes in winding number are avoided, expressions (3.6), (3.7), and (3.12) display the correct properties of a Lyapunov functional: minima on stable attractors, where non-relaxational dynamics maintains it in a constant value, and decreasing value during approach to the attractor. These properties are completely satisfied in the non-chaotic region of parameter space, even in complex situations such as TW competition, as long as large gradients do not appear. It is remarkable that, although the potential is constructed through an expansion around the $k = 0$ TW, its minima identify exactly the remaining TW, its stability, and the non-relaxational terms calculated by subtracting the potential terms to (1.1) give exactly their frequencies. In the phase turbulence regime, however, there are small discrepancies with respect to the theoretical predictions: lack of monotonicity in the approach to the attractor, small fluctuations around the asymptotic value, and small

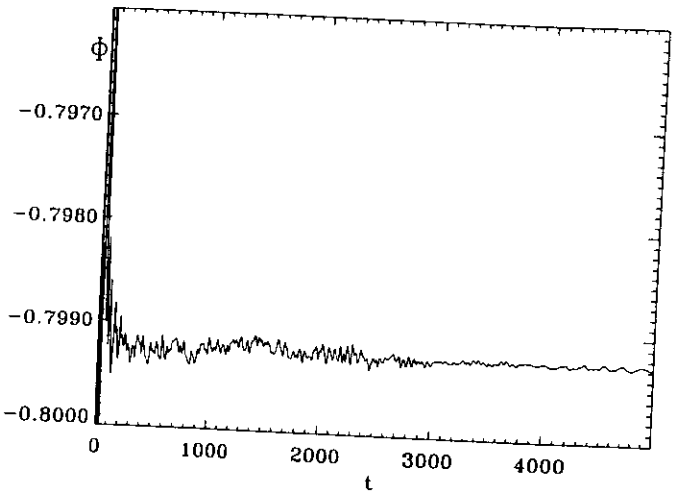

Fig. 12. Same as Fig. 11 but for $c_1 = 2$ and $c_2 = -0.8$. The initial condition was random noise with an amplitude $\epsilon = 0.01$, time step 0.005. In this case 2048 Fourier modes were taken into account. Note the transition occurring arround $t \approx 1000$ to a less fluctuating state.

discrepancy between the values of the potential of TW's and of turbulent configurations, that were predicted to be equal. All these deviations are very small but systematic, and grow as we go deeper in the phase turbulence regime. They can be fixed in principle by calculating more terms in the gradient expansion.

In addition in order to clarify the conceptual status of non-relaxational and non-potential dynamical systems one can ask about the utility of having approximate expressions for the Lyapunov functional of the CGLE. Several applications have been already developed for the case in which (1.1) is perturbed with random noise. In particular the stationary probability distribution is directly related to Φ, and in addition barriers and escape times from metastable TW have been calculated [12,30]. In the absence of random noise, Φ should be still useful in stating the nonlinear stability of the different attractors. However, in practice there will be limitations in the validity of the predictions, since Φ has been constructed in an expansion which is safe only near one particular attractor (the homogeneous TW).

Once known Φ, powerful statistical mechanics techniques (mean field, renormalization group, etc.) can in principle be applied to it to obtain information on the static properties of the CGLE (the dynamical properties, as time-correlation functions, would depend also on the non-relaxational terms N, as in critical dynamics [15]). Zero-temperature Monte Carlo methods can also be applied to sample the phase turbulent attractors, as an alternative to following the dynamical evolution on it. All those promising developments will have to face first with the complexity of Eqs. (3.6), (3.7), and (3.12). Another use of Lyapunov potentials (the one most used in equilibrium thermodynamics) is the identification of attractors by minimization instead of by solving the dynamical equations. In the case of the TW attractors, solving the Euler–Lagrange equations for the minimization of Φ is in fact more complex than solving directly the CGLE with a TW ansatz. But the limit cycle character of the attractors, and their specific form, is derived, not guessed as when substituting the TW ansatz. For the case of chaotic attractors (as in the phase turbulence regime) minimization of potentials can provide a step towards the construction of inertial manifolds. In this respect it should be useful considering the relationships between the Lyapunov potential of Graham and coworkers and other objects based on functional norms used also to characterize chaotic attractors [37,38].

Acknowledgements

We acknowledge very helpful discussions on the subject of this paper with R. Graham. We also acknowledge helpful inputs of E. Tirapegui and R. Toral on the general ideas of non-equilibrium potentials, and from A. Amengual on the numerical code. We acknowledge financial support from DGYCIT (Spain) Projects PB94-1167 and PB94-1172. R.M. also acknowledges partial support from the Programa de Desarrollo de las Ciencias Básicas (PEDECIBA, Uruguay), the Consejo Nacional de Investigaciones Científicas Y Técnicas (CONICYT, Uruguay) and the Programa de Cooperación con Iberoamérica (ICI, Spain).

References

[1] M.C. Cross and P.C. Hohenberg, Rev. Modern Phys. 65 (1993) 851 and references therein.
[2] W. van Saarloos and P. Hohenberg, Physica D 56 (1992) 303 .
[3] P. Kolodner, Phys. Rev. E 50 (1994) 2731.
[4] P. Coullet, L. Gil and F. Roca, Optimal Comm. 73 (1989) 403.
[5] Y. Kuramoto and S. Koga, Progr. Theor. Phys. Suppl. 66 (1981) 1081 .
[6] B.I. Shraiman, A. Pumir, W. van Saarloos, P.C. Hohenberg, H. Chaté and M. Holen, Physica D 57 (1992) 241.
[7] H. Chaté, Nonlinearity 7 (1994) 185.
[8] H. Chaté, Spatiotemporal Pattern in Nonequilibrium Complex Systems (Addison-Wesley, New York, 1994), Santa Fe Institute in the Sciences of Complexity.
[9] H. Chate, New Trends in Nonlinear Dynamics: Nonvariational Aspects (North-Holland, Estella, Spain, 1991), appeared in Physica D 61.
[10] R. Graham and T. Tél, Europhys. Lett. 13 (1990) 1715.
[11] R. Graham and T. Tél; Phys. Rev. A 42 (1990) 4661.
[12] R. Graham and T. Tél, in: Instabilities and Nonequilibrium Structures III, eds. E. Tirapegui and W. Zeller (Reidel, Dordrecht, 1991) p. 125.
[13] O. Descalzi and R. Graham, Phys. Lett. A 170 (1992) 84.
[14] O. Descalzi and R. Graham, Z. Phys. B 93 (1994) 509.
[15] P. C. Hohenberg and B.I. Halperin, Rev. Mod. Phys. 49 (1978) 535.
[16] J.D. Gunton, M. San Miguel and P. Sahni, in: Phase Transitions and Critical Phenomena eds. C. Domb and J. L. Lebowitz (Academic Press, London, 1983) Vol. 8.
[17] R. Graham, in: Theory of continuous Fokker–Plank systems, Vol. 1 of Noise in nonlinear dynamical systems, eds. F. Moss and P.V.E.M. Clintock (Cambridge University Press, Cambridge, 1989) p.225.
[18] R. Graham, in: XXV Years of Nonequilibrium Statistical Mechanics, Vol. 446 of Lecture Notes in Mathematics, eds. L. Brey, J. Marro, M. Rubí and M. San Miguel (Springer, Berlin, 1995).
[19] M. Caponeri and S. Ciliberto, Phys. Rev. Lett. 64 (1990) 2775.
[20] M. Caponeri and S. Ciliberto, Physica D 58 (1992) 365.
[21] H. Calisto, E. Cerdá and E. Tirapegui, J. Statist. Phys. 69 (1992) 1115.
[22] M. San Miguel and F. Sagués, Phys. Rev. A 36 (1987) 1883.
[23] P. Szépfalusy and T. Tél, Phys. Rev. A 112 (1982) 146.
[24] S. Rica and E. Tirapegui, Phys. Rev. Lett. 64 (1990) 878.
[25] T.B.Benjamin and J.E. Feir, J. Fluid Mech. 27 (1967) 417.
[26] A. Newell, Appl. Math. 15 (1974) 157.
[27] W. Eckhaus, Studies in Nonlinear Stability Theory (Springer, Berlin, 1965).
[28] B. Janiaud, A. Pumir, D. Bensimon, V. Croquette, H. Richter and L. Kramer, Physica D 55 (1992) 269.
[29] D. Egolf and H. Greenside, Phys. Rev. Lett. 74 (1995) 1751.
[30] O. Descalzi, Ph.D. Thesis, University of Essen (1993).
[31] R. Graham, in: Fluctuations, Instabilities and Phase Transitions, ed. T. Riste (Plenum Press, New York, 1975) p.270.
[32] D. Walgraef, G. Dewl and P. Borkmans, Adv. Chem. Phys. 49 (1982) 311.
[33] D. Walgraef, G. Dewl and P. Borkmans, J. Chem. Phys. 78 (1983) 3043.
[34] H. Sakaguchi, Progr. Theor. Phys. 84 (1990) 792.
[35] S. Chan, J. Chem. Phys. 67 (1977) 5755.
[36] R. Montagne, E. Hernández-García and M. San Miguel, to be published.
[37] C.R. Doering, J.D. Gibbon, D.D. Holm and B. Nicolaenko, Nonlinearity 1 (1988) 279.
[38] M. Bartuccelli, P. Constantin, C.R. Doering, J.D. Gibbon and M. Gisselfält, Physica D 44 (1990) 421.

Winding Number Instability in the Phase-Turbulence Regime of the Complex Ginzburg-Landau Equation

R. Montagne,* E. Hernández-García, and M. San Miguel

Departament de Física, Universitat de les Illes Balears and Instituto Mediterraneo de Estudios Avanzados, IMEDEA (CSIC-UIB), E-07071 Palma de Mallorca, Spain

(Received 29 March 1996)

We give a statistical characterization of states with nonzero winding number in the phase turbulence (PT) regime of the one-dimensional complex Ginzburg-Landau equation. We find that states with winding numbers larger than critical ones are unstable in the sense that they decay to states with smaller winding numbers. The transition from phase to defect turbulence is interpreted as an ergodicity breaking transition which occurs when the range of stable winding numbers vanishes. Asymptotically stable states which are not spatiotemporally chaotic are described within the PT regime of a nonzero winding number. [S0031-9007(96)00561-3]

PACS numbers: 05.45.+b, 05.70.Ln, 82.40.Bj

Spatiotemporal complex dynamics [1,2] is one of the present focuses of research in nonlinear phenomena. Much effort has been devoted to the characterization of different dynamical phases and transitions between them for model equations such as the complex Ginzburg-Landau equation (CGLE) [1,3–11]. One of the main questions driving these studies is whether concepts brought from statistical mechanics can be useful for describing complex nonequilibrium systems [3,12]. In this paper we give a characterization of the spatiotemporal configurations that occur in the phase turbulence (PT) regime of the CGLE (described below), for a finite system, in terms of a global wave number. This quantity plays the role of an order parameter classifying different phases. We show that in the PT regime there is an instability such that a conservation law for the global wave number occurs only for wave numbers within a finite range that depends on the point in parameter space. Our study is statistical in the sense that averages over ensembles of initial conditions are used. Our results allow a characterization of the transition from PT to defect or amplitude turbulence (DT) (another known dynamical regime of the CGLE) in terms of the range of conserved global wave numbers: As one moves in parameter space, within the PT regime and towards the DT regime, this range becomes smaller. The transition is identified with the point in parameter space at which such a stable range disappears.

The CGLE is an amplitude equation for a complex field $A(\mathbf{x},t)$ describing universal features of the dynamics of extended systems near a Hopf bifurcation [1,7]

$$\partial_t A = A + (1 + ic_1)\nabla^2 A - (1 + ic_2)|A|^2 A. \quad (1)$$

Binary fluid convection [13], transversally extended lasers [14], chemical turbulence [15], and bluff body wakes [16], among other systems, can be described by the CGLE in the appropriate parameter range. We will restrict ourselves in this paper to the one-dimensional case, that is $A = A(x,t)$, with $x \in [0,L]$. For this situation a major step towards the analysis of phases and phase transitions in (1) was the identification [3–5] of different chaotic regimes in different regions of the parameter space $[c_1,c_2]$ (see Fig. 1). Equation (1) has plane-wave solutions $A_k = \sqrt{1-k^2}e^{ikx}$ with $k \in [-1,1]$. When $c_1c_2 > -1$ there is a range of wave numbers $[-k_E,k_E]$ such that the plane-wave solutions with wave numbers in this range are linearly stable. They become unstable outside this range (the Eckhaus instability [6]). The limit of this range k_E approaches zero as the product c_1c_2 approaches -1, so that the range of stable plane waves vanishes by approaching from below the line $c_1c_2 = -1$ (the Benjamin-Feir or Newell line, labeled BF in Fig. 1). Above that line no plane wave is stable and different turbulent states exist. The authors of [3–5] identified three different regimes in different regions above the BF line (Fig. 1): PT, DT, and bichaos. Among these regimes, the transition between PT and DT has received special attention [3,10,17]. In spite of the fact that there are some indications that this transition can be ill defined in the $L \to \infty$ limit [5,9,10], the PT regime is

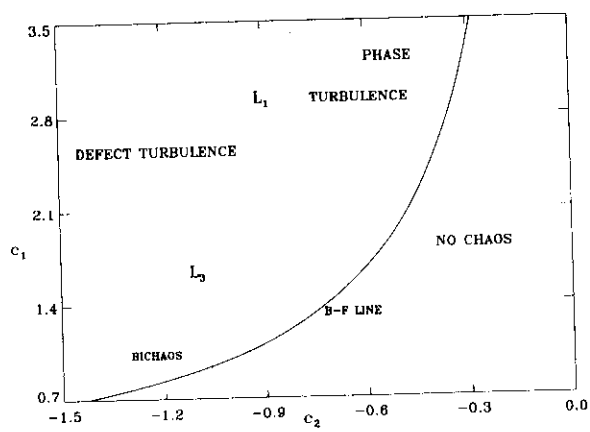

FIG. 1. Regions of the parameter $[c_1,c_2]$ space for the CGLE displaying different kinds of regular and chaotic behavior. Lines L_1, L_3 were determined in [3–5].

0031-9007/96/77(2)/267(4)$10.00

robustly observed for any finite size system and for finite observation times, with the transition to DT appearing at a quite well-defined line (L_1 in Fig. 1) [9]. In the DT region the modulus $|A|$ of $A = |A|e^{i\phi}$ becomes zero at some instants and places (called *defects*), so that the phase ϕ becomes undefined and the winding number $\nu \equiv \frac{1}{2\pi}\int_0^L \partial_x \phi dx$ changes value during evolution. In contrast, dynamics maintains the modulus of A far from zero in the PT region, so that ν is thought to be a constant of motion there. A global wave number of the configuration can be defined as $k \equiv 2\pi\nu/L$. In the bichaos regime one may observe either DT, PT, or a coexistence of them depending on the initial conditions [5]. These different regimes were originally identified from the analysis of the space-time density of *defects*. If this picture is correct, one can speculate that the transition between DT and PT would be a kind of ergodicity breaking transition [18] as in other systems described by statistical mechanics. DT would correspond to a "disordered" phase and ν classifies different "ordered" phases in PT. However, we note that most studies of the PT regime have considered in detail only the case of $\nu = 0$. In fact the phase diagram in Fig. 1 was constructed for this case. In order to provide a better understanding of the PT-DT transition we undertake in this Letter a systematic study of PT configurations with $\nu \neq 0$.

Typical configurations of the PT state of zero winding number consist of pulses in $|A|$, corresponding to phase sinks, that travel and collide rather irregularly on top of a $k = 0$ unstable background wave (that is, a uniform oscillation) [3,5]. The phase of these configurations strongly resembles solutions of the Kuramoto-Shivashinsky (KS) equation. Quantitative agreement has been found between the $\nu = 0$ PT states of the CGLE and solutions of the KS equation near the BF line [10]. The more obvious effect of a nonzero ν is the appearance of a uniform drift added to the irregular motion of the pulses. In addition, Chaté [4,5] reported an earlier breakdown of the PT regime when $\nu \neq 0$. Our results below show that not all the winding numbers are in fact allowed in the PT region at long times. PT states with too large $|\nu|$ are only transients and decay to states within a band of allowed winding numbers. The width of this band shrinks to zero when approaching the line L_1. In addition we find that the allowed nonzero winding number states are not of a single type. We have identified three basic types of asymptotic states for $\nu \neq 0$, which we describe below.

In order to study the dynamics of states with $\nu \neq 0$ we have performed simulations extensively covering the PT region of parameters of Fig. 1. Only a small part of the simulations is shown here, and the rest will be reported elsewhere. We use a pseudospectral code with periodic boundary conditions and second-order accuracy in time. Spatial resolution was typically 512 modes, with runs of up to 4096 modes to confirm the results. We work at fixed system size $L = 512$. The initial condition in our simulation is a plane wave of the desired winding number, slightly perturbed by a white Gaussian random field. The initial evolution of the spatial power spectrum is well described by the linear stability analysis around the initial plane wave: Typically the perturbation grows mostly around the most unstable wave numbers identified from such linear analysis. After some time the system reaches a state similar to the $\nu = 0$ PT, except for a nonzero average velocity of the chaotically traveling pulses. We call this state *riding PT*. Its spatial power spectrum is broad and unsteady, with the more active wave numbers located around the one determined by the initial winding number. We observe that when this winding number is small, it remains constant in time, and the system either remains in the *riding PT* state or approaches one of the more regular asymptotic states that will be described below. If $|\nu|$ is initially too high, the competition between wave numbers leads to phase slips that reduce $|\nu|$ until a value inside an allowed range is reached. Then the system evolves as before.

We present in Fig. 2 the temporal evolution of $\overline{\nu}(t)$, the average of $\nu(t)$ over 50 independent realizations of the random perturbation added to the initial plane wave for a fixed point in parameter space. The variance among the sample of 50 realizations is also shown. Three initial values ν_i of the winding number are shown. $\overline{\nu}(t)$ typically presents a decay from ν_i to the final winding number ν_f. The decay is found to take place in a characteristic time τ that we quantify as the time for which half of the jump in ν has been attained. Figure 3 shows $1/\tau$ for different values of ν_i. The different curves correspond to different values of c_2 with fixed c_1. Similar results were obtained for c_2 fixed and varying c_1. τ increases with an apparent divergence as ν_i approaches a particular value ν_c which is a function of c_1 and c_2. We estimate this ν_c by fitting linearly the data for $1/\tau$. Other fits involving nontrivial

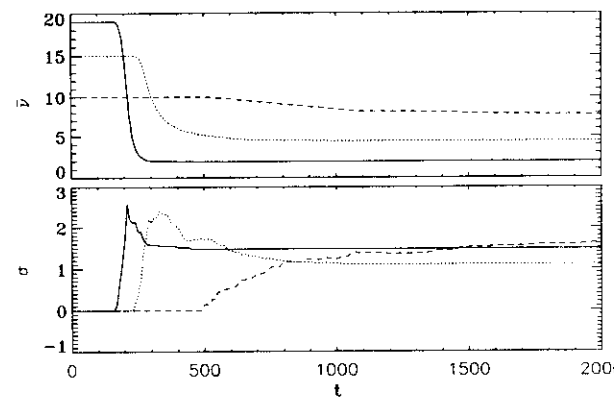

FIG. 2. (a) Temporal evolution of $\overline{\nu}(t)$ for three different initial winding numbers $\nu_i = 19$ (solid), 15 (dotted), 10 (dashed). $c_1 = 2.1, c_2 = -0.75$. (b) Winding number standard deviation σ.

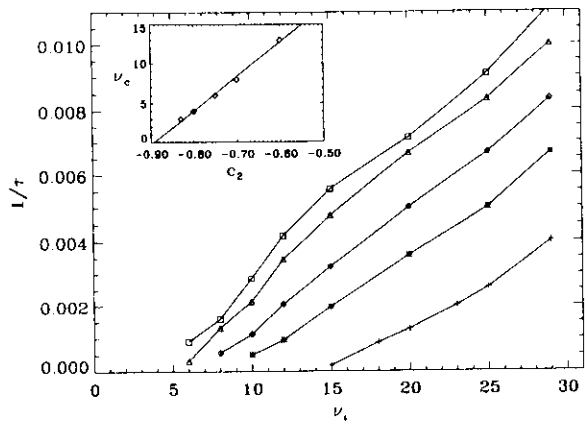

FIG. 3. Inverse of the characteristic time for winding number relaxation as a function of the initial winding number. The value of c_1 is fixed ($c_1 = 2.1$) and c_2 varies from near the BF line ($c_2 = -1/2.1$) to the L_1 line ($c_2 \approx -0.9$). Different symbols correspond to $c_2 = -0.6$ (+), $c_2 = -0.7$ (*), $c_2 = -0.75$ ($\diamond$), $c_2 = -0.8$ ($\triangle$), and $c_2 = -0.83$ ($\square$). The inset shows the critical winding number (ν_c) as a function of c_2.

critical exponents have been tried, but they do not improve the simpler linear one in a significant manner. A very similar value of ν_c is obtained by simply determining the value of ν_i below which $\nu(t)$ does not change in any of the realizations. Values of ν_c from some of the simulations are in the inset of Fig. 3. ν_c vanishes as c_2 approaches the transition line L_1 (or L_3 when passing through the bichaos region). For example, the linear fitting of the data in the inset of Fig. 3 and extrapolation towards zero ν_c reproduces the value for L_1 of [3,5] ($c_2 \approx -0.9$ for $c_1 = 2.1$) within the fitting error in c_2 of ± 0.02.

The winding number instability found here in the PT region is strikingly similar to the Eckhaus instability of traveling waves below the BF line of Fig. 1 [6]: There is a range of allowed winding numbers such that configurations outside this range undergo phase slips until an allowed ν is reached. The difference is that below the BF line, the attractor for each stable ν is a traveling plane wave of wave number k, whereas each ν, or an equivalent global wave number, characterizes phase turbulent attractors above the BF line. The allowed range of traveling waves shrinks to zero when (c_1, c_2) approaches the BF from below, whereas above BF, the allowed ν range shrinks to zero when approaching the L_1 line from the right. In this picture, the transition PT-DT appears as the *BF line* associated with an Eckhaus-like instability for phase turbulent waves. Such winding number instability gives rise to a transition between states of different global wave numbers, but none of these states is a perfect traveling wave (TW) state with a well-defined uniform wave number. The transition is thus reminiscent of the one observed for an Eckhaus instability in the presence of stochastic noise [19]. In the latter case a local wave number independent of position cannot be defined because of noise, while for phase turbulent waves the disorder is generated by the system dynamics. The comparison is also instructive because it can be shown that, for the one-dimensional stochastic case, there is no true long range order, and therefore no true phase transition in the infinite size limit [20]. But for finite sizes and finite observation times, well-defined effective transitions and even critical exponents can be introduced [19]. The PT-DT transition in the CGLE can be an effective transition of this kind. In order to further characterize the robustness of the effective transition an analysis of system size effects should be performed. Preliminary results indicate that the ν_c obtained for each (c_1, c_2) point grows linearly with system size L, as it should happen for a well-defined extensive quantity.

Finally, we consider the nature of the asymptotic states allowed within the band of "stable" ν. We have numerically found three basic types of states in the PT region of parameters with nonzero ν. Figure 4 shows in gray levels the value of $\partial_x \phi(x,t)$ as a function of x and t. The state shown in the top left is the familiar [5] *riding PT*, which is similar to the PT usually seen for $\nu = 0$ (wiggling pulses in the gradient of the phase) except for a systematic drift in a direction determined by ν. The other two states do not show spatiotemporal chaos. They can be described as the motion in time of a spatially rigid pattern on the top of a plane wave (with $k \neq 0$) background and with periodic boundary conditions. The state shown in the top right consists of equidistant pulses traveling uniformly. They are the quasiperiodic states described in [6]. The state shown in the bottom left, which we call *frozen turbulence*, consists of pulses uniformly traveling on a plane wave background, as in the quasiperiodic case, but now the pulses are not equidistant from each other. The spatial power spectrum is shown for this latter case. It is a broad spectrum in the sense that the inverse of its width, which gives a measure of the correlation length, is small compared with the system size. This is due to the irregular positions of the pulses. In addition, the spectrum is constant in time, which makes this frozen state different from riding PT and reflects that the pattern moves rigidly. The existence of the two states with no spatiotemporal chaos (quasiperiodic and frozen turbulence) described above can be understood by analyzing the phase equation valid near the BF instability. In the case of a nonzero ν it contains terms breaking the left-right symmetry [6,21], and it is known as a Kawahara equation [22]. Its uniformly traveling solutions are related to the rigidly propagating patterns of Figs. 1(b) and 1(c). These solutions can be analyzed with the tools of Shilnikov theory [23]. The details will be discussed elsewhere.

In addition to the pure three basic states, there are configurations in which they coexist at different places of space, giving rise to a kind of *intermittent* configuration, some of them already observed in [4]. The main results reported here, that is the existence of an Eckhaus-like

instability for phase-turbulent waves, the identification of the transition PT-DT with the vanishing of the range of stable winding numbers, and the coexistence of different kinds of PT attractors should in principle be observed in systems for which PT and DT regimes above a Hopf bifurcation are known to exist [16]. We note in addition that the experimental observation of what seems to be an Eckhaus instability for nonregular waves has been already reported in [24].

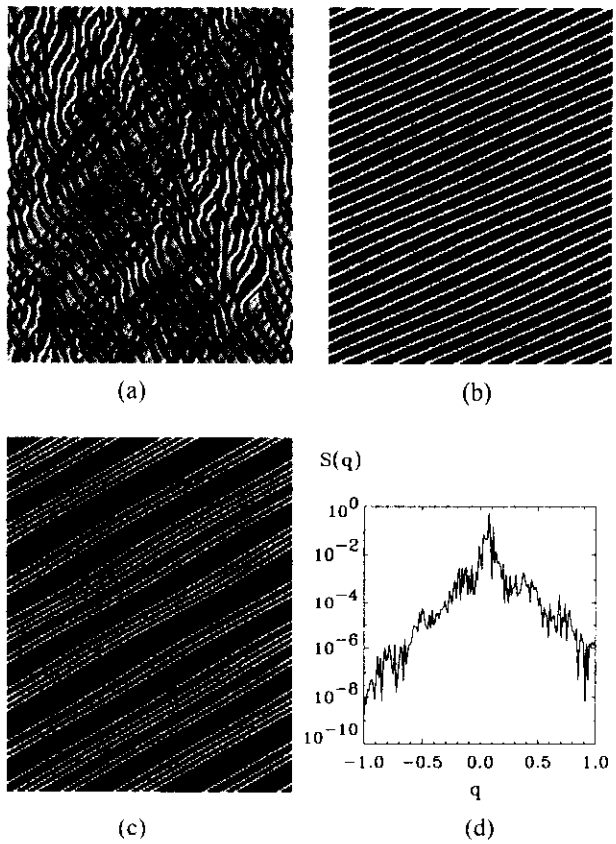

FIG. 4. Spatiotemporal evolution of $\partial_x\phi(x,t)$ with time running upwards and x in the horizontal direction. The lighter grey corresponds to the maximum value of $\partial_x\phi(x,t)$ and the darker grey corresponds to the minimum value. Different scales of grey are used in each case in order to see the significant structures. (a) Last 10^2 time units of a run 10^4 time units long for a *riding PT* state at $c_1 = 2.1$ and $c_2 = -0.83$. The initial condition was a TW with $\nu_i = 20$ that decayed to $\nu_f = -1$ after a short time. (b) Last 10^2 time units of a run 10^5 time units long for a quasiperiodic state. The initial condition is random noise with an amplitude of 0.05. $c_1 = 2.0$ and $c_2 = -0.8$. (c) Last 10^2 time units of a run 10^4 time units long for a frozen turbulence state. The initial condition is a TW of $\nu_i = 12$ that decayed to $\nu_f = 6$ after a short time. $c_1 = 1.75$ and $c_2 = -0.8$. (d) Spatial power spectrum $S(q)$ as a function of wave number for the frozen turbulence configuration shown in (c). This specimen is constant in time.

Financial support from DGYCIT (Spain) Projects No. PB94-1167 and No. PB94-1172 is acknowledged. R. M. also acknowledges partial support from the Programa de Desarrollo de las Ciencias Básicas (PEDECIBA, Uruguay), the Consejo Nacional de Investigaciones Científicas Y Técnicas (CONICYT, Uruguay), and the Programa de Cooperación con Iberoamérica (ICI, Spain).

*On leave from Universidad de la República, Uruguay.

[1] M. Cross and P. Hohenberg, Rev. Mod. Phys. **65**, 851 (1993), and references therein.
[2] M. Cross and P. Hohenberg, Science **263**, 1569 (1994).
[3] B. Shraiman *et al.*, Physica (Amsterdam) **57D**, 241 (1992).
[4] H. Chaté, Nonlinearity **7**, 185 (1994).
[5] H. Chaté, in *Spatiotemporal Patterns in Nonequilibrium Complex Systems*, edited by P. E. Cladis and P. Palffy-Muhoray (Addison-Wesley, New York, 1995).
[6] B. Janiaud *et al.*, Physica (Amsterdam) **55D**, 269 (1992).
[7] W. van Saarloos and P. Hohenberg, Physica (Amsterdam) **56D**, 303 (1992).
[8] D. Egolf and H. Greenside, Nature (London) **369**, 129 (1994).
[9] H. Chaté and P. Manneville, in *A Tentative Dictionary of Turbulence*, edited by P. Tabeling and O. Cardoso (Plenum, New York, 1995).
[10] D. Egolf and H. Greenside, Phys. Rev. Lett. **74**, 1751 (1995).
[11] R. Montagne, E. Hernández-García, and M. San Miguel (to be published).
[12] P. C. Hohenberg and B. I. Shraiman, Physica (Amsterdam) **37D**, 109 (1989).
[13] P. Kolodner, S. Slimani, N. Aubry, and R. Lima, Physica (Amsterdam) **85D**, 165 (1995).
[14] P. Coullet, L. Gil, and F. Roca, Opt. Commun. **73**, 403 (1989).
[15] Y. Kuramoto and S. Koga, Progr. Theor. Phys. Suppl. **66**, 1081 (1981).
[16] T. Leweke and M. Provansal, Phys. Rev. Lett. **72**, 3174 (1994).
[17] H. Sakaguchi, Prog. Theor. Phys. **84**, 792 (1990).
[18] R. Palmer, in *Lectures in the Sciences of Complexity*, edited by D. L. Stein (Addison-Wesley, New York, 1989).
[19] E. Hernández-García, J. Viñals, R. Toral, and M. San Miguel, Phys. Rev. Lett. **70**, 3576 (1993).
[20] J. Viñals, E. Hernández-García, R. Toral, and M. San Miguel, Phys. Rev. A **44**, 1123 (1991); E. Hernández-García, M. San Miguel, R. Toral, and J. Viñals, Physica (Amsterdam) **61D**, 159 (1992).
[21] H. Sakaguchi, Prog. Theor. Phys. **83**, 169 (1990).
[22] T. Kawahara, Phys. Rev. Lett. **51**, 381 (1983).
[23] S. Wiggings, *Introduction to Applied Nonlinear Dynamical Systems and Chaos* (Springer, New York, 1990).
[24] L. Pan and J. de Bruyn, Phys. Rev. E **49**, 2119 (1994).

Wound-up phase turbulence in the Complex Ginzburg-Landau Equation

R. Montagne*[‡§], E. Hernández-García[‡§], A. Amengual[‡], and M. San Miguel[‡§]
[‡] *Departament de Física, Universitat de les Illes Balears, E-07071 Palma de Mallorca, Spain*
[§] *Instituto Mediterráneo de Estudios Avanzados, IMEDEA[†] (CSIC-UIB), E-07071 Palma de Mallorca, Spain*
(December 16, 1996)

We consider phase turbulent regimes with nonzero winding number in the one-dimensional Complex Ginzburg-Landau equation. We find that phase turbulent states with winding number larger than a critical one are only transients and decay to states within a range of allowed winding numbers. The analogy with the Eckhaus instability for non-turbulent waves is stressed. The transition from phase to defect turbulence is interpreted as an ergodicity breaking transition which occurs when the range of allowed winding numbers vanishes. We explain the states reached at long times in terms of three basic states, namely *quasiperiodic* states, *frozen turbulence* states, and *riding turbulence* states. Justification and some insight into them is obtained from an analysis of a phase equation for nonzero winding number: rigidly moving solutions of this equation, which correspond to quasiperiodic and frozen turbulence states, are understood in terms of periodic and chaotic solutions of an associated system of ordinary differential equations. A short report of some of our results has been published in [*Montagne et al., Phys. Rev. Lett.* **77**, *267 (1996)*].

PACS: 05.45.+b,82.40.Bj,05.70.Ln

I. INTRODUCTION

A. The complex Ginzburg-Landau equation and its phase diagram

Spatio-temporal complex dynamics [1, 2, 3] is one of the present focus of research in nonlinear phenomena. This subject lies at the intersection of two important lines of thought: on the one hand the generalization of the ideas of dynamical systems theory to high dimensional situations[4, 5, 6], and on the other the application of some concepts and tools developed in the field of statistical mechanics, specially in the study of phase transitions, to the analysis of complex nonequilibrium systems [7, 8, 9].

An important effort has been devoted to the characterization of different dynamical states and transitions among them for model equations such as the Complex Ginzburg-Landau Equation (CGLE) [1, 4, 7, 10, 11, 12, 13, 14, 15, 16, 17]. The CGLE is an equation for a complex field $A(\mathbf{x},t)$:

$$\partial_t A = A + (1+ic_1)\nabla^2 A - (1+ic_2)\mid A\mid^2 A\ . \tag{1.1}$$

$A(\mathbf{x},t)$ represents the slowly varying, in space and time, complex amplitude of the Fourier mode of zero wavenumber when it has become unstable through a Hopf bifurcation (the signs used in (1.1) assume it to be supercritical). The CGLE is obtained universally when analyzing the dynamics sufficiently close to the bifurcation point. In one dimensional geometries, (1.1) or a coupled set of similar equations with additional group velocity terms describe also the evolution of the amplitudes of Hopf-bifurcated traveling waves [1, 14, 18]. Binary fluid convection [19], transversally extended lasers [20, 21], chemical turbulence[22, 23], bluff body wakes [24], the motion of bars in the bed of rivers [25], and many other systems have been described by the CGLE in the appropriate parameter range. We will restrict ourselves in this paper to the one-dimensional case, that is $A = A(x,t)$, with $x \in [0, L]$. As usual, we will use periodic boundary conditions in x.

The one-dimensional Eq. (1.1) has traveling wave (TW) solutions

$$A_k = \sqrt{1-k^2}e^{i(kx-\omega_k t)},\ \omega_k = c_2 + (c_1 - c_2)k^2 \tag{1.2}$$

with $k \in [-1,1]$. When $1 + c_1c_2 > 0$ there is a range of wavenumbers $[-k_E, k_E]$ such that TW solutions with wavenumber in this range are linearly stable. Waves with k outside this range display a sideband instability (the

---

*on leave from Universidad de la República (Uruguay).
[†]URL: http://www.imedea.uib.es/Nonlinear

Eckhaus instability [1, 13, 26]). The limit of this range, k_E, vanishes as the quantity $1+c_1c_2$ approaches zero, so that the range of stable traveling waves vanishes by decreasing $1+c_1c_2$. The line $1+c_1c_2=0$, is the Benjamin–Feir–Newell line[27, 28], labeled BFN in Fig.1. Above that line, where $1+c_1c_2<0$, no traveling wave is stable and different turbulent states exist. A major step towards the analysis of phases and phase transitions in (1.1) was the numerical construction in [7, 11, 12] of a phase diagram that shows which type of regular or chaotic behavior occurs in different regions of the parameter space $[c_1, c_2]$. Fig. 1 has been constructed from the data in [7, 11, 12]. Above the BFN line, three types of turbulent behavior are found, namely *phase turbulence* (PT), *defect* or *amplitude turbulence* (DT), and *bichaos* (BC).

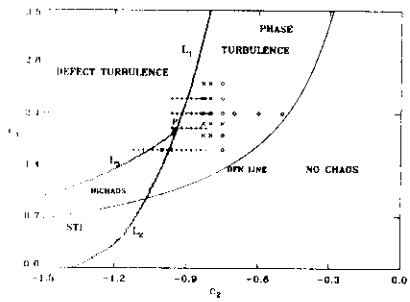

FIG. 1. Regions of the parameter space $[c_1, c_2]$ for the CGLE displaying different kinds of regular and chaotic behavior. Lines L_1, L_3 were determined in[7, 11, 12]. See the text in Section II for the explanation of the different symbols.

Phase turbulence is a state in which $A(x,t)=|A|e^{i\varphi}$ evolves irregularly but with its modulus always far from $|A|=0$. Since the modulus never vanishes, periodic boundary conditions enforce the *winding number* defined as

$$\nu \equiv \frac{1}{2\pi}\int_0^L \partial_x \varphi dx \tag{1.3}$$

to be a constant of motion, fixed by the initial condition. ν is always an integer because of periodic boundary conditions . The quantity $k \equiv 2\pi\nu/L$ can be thought of as an *average* or *global wavenumber*. To the left of line L_1 (region DT), in contrast, the modulus of A becomes zero at some instants and places (called *defects* or *phase slips*). In such places the phase φ becomes undefined, so allowing ν to change its value during evolution. BC is a region in which either PT, DT, or spatial coexistence of both can be observed depending on initial conditions. It should be noted that chaotic states exist also below the BFN line: To the left of the line L_2, a chaotic attractor called *Spatio Temporal Intermittency* (STI) coexists with the stable traveling waves [11]. A diagram qualitatively similar to Fig. 1 has also been found for the two-dimensional CGLE [29, 30]. Despite the relevance of ν in the dynamics of the CGLE, most studies of the PT regime have only considered in detail the case of $\nu=0$. In fact the phase diagram in Fig. 1 was constructed [7, 11, 12] using initial conditions that enforce $\nu=0$. Apart from some limited observations[12, 13, 30], systematic consideration of the $\nu\neq 0$ (*wound*) disordered phases has started only recently [10, 31, 32]. States with $\nu\neq 0$ are precisely the subject of the present paper.

B. The PT-DT transition

Among the regimes described above, the transition between PT and DT has received special attention [7, 10, 16, 31, 32, 33]. The PT regime is robustly observed for the large but finite sizes and for the long but finite observation times allowed by computer simulation, with the transition to DT appearing at a quite well defined line (L_1 in Fig. 1) [15, 30], but it is unknown if the PT state would persist in the thermodynamic limit $L\to\infty$. One possible scenario is that in a system large enough, and after waiting enough time, a defect would appear somewhere, making thus the conservation of ν only an approximate rule. In this scenario, a PT state is a long lived metastable state. In the alternative scenario, the one in which PT and the transition to DT persist even in the thermodynamic limit, this

transition would be a kind of ergodicity breaking transition [10, 34] in which the system restricts its dynamics to the small portion of configuration space characterized by a particular ν. DT would correspond to a "disordered" phase and different "ordered" phases in the PT region would be classified by its value of ν. The idea of using a quantity related to ν as an order parameter [10] has also been independently proposed in [31].

The question of which of the scenarios above is the appropriate one is not yet settled. Recent investigations seem to slightly favor the first possibility [12, 15, 16, 30]. The most powerful method in equilibrium statistical mechanics to distinguish true phase transitions from sharp crossovers is the careful analysis of finite-size effects [35]. Such type of analysis has been carried out in [15, 30] , giving some evidence (although not definitive) that the PT state will not properly exist in an infinite system or, equivalently, that the L_1 line in Fig. 1 approaches the BFN line as $L \to \infty$. Here we present another finite-size scaling analysis, preliminarily commented in [10], based on the quantity ν as an order parameter. Our result is inconclusive, perhaps slightly favoring the vanishing of PT at large system sizes. In any case, the PT regime is clearly observed in the largest systems considered and its characterization is of relevance for experimental systems, that are always finite. In this paper we characterize this PT regime in a finite system as we now outline.

C. Outline of the paper

We show that in the PT regime there is an instability such that a conservation law for the winding number occurs only for ν within a finite range that depends on the point in parameter space. PT states with too large $|\nu|$ are only transients and decay to states within a band of allowed winding numbers. Our results, presented in Section II, allow a characterization of the transition from PT to DT in terms of the range of conserved ν: as one moves in parameter space, within the PT regime and towards the DT regime, this range becomes smaller. The transition is identified with the line in parameter space at which such stable range vanishes. Analogies with known aspects of the Eckhaus and the Benjamin-Feir instabilities are stressed. States with $\nu \neq 0$ found in the PT region of parameters at late times are of several types, and Section III describes them in terms of three [10] elementary *wound* states. Section IV gives some insight into the states numerically obtained by explaining them in terms of solutions of a phase equation. In addition, theoretical predictions are made for such states. The paper is closed with some final remarks. An Appendix explains our numerical method.

II. THE WINDING NUMBER INSTABILITY

The dynamics of states with non-zero winding number and periodic boundary conditions has been studied numerically in the PT region of parameters. In order to do so we have performed numerical integrations of Eq. (1.1) in a number of points, shown in Fig. 1. Points marked as $\diamond$ correspond to parameter values where intensive statistics has been performed. The points overmarked with $\times$ correspond to places where finite-size scaling was analyzed. Finally the symbol + correspond to runs made in order to determine accurately the PT-DT transition line (L_1). Our pseudospectral integration method is described in the Appendix. Unless otherwise stated, system size is $L = 512$ and the spatial resolution is typically 512 modes, with some runs performed with up to 4096 modes to confirm the results. The initial condition is a traveling wave, with a desired initial winding number ν_i, slightly perturbed by a random noise of amplitude ϵ. By this amplitude we specifically mean that a set of uncorrelated Gaussian numbers of zero mean and variance ϵ^2 was generated, one number for each collocation point in the numerical lattice. Only results for $\nu_i > 0$ are shown here. The behavior for $\nu_i < 0$ is completely symmetrical.

The initial evolution is well described by the linear stability analysis around the traveling wave [13, 14, 36, 26]. Typically, as seen from the evolution of the power spectrum, unstable sidebands initially grow. This growth stops when an intense competition among modes close to the initial wave and to the broad sidebands is established. Configurations during this early nonlinear regime are similar to the ones that would be called *riding turbulence* and described in Section III. At long times the system approaches one of several possible dynamical states. In general, they can be understood in terms of three of them, which are called basic states. In the next section these final states are discussed. When the initial winding number is above a critical value ν_c, which depends on c_1 and c_2, there is a transient period between the early competition and the final state during which the winding number changes.

In Fig. 2a we show in grey levels the phase $\varphi(x,t)$ for a given run with parameters $c_1 = 2.1$ and $c_2 = -0.6$. The space-time defects appear as dislocations in this representation. In Fig. 2b the winding number has been plotted as a function of time. The winding number changes from the initial value $\nu_i = 20$ to the final value $\nu_f = 14$. The discrete jumps in ν are due to the integer nature of this quantity, and they are smeared out when averages over several realizations are performed. The resemblance with the dynamics of the Eckhaus instability of regular waves

is striking. In fact, since the changes in ν occur on top of a chaotic wave, the analogy is stronger with the Eckhaus instability in the presence of stochastic fluctuations [37, 38]. In the latter case a local wavenumber independent of position cannot be defined because of noise, while for phase turbulent waves the disorder is generated by the system dynamics. Nevertheless in both cases the configurations can be characterized by a global wavenumber such as $\bar{k}$ or ν. The analogy is also instructive since it can be shown [38, 39] that for the one-dimensional relaxational dynamics considered in [37, 38, 39] (which is related to Eq.(1.1) with $c_1 = c_2 = 0$) there is no long range order in the system, so that there is no proper phase transition in the thermodynamic $L \to \infty$ limit. Despite this, for large but finite sizes and long but finite times, sharp transitions are observed and critical exponents and scaling functions can be consistently introduced [37]. This example should make clear that even in the case that the PT-DT transition would not exist in the thermodynamic limit, its characterization in large finite systems is justified. The development of phase slips from PT waves of high enough ν_i can be viewed as a kind of Eckhaus-like instability for turbulent waves, whereas the usual Eckhaus instability [13] appears for regular waves. This similarity was one of the main motivations for the kind of analysis that follows.

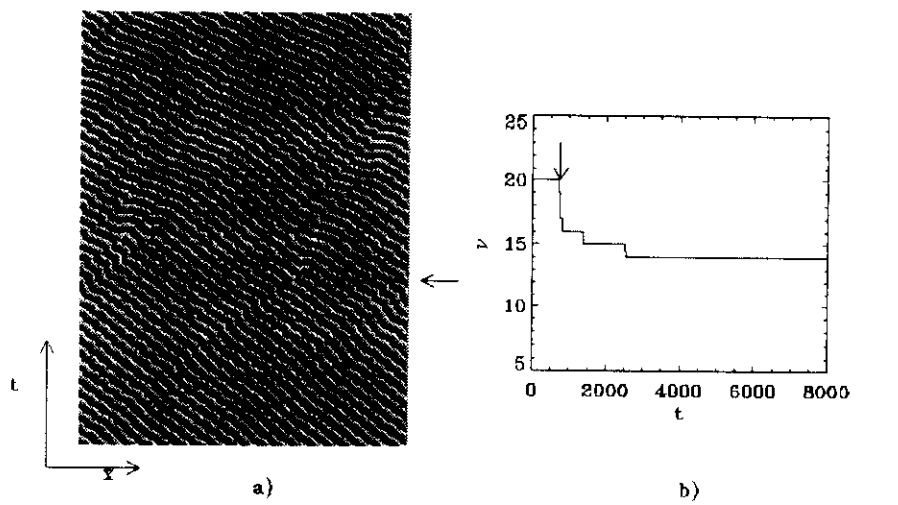

FIG. 2. a) Spatiotemporal evolution of the phase $\varphi(x,t)$ coded in grey levels with time running upwards and x in the horizontal direction. The lighter grey correspond $\varphi(x,t) = -\pi$ and darker to $\varphi(x,t) = \pi$. The time interval shown in the picture goes from $t = 500$ to 1000 time units of a total run of 10^4. $c_1 = 2.1$, $c_2 = -0.60$, and the initial condition was a TW with $\nu_i = 20$ that decayed to $\nu_f = 14$. The arrow indicates the time at which ν begins to change. b) The complete time evolution of the winding number for this initial condition.

For each point in parameter space and initial winding number considered, we have averaged over 50 independent random realizations of the white Gaussian perturbation added to the initial wave. Figs. 3a and 3b show the temporal evolution of this average $\bar{\nu}(t)$ and its variance σ for $c_1 = 2.1$ and $c_2 = -0.83$. Four values of the initial winding number ($\nu_i = 10, 15, 20, 25$) are shown. Typically, the curve $\bar{\nu}(t)$ decays from ν_i to a final winding number ν_f.

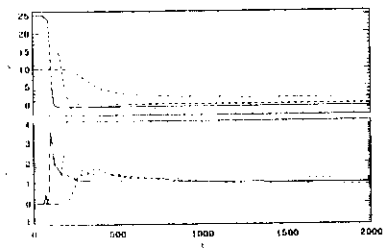

FIG. 3. a) Temporal evolution of $\bar{\nu}(t)$ for four different initial winding numbers $\nu_i = 25$ (solid), 20(dotted), 15 (dashed) 10 (dashed-dotted). $c_1 = 2.1, c_2 = -0.83$ (PT regime). b) Winding number standard deviation σ.

The variance displays the behavior typical of a decay from a unstable state [40], namely a pronounced maximum at the time of fastest variation of $\bar{\nu}(t)$. The final value of σ gives the dispersion in the final values of the winding numbers. Although the behavior shown in Fig. 3 is very similar to the observed in [37] for a stochastic relaxational case, the scaling laws found there do not apply here. The main qualitative difference is that in a range of ν_i the sign of the average final $\bar{\nu}$ is here opposite to the initial one. In addition for some of the initial winding numbers (i.e. $\nu_i = 20$ in Fig. 3) $\bar{\nu}(t)$ is not monotonously decaying, showing a small recovery after the fast decrease in $\bar{\nu}$. These features are also observed for other values of $[c_1, c_2]$, so that figure 3 is typical for $[c_1, c_2]$ in the PT region of Fig. 1. For comparison we show $\bar{\nu}(t)$ and its variance in Fig. 4 for the point $c_1 = 1.6$ and $c_2 = -1.0$, in the "bichaos" region. The main difference is the existence of fast fluctuations in $\bar{\nu}$ and σ. They are related to the characteristic dynamics of the bichaos regime: The final state depends on the initial conditions and it can correspond to PT, DT or even coexistence of both. In the 50 realizations performed all these possibilities were found. When DT appears, there are big fluctuations of the winding number around $\nu = 0$ that produce the wiggling on the averaged value. More than 50 realizations should be performed to smooth out such big fluctuations.

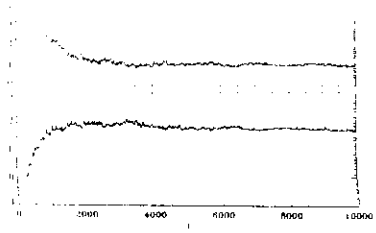

FIG. 4. a) Temporal evolution of $\nu(t)$ for an initial winding number of $\nu_i = 4$ in the bichaos regime. $c_1 = 1.6, c_2 = -1.0$. b) Winding number standard deviation σ.

Returning to the PT parameter regime (Fig. 3) the decay of the initial state is seen to take place during a characteristic time which depends on ν_i. We quantify this time τ as the time for which half of the jump in ν is attained. τ increases as ν_i decreases, and there is a critical value of ν_i, ν_c, such that no decay is observed for $\nu_i < \nu_c$. Then τ diverges (critical slowing down) when ν_i approaches ν_c from above. This gives a sensible procedure to determine ν_c: Figs. 5a and 5b show $1/\tau$ as a function of ν_i. In Fig. 5a, c_1 is fixed and the different symbols correspond to different values of c_2. In Fig. 5b, c_2 is fixed and the symbols correspond to different values of c_1. The values of ν_c have been estimated by extrapolating to $1/\tau = 0$ a linear fit to the points of smallest ν_i in each sequence. Motivated by [37] we have tried to fit the divergence of τ with nontrivial critical exponents, but we have found no significant improvement over the simpler linear fit. The values of ν_c so obtained are plotted in the insets of Figs. 5a and 5b. The range of conserved winding numbers $[-\nu_c, \nu_c]$ is analogous to the Eckhaus range of stable wavenumbers when working below the BFN line. ν_c can also be obtained by directly determining the value of ν_i below which $\nu(t)$ does not change in any of the realizations. This method can only give integer values of ν_c whereas the method based on τ gives a real number which is preferable when looking for continuous dependences of ν_c on system parameters. The two methods however give consistent results within the discretization indeterminacy.

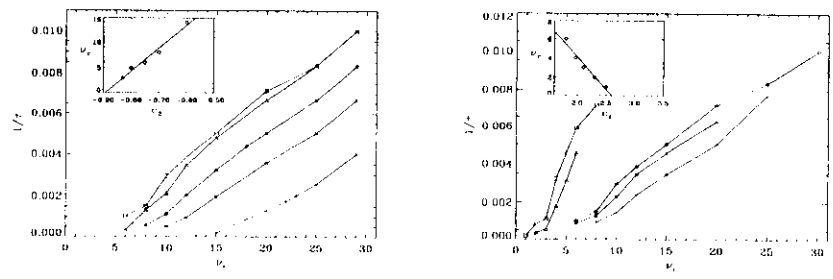

FIG. 5. a) Inverse of the characteristic time for winding number relaxation as a function of the initial winding number. The value of c_1 is fixed ($c_1 = 2.1$) and c_2 varies from near the BFN line ($c_2 \simeq -0.48$) to the L_1 line ($c_2 \approx -0.9$). Different symbols correspond to $c_2 = -0.6$ (+), $c_2 = -0.7$ ($*$), $c_2 = -0.75$ ($\diamond$), $c_2 = -0.8$ ($\triangle$), $c_2 = -0.83$ ($\square$). The inset shows the critical winding number (ν_c) as a function of c_2. b) Idem but the value of c_2 is fixed ($c_2 = -0.83$) and c_1 varies from near the BFN line ($c_1 \simeq 1.33$) to $c_1 = 2.5$. Different symbols correspond to $c_1 = 1.6$ (+), $c_1 = 1.8$ ($*$), $c_1 = 1.96$ ($\diamond$), $c_1 = 2.1$ ($\triangle$), $c_1 = 2.3$ ($\square$), $c_1 = 2.5$ ($\times$). The inset shows the critical winding number (ν_c) as a function of c_1

The insets of Fig. 5a and Fig. 5b indicate a clear decrease in ν_c as the values of c_1 and c_2 approach the L_1 line. In fact we know that ν_c should be zero to the left of L_1, since no wave maintains its winding number constant there. This lead us to a sensible method for determining the position of line L_1 [10], alternative to the one based in the density of defects used in [7]. It consists in extrapolating the behavior of ν_c to $\nu_c = 0$. A simple linear fit has been used. The same method to determine the line L_1 has been independently introduced in [31, 32]. The coefficients of the linear fit are not universal: they depend of the particular path by which the line L_1 is approached. With this method the line L_1 is determined as the line at which the range of conserved winding numbers $[-\nu_c, \nu_c]$ shrinks to zero. The analogy with the Eckhaus instability of regular waves is again remarkable: in the same way as the range of Eckhaus-stable wavenumbers shrinks to zero when approaching the BFN line from below, the allowed ν range shrinks to zero when approaching the L_1 line from the right. The difference is that below the BFN line the values of the wavenumber characterizes plane-wave attractors, whereas above that line, ν characterizes phase-turbulent waves. In this picture, the transition line PT–DT appears as the *BFN line* associated to an Eckhaus-like instability for phase turbulent waves. For the case of Fig. 5a the PT–DT transition is located at $c_1 = 2.1, c_2 = -0.89 \pm 0.02$, and $c_1 = 2.60 \pm 0.02, c_2 = -0.83$ for the case of Fig. 5b. The agreement with the position of the line as determined by [7, 12], where system sizes similar to ours are used, is good. For example for $c_1 = 2.1$ their value for L_1 is $c_2 = -0.92$. The points marked as

+ in Fig. 1 correspond to runs used to determine the position of the transition line L_1 directly as the line at which defects appear in a long run even with $\nu = 0$. All these ways of determining L_1 give consistent results. Below the point P, ν_c goes to zero when the parameters approach the line L_3, not L_1, thus confirming the known behavior that below point P in Fig. 1 the line separating phase turbulence from defect turbulence when coming from the PT side is actually L_3.

The use of a linear fit to locate the line L_1 is questionable and more complex fits have been tested. However, the simplest linear fit has been found of enough quality for most of the the situations checked. Clearly some theoretical guide is needed to suggest alternative functional forms for $\nu_c(c_1, c_2)$. We notice that the analogous quantity below the BFN line, the Eckhaus wavenumber limit, behaves as $q_E \sim \sqrt{\epsilon}$ for small ϵ, being ϵ the difference between either c_1 or c_2 and its value at the BFN line. From the insets in Figs. 5a or 5b, this functional form is clearly less adequate than the linear fit used.

Another interesting point to study is the dependence of the final average winding number $\bar{\nu}_f$ on the initial one ν_i. Fig. 6 shows an example using $c_1 = 2.1$ and $c_2 = -0.8$. The behavior for other values of the parameters is qualitatively similar. $\bar{\nu}_f$ remains equal to the initial value if $\nu_i \leq 5$ during the whole simulation time, so that $\nu_c \approx 5$, a value consistent with the one obtained from the divergence of τ and plotted in the inset of Fig. 5a. For $\nu_i > \nu_c$, the final winding number is always smaller than the initial one. By increasing ν_i a minimum on $\bar{\nu}_f$ is always observed, and then $\bar{\nu}_f$ tends to a constant value. Figure 6 also shows the winding number associated with one of the two Fourier modes of fastest growth obtained from the linear stability analysis of the initial traveling wave. The one shown is the lowest, the other one starts at $\bar{\nu}_f = 28$ and grows further up. Obviously they do not determine the final state in a direct way. This is consistent with the observation mentioned above that the winding number instability does not develop directly from the linear instability of the traveling wave, but from a later nonlinear competition regime.

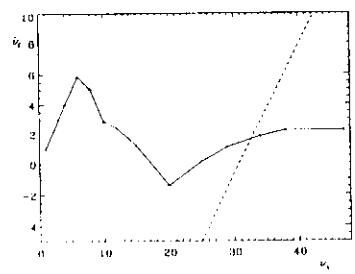

FIG. 6. The final averaged winding number ($\bar{\nu}_f$) as a function of the initial one ν_i. The initial condition is a TW with winding number ν_i for $c_1 = 2.1$ and $c_2 = -0.8$. The dashed line corresponds to the lowest of the two Fourier modes of fastest growth in the linear regime as a function of ν_i.

As stated in the introduction, a powerful way of distinguishing true phase transitions from effective ones is the analysis of finite-size scaling [35]. We have tried to analyze size-effects from the point of view of ν as an order parameter. In the DT state such kind of analysis was performed in [41]. Egolf showed that the distribution of the values taken by the ever-changing winding number is a Gaussian function of width proportional to $\sqrt{L}$. This is exactly the expected behavior for order parameters in disordered phases. In the thermodynamic limit the intensive version of the order parameter, ν/L, would tend to zero so that the disordered DT phase in the thermodynamic limit is characterized by a vanishing intensive order parameter. For the PT states to be true distinct phases, the existence of a nonvanishing ν_c such that ν is constant for $|\nu| < \nu_c$ is not enough. The range of stable winding numbers should also grow at least linearly with L for this range to have any macroscopic significance. The analysis of the growth of ν_c with system size has been performed in points $c_1 = 2.1, c_2 = -0.8$ and $c_1 = 1.96, c_2 = -0.83$ of parameter space. ν_c, determined as explained before, is plotted in Fig. 7 for several system sizes for which the statistical sample of 50 runs was collected for each ν_i.

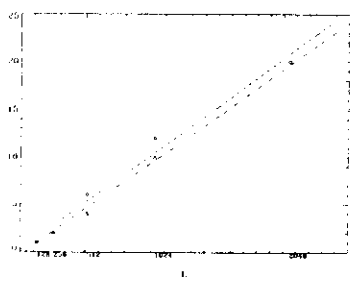

FIG. 7. The critical winding number (ν_c) as a function of the length L of the system is shown. Different symbols correspond to $c_1 = 2.1$ and $c_2 = -0.8$ ($\triangle$), and $c_1 = 1.96$, and $c_2 = -0.83$ ($\diamond$). The straight lines are linear fits to the two sets of data.

There is a clear increasing, close to linear, of ν_c as a function of L, thus indicating that for this range of system sizes the range of allowed winding numbers is an extensive quantity and then each ν is a good order parameter for classifying well defined PT phases. It should be noted however that for the larger system size for which extensive statistics was collected ($L = 2048$) data seem to show a tendency towards saturation. Thus our study should be considered as not conclusive, and larger systems sizes need to be considered.

III. DIFFERENT ASYMPTOTIC STATES IN THE PT REGION

Typical configurations of the PT state of zero winding number consist of pulses in the modulus $|A|$, acting as phase sinks, that travel and collide rather irregularly on top of the $k = 0$ unstable background wave (that is, a uniform oscillation)[7, 12]. The phase of these configurations strongly resembles solutions of the Kuramoto-Shivashinsky (KS) equation. Quantitative agreement has been found between the phase of the $\nu = 0$ PT states of the CGLE and solutions of the KS equation near the BFN line[16].

For states with $\nu \neq 0$ a typical state[12] is the one in which an average speed (in a direction determined by the sign of ν) is added to the irregular motion of the pulses. We have found that in addition to these configurations there are other attractors in the PT region of parameters. We have identified [10] three basic types of asymptotic states for $\nu \neq 0$, which we describe below. Other states can be described in terms of these basic ones. Except when explicitly stated, all the configurations described in this Section have been obtained by running for long times Eq. (1.1) with the initial conditions described before, that is small random Gaussian noise added to an unstable traveling wave. The winding number of these final states is constant and is reached after a transient period in which the winding number might have changed.

Figs. 8, 9 and 11 show examples of the basic states that we call *riding PT* (Fig. 8), *quasiperiodic states* (Fig. 9) and *frozen turbulence* (Fig. 11). For each figure: Panel (a) corresponds to a grey scale space–time plot of $\partial_x \varphi(x,t)$. Panel (b) shows the value of this quantity and the modulus of the field ($\mid A \mid$) as a function of position at the time indicated by an arrow in panels (a) and (d). Panel (c) shows the spatial power spectrum $S(q,t)$ of $A(x,t)$ for the same time. Finally, panel (d) shows the quantity $W = \int \mid \partial_t S(q,t) \mid dq$, which is a global measure of the temporal change in the spatial power spectrum.

Riding PT. This state (see Fig. 8) is the most familiar one [12]: wiggling pulses in the gradient of the phase with a systematic drift in a direction determined by ν. The modulus of the field consists of a disordered spatial sequence of small pulses and shocks, with $A(x,t)$ always far from zero. The spatial power spectrum $S(q)$ has a peak corresponding to the global wave number k (associated in this case with $\nu = -1$, so that $k = 2\pi\nu/L = -0.012$) and a broad background associated with the turbulent motion "riding" on the traveling wave. The time evolution of W shows a decay towards a fluctuating non-zero value, indicating that the power spectrum is continuously changing in time as corresponds to the turbulent state reached by the system.

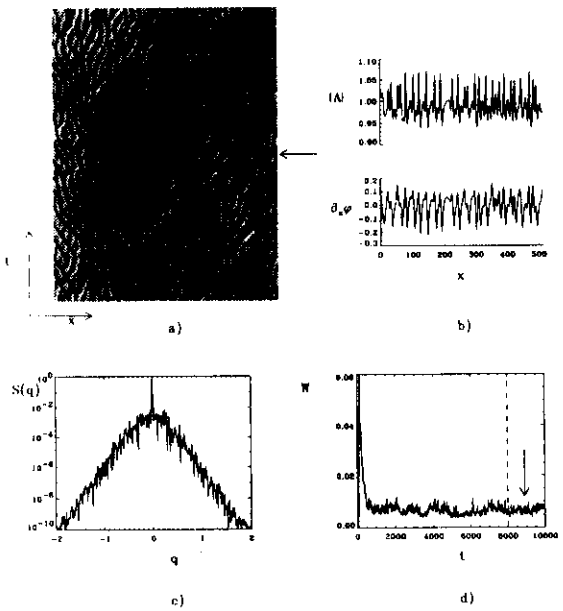

FIG. 8. a) Spatiotemporal evolution of $\partial_x\varphi(x,t)$. The lighter grey correspond to the maximum value of $\partial_x\varphi(x,t)$ and darker to the minimum. Last 2000 time units of a run 10^4 time units long for a *riding* PT state at $c_1 = 2.1$, and $c_2 = -0.83$. The initial condition was a TW with $\nu_i = 20$ that decayed to $\nu_f = -1$ after a short time. b) A snapshot of $\mid A(x,t) \mid$ and $\partial_x\varphi(x,t)$ as a function of x for $t = 8900$ which is indicated by an arrow in a) and d). c) Spatial power spectrum $S(q)$ as a function of wavenumber at the same time $t = 8900$. d)The time evolution of the quantity W defined in the text. The dashed line indicates the initial time for picture a).

Quasiperiodic states. These states (an example is shown in Fig. 9) can be described as the motion of equidistant pulses in the gradient of the phase that travel at constant speed on top of the background wave. The fact that the periodicity of the pulses and that of the supporting wave are not the same justify the name of *quasiperiodic*. We show later that these states correspond to the ones described in Ref. [13]. In Fig. 9a, the modulus $\mid A \mid$ and the gradient of the phase clearly exhibit uniformly traveling pulses. The spatial power spectrum $S(q)$ (Fig. 9c) clearly shows the quasiperiodic nature of this state: a central peak, corresponding to the dominant traveling wave, with equally spaced peaks surrounding it, showing the periodicity of the pulses. The peaks are not sharp because this configuration has been obtained from a random perturbation. The decrease of W in Fig. 9d indicates that the peaks are narrowing. Its asymptotic approach to zero indicates that the amplitudes of the main modes reach a steady value and $S(q)$ becomes time independent.

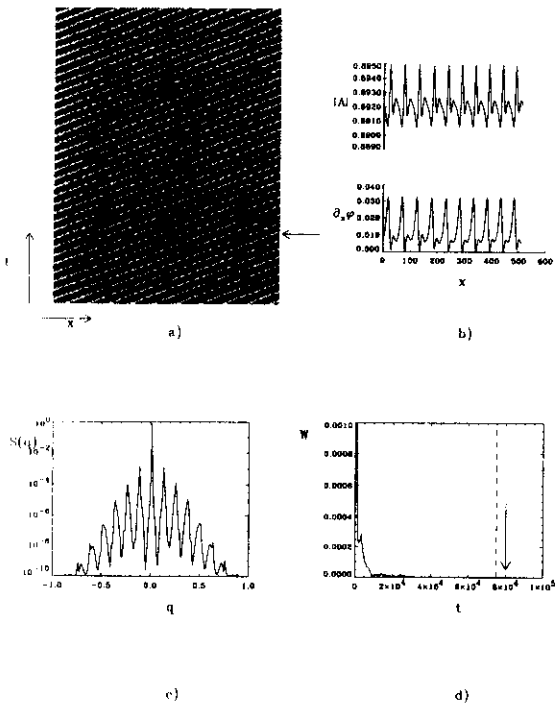

FIG. 9. Same as in Fig. 8 but for last 35000 time units of a run 10^5 time units long for a quasiperiodic state. The initial condition is random noise with an amplitude of 0.05. $c_1 = 2.0$, and $c_2 = -0.8$. b) and c) correspond to a time $t = 8 \times 10^4$.

More perfect quasiperiodic configurations can be obtained from initial configurations that are already quasiperiodic. Figure 10 shows the quantity W for a state generated at $c_1 = 2.1$ and $c_2 = -0.6$ from an initial traveling wave with a sinusoidal perturbation. The initial traveling wave had $\nu_i = 18$ and the winding number of the sinusoidal perturbation was $\nu = 22$. The travelling wave decayed to a state with $\nu_f = 10$ of the quasiperiodic type, cleaner than before. The spatial power spectrum (shown in the inset at the time indicated by an arrow in the main picture) shows the typical characteristics of a quasiperiodic state.

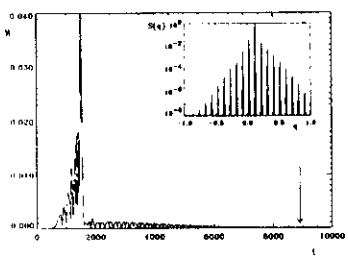

FIG. 10. a)The time evolution of W for a quasiperiodic state. The initial condition is a TW sinusoidally perturbed for $c_1 = 2.1$ and $c_2 = -0.6$. In the inset the spatial power spectrum $S(q)$ as a function of wavenumber at the time $t = 8900$ indicated by an arrow in the main picture.

Frozen turbulence. This state (see Fig. 11) was first described in [10]. It consists of pulses in $\partial_x \varphi$ traveling at constant speed on a traveling wave background, as in the quasiperiodic case, but now the pulses are not equidistant from each other (see Fig. 11b). The power spectrum at a given time is quite different from the one of a quasiperiodic state. It is similar, instead, to the power spectrum obtained in the *riding PT* state: $S(q)$ is a broad spectrum in the sense that the inverse of the width, which gives a measure of the correlation length, is small compared with the system size. Here however W relaxes to zero, so that the power spectrum finally stops changing (thereby the name *frozen*).

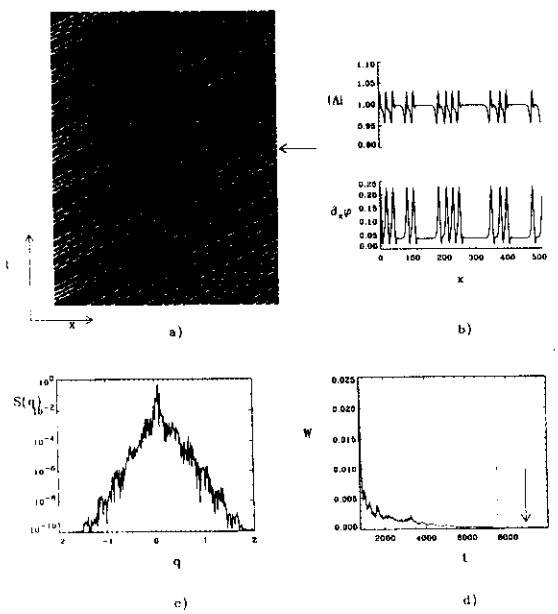

FIG. 11. Same as in Fig. 9 but for last 2500 time units of a run 10^4 time units long for a frozen turbulence state. The initial condition was a TW of $\nu_i = 12$ that decayed to $\nu_f = 6$ after a short time. $c_1 = 1.75$ and $c_2 = -0.8$. The time of b) and c) is $t = 8900$, indicated by an arrow as in previous figures.

This behavior is an indicator of the fact [10], obvious from Fig. 11, that the pattern approaches a state of rigid motion for the modulation in modulus and gradient of the phase of the unstable background plane wave. That is, the field $A(x,t)$ is of the form:

$$A(x,t) = g(x - vt)e^{i(kx - \omega_k t + \alpha(t))} \tag{3.1}$$

where g is a uniformly translating complex modulation factor. It is easy to see that configurations of the form (3.1) have a time-independent spatial power spectrum. Torcini [31] noticed in addition that the function $\alpha(t)$ is linear in t so that the solutions are in fact of the form

$$A(x,t) = f(x - vt)e^{i(kx - \omega t)} \tag{3.2}$$

where again $f(x - vt)$ is a complex valued function and ω can differ from ω_k. f and g differ only in a constant phase. The envelopes $g(x - vt)$ or $f(x - vt)$ turn out to be rather irregular functions in the present *frozen turbulence* case, whereas they are periodic in the quasiperiodic configurations discussed above.

After presenting the basic states, we continue addressing some interesting mixed states that can be described in terms of them. Most of the configurations ending up in the frozen turbulence or in the quasiperiodic states have long time transients of the riding turbulence type. Only at long times a decay to rigid propagation occurs. There are cases in which a different type of decay happens. For example Fig. 12 shows a case in which the system jumps from a very strong riding turbulence regime to another state, also of the riding turbulence type, but much more regular. The quantity W, shown in Fig. 12b, turns out to be a valuable tool in distinguishing the different regimes: a superficial look at Fig. 12a could be easily misunderstood as indicating the approach of the system towards a frozen turbulence state, but the lack of decay towards zero of W identifies the final state as riding turbulence. The arrows indicate the jump to the second state. Fig. 13 shows a state characterized by a recurrence between two different riding turbulence states, showing a kind of temporal intermittency.

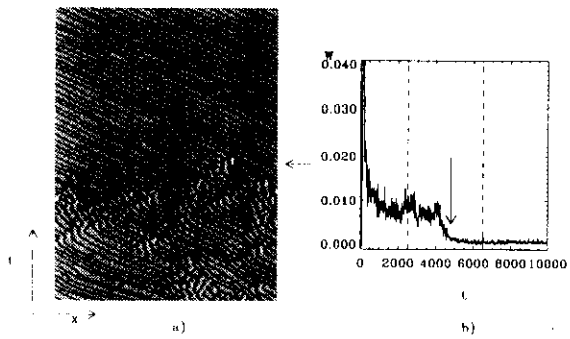

FIG. 12. a) Spatiotemporal evolution of $\partial_x\varphi(x,t)$ for a riding turbulence state that decays onto another one. $c_1 = 2.5$, $c_2 = -0.75$. The initial condition was a TW of $\nu_i = 20$ that decayed to $\nu_f = -2$ in a short time. b) Time evolution of W. The dashed lines indicate the time interval shown in a) (from $t_1 = 2500$ to $t_2 = 6500$ of a run 10^5 time units long). The arrow indicates the transition from one of the riding turbulence regimes to the other one.

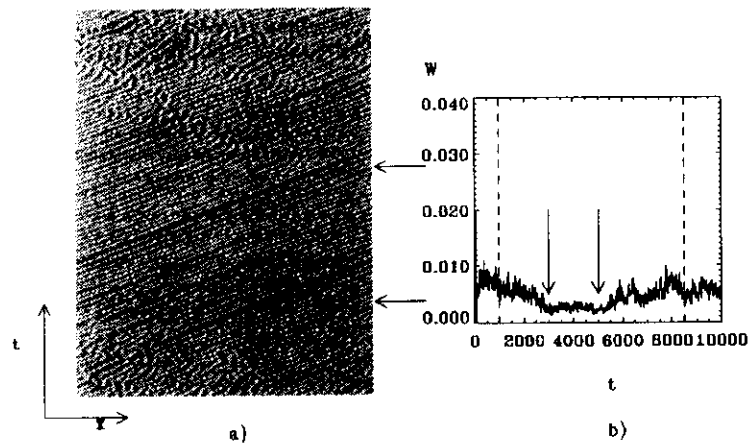

FIG. 13. a) Spatiotemporal evolution of $\partial_x\varphi(x,t)$ showing intermittency between riding turbulence states. $c_1 = 2.1$, $c_2 = -0.83$. The initial condition is a TW of $\nu_i = 1$ that did not change. b)Time evolution of W. The dashed lines indicate the time interval shown in a) (from $t_1 = 1000$ to $t_2 = 8500$ of a run 10^4 time units long). The arrows indicate the end of a riding turbulence regime and the beginning of another one.

Finally Fig. 14 shows a riding turbulence state with zero winding number. This is not however a typical configuration, since usually for $\nu = 0$ there is no preferred direction for the pulses to drift, whereas the figure shows that in fact there is a local drift at some places of the system. It turns out that this state can be understood as composed by two domains of different local winding number: $\nu = 1$ and $\nu = -1$, so that globally $\nu = 0$. The pulses travel either in one direction or in the other depending of the region of the system in which they are. In Fig. 14b a snapshot of the gradient of the phase $\partial_x\varphi(x,t)$ and the phase itself $\varphi(x,t)$ is shown. Lines showing the average trend in the phase are plotted over the phase, clearly identifying the two regions in the system. This coexistence of the different basic states at different places of space, or at different times as in Fig. 13, was already mentioned in [11] where it was argued to give rise to a kind of spatio-temporal intermittent behavior.

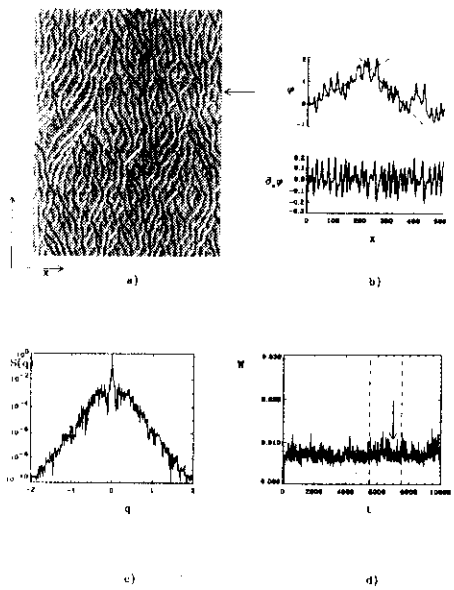

FIG. 14. a) Spatiotemporal evolution of $\partial_x\varphi(x,t)$. The time interval corresponds to 5500 to 7500 time units of a run 10^4 time units long for a *riding PT* state at $c_1 = 2.1$ and $c_2 = -0.83$. The initial condition was a TW with $\nu_i = 0$ that did not change. b) Snapshots of $\varphi(x,t)$ and $\partial_x\varphi(x,t)$ as a function of x at the time $t = 6980$ indicated by an arrow in a) and d). The dashed lines in the graph of $\varphi(x,t)$ indicate average slopes, that is "local" wavenumbers. c) Spatial power spectrum $S(q)$ as a function of wavenumber at the same time $t = 6980$. d)Time evolution of W. Dashed lines indicate the time interval of picture a).

Given the large variety of configurations that are observed, and the very long transients before a jump from one state to another occurs, it would be difficult to conclude from numerical evidence alone that the three kinds of states considered as *basic* above are true asymptotic states. Some analytical insight would be desirable to be sure that these three states are attractors of the dynamics. The next Section is devoted to provide such analytical justification.

IV. ASYMPTOTIC STATES IN TERMS OF THE PHASE DYNAMICS

The question on whether it is possible or not to describe the PT regime of the CGLE from a closed equation for the phase alone has been posed by several authors[15, 16, 30, 42, 43]. A phase equation is obtained by considering a long wavelength perturbation of a plane-wave solution in the CGLE (1.1). It is clear that this phase equation will only describe phase dynamics close to the homogeneous plane-wave (that is the one with $\nu = 0$) if the perturbation is made around the spatially-homogeneous solution. In order to get a description of PT at $\nu \neq 0$ the expansion should be done for a perturbation on a traveling wave solution with wavenumber (k) different from zero,

$$A = (\sqrt{1-k^2} + a(x,t))e^{i(kx+\phi(x,t))}\,, \tag{4.1}$$

Here k is taken as $k = \frac{2\pi}{L}\nu$. If A satisfies periodic boundary conditions the same conditions apply to ϕ because any global phase winding is included in k (the total phase is $\varphi = kx + \phi$). From general symmetry arguments the general phase equation for $k \neq 0$ should read, up to fourth order in gradients:

$$\begin{aligned}\partial_t\phi = \Omega_0 - v_g\partial_x\phi - D_2\partial_x^2\phi + D_{11}(\partial_x\phi)^2 + D_3\partial_x^3\phi + D_{12}(\partial_x\phi)(\partial_x^2\phi) \\ - D_4\partial_x^4\phi + D_{13}(\partial_x\phi)(\partial_x^3\phi) + D_{22}\left(\partial_x^2\phi\right)^2 + D_{112}(\partial_x\phi)^2(\partial_x^2\phi) + \ldots\,.\end{aligned} \tag{4.2}$$

When $v_g = D_3 = D_{12} = D_{13} = D_{22} = D_{112} = 0$, Eq. (4.2) reduces to the Kuramoto–Sivashinsky (KS) equation [44, 45] that is the lowest order nonlinear phase equation for the case $k = 0$. For $k \neq 0$, Eq. (4.2) was systematically derived up to third order in gradients in [36]. An easy way of obtaining the values of all the coefficients in (4.2) was discussed in [46]: First, Ω_0 is related to the frequency of the plane-wave solutions:

$$\Omega_0 = -\omega_k = -c_2 - (c_1 - c_2)k^2 \tag{4.3}$$

Second, the linear terms can be obtained from the eigenvalue $\lambda(k,q)$ corresponding to the phase-like branch in the linear stability analysis of the wave of wavenumber k with respect to perturbations of wavenumber q[13, 14, 36, 26]:

$$\lambda(k,q) = -iv_g q + D_2 q^2 - iD_3 q^3 - D_4 q^4 + \mathcal{O}(q^5) \tag{4.4}$$

with

$$v_g = 2k(c_1 - c_2) \tag{4.5}$$

$$D_2 = -(1 + c_1 c_2) + \frac{2k^2(1 + c_2^2)}{1 - k^2} \tag{4.6}$$

$$D_3 = \frac{2k(1 + c_2^2)\left[-c_1 + (c_1 + 2c_2)k^2\right]}{(1 - k^2)^2} \tag{4.7}$$

$$D_4 = \frac{1}{2(1 - k^2)^3}\left\{c_1^2(1 + c_2^2) - 2k^2(1 + c_2^2)(c_1^2 + 6c_1c_2) + k^4\left[4 + (1 + c_2^2)(c_1^2 + 12c_1c_2) + c_2^2(24 + 20c_2^2)\right]\right\} . \tag{4.8}$$

Third, the nonlinear terms can be obtained from the following consistency relationship: If (4.1) is an exact solution of the CGLE, then $\phi(x,t)$ satisfies the phase equation with coefficients depending on k. In addition if $(\sqrt{1 - k_1^2} + a_1(x,t))e^{i(k_1 x + \phi_1(x,t))}$ is another exact solution of the CGLE, then $\phi_1(x,t)$ satisfies a similar phase equation but with coefficients depending on k_1 instead of k. But this solution can be written as $(\sqrt{1 - k_1^2} + a_1(x,t))e^{i(kx + (k_1 - k)x + \phi_1(x,t))}$ so that $(k_1 - k)x + \phi_1(x,t)$ is also solution of the phase equation with coefficients depending on k (with different boundary conditions). By combining the two equations satisfied by ϕ_1 and expanding the coefficients depending on k_1 as a power series around k (assuming $k_1 - k$ small) the following relationships between linear and nonlinear terms are obtained:

$$D_{11} = -\frac{1}{2}\frac{\partial v_g}{\partial k} , \quad D_{12} = -\frac{\partial D_2}{\partial k} , \quad D_{13} = \frac{\partial D_3}{\partial k} , \quad D_{112} = -\frac{1}{2}\frac{\partial^2 D_2}{\partial k^2} \tag{4.9}$$

So that

$$D_{11} = c_2 - c_1 \tag{4.10}$$

$$D_{12} = -\frac{4k(1 + c_2^2)}{(1 - k^2)^2} \tag{4.11}$$

$$D_{13} = \frac{2(1 + c_2^2)}{(1 - k^2)^3}\left[-c_1 + 6c_2k^2 + (2c_2 + c_1)k^4\right] \tag{4.12}$$

$$D_{112} = -\frac{2(1 + c_2^2)(3k^2 + 1)}{(1 - k^2)^3} \tag{4.13}$$

The coefficient D_{22} is only obtained following the method to higher order in $(k_1 - k)$. The coefficients up to third order in gradients can be found also in [36] and approximate expressions for them are given in [13].

The traveling wave of wavenumber k becomes unstable when the coefficient D_2 becomes positive. One expects that the first terms in the gradient expansion (4.2) give a good description of the phase dynamics in the weakly nonlinear regime, that is D_2 positive but small (note that for a given $k \neq 0$ this includes part of the region below the BFN line in Fig 1). The arguments presented in [46] imply that the relative importance of the different terms in a multiple scale expansion in which D_2 is the small parameter can be established by considering $\phi \sim \partial_x \sim D_2^{1/2}$. Then the dominant terms close to the instability of wave k are the ones containing Ω_0 and v_g. After them, the terms with coefficients D_3 and D_{11} are the most relevant. Up to this order Eq. (4.2) is a Korteweg–de Vries equation (KdV). The terms with D_2, D_4 and D_{12} appear at the next order. The importance of the terms in D_2 and D_4 for a qualitatively correct description of phase dynamics is obvious since they control the stability properties of the wave of wavenumber k. The

importance of the term with coefficient D_{12} was stressed in [13, 47]: if it is large enough it can change the character of the bifurcation from supercritical to subcritical.

The detailed comparison of the reduced dynamics (4.2) with the complete CGLE phase dynamics is beyond the scope of the present paper. The aim of this Section is to use Eq.(4.2) just to get some understanding of the asymptotic states presented in Section III. To this end we will use the detailed results available from the work of Chang et al. [48]. These results are obtained for the so-called Kawahara equation [49, 50, 47, 48, 51] which is Eq.(4.2) with $D_{12} = D_{13} = D_{22} = D_{112} = 0$. The term D_{12}, which according to Kuramoto estimations [46] is of the same order for small D_2 as the terms in D_2 and D_4, will thus be neglected. It would be certainly necessary to consider the modifications introduced by the term D_{12} into the results of [48]. This will be briefly discussed at the end of this section. At this point it is interesting to note that, to our knowledge, the only quantitative comparison of the phase dynamics with $k \neq 0$ obtained from a phase equation and from CGLE is [31, 32]. But the phase equation used in these references is the one presented in [42], in which the nonlinear terms considered are only those with coefficients D_{11} and D_{13}. In addition D_{11}, D_{13}, and the coefficients of the linear terms are considered only up to first order in k. Despite these limitations, in particular the absence of the D_{12} term, the phase equation is found to reproduce well the phase dynamics of the CGLE, an agreement that degrades when the term in D_{13} is suppressed [52]. Clearly further work is needed to establish firmly the relevance of the different terms in (4.2)[53]. Our study will be restricted to the situation of [48] (that is $D_{12} = D_{22} = D_{13} = D_{112} = 0$) since no study of comparable detail for a more complete equation is available in the literature.

The situation of interest here is the one in which the traveling waves are unstable against a finite band of wavenumbers, so that $D_2,\ D_4 > 0$. Making the following changes of variables in (4.2) with $D_{12} = D_{22} = D_{13} = D_{112} = 0$:

$$\begin{aligned} \chi &= \sqrt{\frac{D_2}{D_4}}\,(x - v_g t)\ , \\ \tau &= \frac{D_2^2}{D_4} t\ , \\ u(\chi,\tau) &= -\frac{D_{11} D_4^{1/2}}{2 D_2^{3/2}} \partial_x \phi(x,t)\ . \end{aligned} \tag{4.14}$$

the Kawahara equation[49, 50, 47, 48, 51] is obtained

$$\partial_\tau u = -\partial_\chi^2 u - 4u\partial_\chi u - \delta\partial_\chi^3 u - \partial_\chi^4 u\ , \tag{4.15}$$

with

$$\delta = -\frac{D_3}{\sqrt{D_2 D_4}} \tag{4.16}$$

Since ϕ is periodic in x, $u(\chi,t)$ is periodic in χ. In addition $\int_0^L u(\chi,\tau)d\chi = 0$. To have some intuition on the meaning of the parameter δ, its expansion at small k reads

$$\delta \approx 2\sqrt{2}\,k\ \mathrm{sign}\,(c_1)\sqrt{\frac{1+c_2^2}{|\,1+c_1c_2\,|}} + \mathcal{O}(k^3)\ . \tag{4.17}$$

It should be noted that δ does not diverge at the BFN line, as the expansion (4.17) seems to suggest, but below it. From Eq. (4.16) it is clear that δ diverges where D_2 vanishes indicating that the corresponding traveling wave of wavenumber k has become Eckhaus unstable.

The Kawahara equation (4.15) has been considered in the context of surface waves on fluid films falling down an inclined or vertical plane [54], and also as a simple generalization of the KS or the KdV equations [49, 50]. It has also been considered in the context of growth shapes [55]. It reduces to KS for $\delta = 0$ (or equivalently for $k = 0$) when written in the original variable φ.

Equation (4.15) has periodic, soliton-like, spatially-irregular, and spatio-temporally chaotic solutions. [49, 50, 51]. In fact, all of these solutions have been analytically shown to exist [48]. All of them except the isolated soliton-like solution [56] are stable in some parameter regimes [48]. These kinds of solutions should manifest themselves (provided the approximate phase description holds) in the time evolution of the phase gradient $\partial_x\varphi$ $(= k + \partial\phi)$ of the solutions of the CGLE (1.1) in the PT regime. The analytical results in [48] thus provide a firm basis for true existence of the numerically observed states described in Section III.

The detailed bifurcation analysis in [48] also gives detailed predictions for the wound states of the CGLE, within the range of validity of the phase description. We will reproduce here some of the results in [48] and reinterpret them

in terms of the gradient of the phase of CGLE solutions. Our interest is centered in the rigidly moving train of pulses (frozen turbulence and quasiperiodic states) observed in several of the numerical simulations reported in Section III. They are of the form (3.2), and because of (4.14) we have

$$u(\chi,\tau) = H(\xi)\ , \tag{4.18}$$

with $\xi = \chi - v\tau$, being v the velocity of the train of pulses we want to describe in units of χ and τ. The partial differential equation (4.15) is reduced to an ordinary differential equation (ODE) for $H(\xi)$:

$$H^{iv} + \delta H''' + H'' + 4HH' - vH' = 0\ . \tag{4.19}$$

The primes denote differentiation with respect to ξ. After an integration:

$$H''' + \delta H'' + H' - vH + 2H^2 = Q\ . \tag{4.20}$$

Q is fixed in a nontrivial way by the condition $\int H d\xi = 0$ which follows from our periodic boundary conditions. This third order ODE can be rewritten as a three-dimensional dynamical system:

$$\begin{aligned} u_1' &= u_2 \\ u_2' &= u_3 \\ u_3' &= cu_1 - u_2 - \delta u_3 - 2(u_1)^2 \end{aligned} \tag{4.21}$$

with

$$\begin{aligned} u_1(\xi) &= H(\chi) - \frac{v}{4} + \sqrt{\frac{c^2}{16} + \frac{Q}{2}}\ , \\ c &= \sqrt{8Q + v^2}\ . \end{aligned} \tag{4.22}$$

Different qualitative behaviors in phase space of the solutions of the dynamical system (4.21) are related to the shape of the solutions of (4.19) [57]. This is illustrated in Fig. 15.

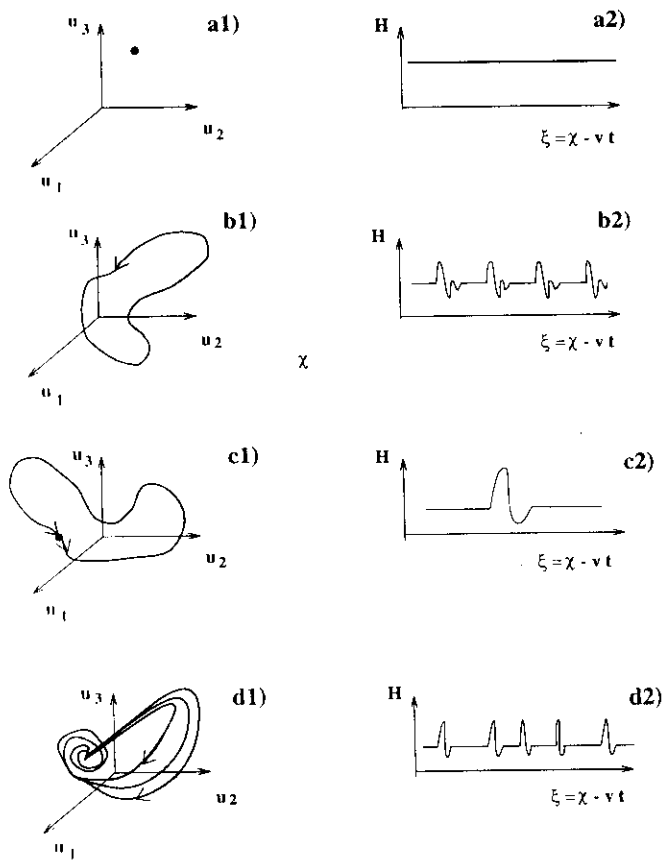

FIG. 15. Schematic relationship between trajectories of the dynamical system (4.21) in phase space (left column) and solutions $u(\chi,\tau) = H(\xi = \chi - v\tau)$ of equation (4.15) (right column). a1) Fixed point of (4.21), a2) uniform solution of (4.15) (traveling wave in the CGLE (1.1)). b1) Periodic solution (limit cycle) of (4.21), b2) periodic train solution of (4.15) (quasiperiodic solution of the CGLE (1.1)). c1) Homoclinic trajectory of (4.21), c2) single pulse of (4.15). d1) Chaotic trajectory of (4.21), d2) spatially irregular solution of (4.15) (frozen turbulence in the CGLE).

We stress that all the solutions of (4.19) represent uniformly translating solutions of (4.15). No information is given on more complicated solutions of (4.15). The left column of Fig. 15 shows the possible trajectories of the dynamical system (4.21) while the right column shows the corresponding solution of (4.20), or equivalently $u(\chi,\tau) = H(\xi = \chi - c\tau)$ in equation (4.15). For a fixed point in (4.21) (fig. 15a1) we get a homogeneous solution in (4.15) (fig. 15a2) and (via (4.14)) a traveling wave solution in the CGLE (1.1). For a periodic trajectory in (4.21) (fig. 15b1) we get a train of periodic pulses in the solution of (4.15) (fig. 15b2) and a quasiperiodic solution in CGLE (1.1). An homoclinic trajectory in (4.21) (fig. 15c1) corresponds to a single pulse solution in (4.15) (fig. 15c2). Finally for a chaotic trajectory in (4.21) (fig. 15d1) we have an irregular solution $H(\xi)$ that corresponds to a rigidly traveling spatially irregular solution of (4.15) (fig. 15d2). The chaotic solutions of (4.21) are of the Shil'nikov type [48]. This means that the disordered configurations $H(\xi)$ (and thus u and $\partial_x\varphi$) consist on nearly identical pulses irregularly spaced. This corresponds to the state named *frozen turbulence* for solutions of the CGLE.

The detailed analysis of [48] is done on the one hand by following the sequence of bifurcations of the state in which H is a constant and of the state in which H is close to the KdV soliton (with adequate rescaling Eq. (4.15) reduces to the KdV in the limit $\delta \to \infty$). On the other hand the powerful global theorems of Shil'nikov and their generalizations [58, 59, 60, 61] are used to establish the structure of the solutions of (4.21). The results of [48] relevant to our purposes can be summarized as follows (they can be read-off from figure 3 of Ref. [48]):

1. Periodic solutions of (4.21) exist for all values of δ provided $\mid c \mid > \mid \delta \mid$. They are organized in a variety of branches. Solutions in the same branch differ by their periodicity, and each branch ends in a different kind of solitary-wave solution (infinite spatial period). The shape of the different solitary wave solutions characterizes the different branches.

2. For $\mid \delta \mid \gtrsim 1.1$ only one of the branches of periodic solutions (the *main branch*) remains.

3. Chaotic solutions to (4.21) exist only for $\mid \delta \mid \lesssim 0.84$.

In addition Chang et al. [48] obtained results also for the full equation (4.15), without the restriction to rigidly traveling waves. Their numerical and analytical results can be summarized as

4. Periodic solutions in the main branch with its wavenumber within a given range are linearly stable for all δ. A more precise determination of the range of stable wavenumbers for large δ was performed in [47].

5. In addition to the periodic solutions there are also spatio-temporal chaotic attractors for all δ.

6. If $\mid \delta \mid > 1.1$ only two of these strange attractors remain. For $\mid \delta \mid > 3$ their basin of attraction seems to be much smaller than the one of the periodic solutions.

Expression (4.16) with (4.5)-(4.13) gives the relation between δ and the parameters of the CGLE. $\mid \delta \mid = \infty$ corresponds in Fig. 1 to the line at which the wave of wavenumber k becomes Eckhaus unstable. It is approximately parallel and below the BFN line. The other lines of constant δ, for fixed k, are also approximately parallel to the BFN line, and decreasing $\mid \delta \mid$ corresponds to entering into the PT region and going deep into it. All these lines concentrate onto the BFN line as k approaches zero: for $k = 0$, $\delta = 0$ except on the BFN line $1 + c_1 c_2 = 0$ where δ is undefined. We now rephrase the conclusions above in terms of the three basic asymptotic states of the CGLE in the PT regime. They will be valid as long as the phase description (4.15) remains accurate.

1. There are PT solutions of the quasiperiodic type for all values of the parameters (as long as the phase description remains valid). Bounds on their velocity can be in principle obtained, but this is nontrivial since Q is only known in an implicit way.

2. Increasing $\mid \delta \mid$ by approaching the Eckhaus instability for a given k ($D_2 = 0$), or by increasing the winding number reduces the variety of quasiperiodic solutions.

3. Frozen turbulence solutions exist only for $\mid \delta \mid \lesssim 0.84$, that is far enough from the line $D_2 = 0$ or for small enough winding number.

4. There are linearly stable solutions in the main quasiperiodic branch for all values of the parameters.

5. There are also riding turbulence attractors for all values of parameters.

6. For $|\delta| > 3$, that is at high winding number or close enough to the line $D_2 = 0$ the quasiperiodic solutions have a basin of attraction larger than the riding turbulence ones.

A general feature of these conclusions is that the important quantity is D_2, that is the distance in parameter space from the line at which the k-wave became Eckhaus unstable. This line is *below* the BFN line for $k \neq 0$. Thus not only traveling waves, but also quasiperiodic, frozen turbulence, and riding turbulence attractors should exist below the BFN line for $k \neq 0$. In practice it is relatively easy to find quasiperiodic states below but close the BFN line, but we have been unable to find the other two states so far. The difficulty in finding riding turbulence states can be a consequence of the small range of winding numbers for which they are stable ($|\nu| = L|k|/(2\pi) < \nu_c$) so that the observability condition $|\delta| < 3$ immediately brings us above the BFN line. Another possibility is that the instability of the $\nu = 0$ plane-wave attractor at the BFN line has consequences of a global character beyond the validity of the phase description.

The above predictions imply that the more promising zone for obtaining quasiperiodic solutions starting from random perturbations on a traveling wave of given winding number is for parameter values close and above $D_2 = 0$, or for high winding number ($|\delta| > 3$). In any case no frozen turbulence should be observed in that zone.

Some qualitative aspects of the conclusions above have been shown to be correct. In particular Torcini and collaborators [31, 32] have shown that the average maximal Lyapunov exponent, quantifying the proportion of initial conditions that fall into the spatio-temporal chaotic strange attractors, is a decreasing function of ν.

Our numerical solutions also agree with the prediction that quasiperiodic solutions show up more easily for small D_2. However, their basin of attraction appears to be much smaller than the implied by the conclusions of the phase description since it is reached with very low probability from our initial conditions. This is specially true above the BFN line. The reason for this is probably the effect of the neglected term D_{12}, which is known to reduce the range of stable periodic solutions [47] and even to eliminate it by making the bifurcation subcritical [13]. Above the BFN line the attractor that we observe more frequently at high winding number from our initial conditions is the frozen turbulent state.

A more detailed checking of the predictions above would be desirable. This is however beyond the scope of the present paper since a detailed theoretical analysis of the global properties of the phase space for the equation containing the term D_{12} would be probably needed beforehand. A promising alternative can be the study of the exact equation for $f(x - vt)$ in (3.2) obtained in [32].

V. FINAL REMARKS

One-dimensional wound-up phase turbulence has been shown to be much richer than the case $\nu = 0$. The main results reported here, that is the existence of winding number instability for phase-turbulent waves, the identification of the transition PT-DT with the vanishing of the range of stable winding numbers, and the coexistence of different kinds of PT attractors should in principle be observed in systems for which PT and DT regimes above a Hopf bifurcation are known to exist [24]. To our knowledge, there are so far no observations of the ordered PT states described above. There are however experimental observations of what seems to be an Eckhaus-like instability for non-regular waves in the printer instability system [62]. This suggests that the concept of a turbulent Eckhaus instability can be of interest beyond the range of situations described by the CGLE. A point about which our study is inconclusive is the question on the existence of PT in the thermodynamic limit. The identification of ν as an order parameter identifies the continuation of Fig. 7 towards larger system sizes as a way of resolving the question. It should be noted however that although a linear scaling of the order parameter with system size is usual in common phase transitions, broken ergodicity phase transitions, as the present one, generate usually a number of ordered phases growing exponentially with L, not just linearly [34, 63]. We notice that the results of Section III show that the states of a given ν are not *pure phases*, but different attractors are possible for given ν. An order parameter more refined than ν should be able to distinguish between the different attractors and, since some of them are disordered, the result of an exponentially large number of phases at large L would be probably recovered. The results presented in Section IV give a justification for the existence of the several wound states observed, an especific predictions have been formulated on the basis of previous analitical and numerical results. Further work is needed however to clarify the importance of the different terms in (4.2) and the validity of a phase description.

VI. ACKNOWLEDGMENTS

Helpful discussions with L. Kramer, W. van Saarloos, H. Chaté, A. Torcini, P. Colet and D. Walgraef are acknowledged. Financial support from DGYCIT (Spain) Projects PB94-1167 and PB94-1172 is acknowledged. R.M. also acknowledges partial support from the Programa de Desarrollo de las Ciencias Básicas (PEDECIBA, Uruguay), and the Consejo Nacional de Investigaciones Científicas Y Técnicas (CONICYT, Uruguay).

APPENDIX A: NUMERICAL INTEGRATION SCHEME

The time evolution of the complex field $A(x,t)$ subjected to periodic boundary conditions is obtained numerically from the integration of the CGLE in Fourier space. The method is pseudospectral and second-order accurate in time. Each Fourier mode A_q evolves according to:

$$\partial_t A_q(t) = -\alpha_q A_q(t) + \Phi_q(t) \,, \tag{A1}$$

where α_q is $(1+ic_1)q^2 - 1$, and Φ_q is the amplitude of mode q of the non-linear term in the CGLE. At any time, the amplitudes Φ_q are calculated by taking the inverse Fourier transform $A(x,t)$ of A_q, computing the non-linear term in real space and then calculating the direct Fourier transform of this term. A standard FFT subroutine is used for this purpose [64].

Eq. (A1) is integrated numerically in time by using a method similar to the so called two-step method [65]. For convenience in the notation, the time step is defined here so as the time is increased by $2\delta t$ at each iteration.

When a large number of modes q is used, the linear time scales α_q can take a wide range of values. A way of circumventing this stiffness problem is to treat exactly the linear terms by using the formal solution:

$$A_q(t) = e^{-\alpha_q t}\left(A_q(t_0)e^{\alpha_q t_0} + \int_{t_0}^{t} \Phi_q(s)e^{\alpha_q s}ds\right) \,. \tag{A2}$$

From here the following relationship is found:

$$\frac{A_q(t+\delta t)}{e^{-\alpha_q \delta t}} - \frac{A_q(t-\delta t)}{e^{\alpha_q \delta t}} = e^{-\alpha_q t}\int_{t-\delta t}^{t+\delta t} \Phi_q(s)e^{\alpha_q s}ds \,. \tag{A3}$$

The Taylor expansion of of $\Phi_q(s)$ around $s=t$ for small δt gives an expression for the r.h.s. of Eq. (A3):

$$\Phi_q(t)\frac{e^{\alpha_q \delta t} - e^{-\alpha_q \delta t}}{\alpha_q} + \mathcal{O}(\delta t^3) \,. \tag{A4}$$

Substituting this result in (A3) we get:

$$A_q(n+1) = e^{-2\alpha_q \delta t}A_q(n-1) + \frac{1-e^{-2\alpha_q \delta t}}{\alpha_q}\Phi_q(n) + \mathcal{O}(\delta t^3) \,. \tag{A5}$$

where expressions of the form $f(n)$ are shortcuts for $f(t=n\delta t)$. Expression (A5) is the so called "slaved leap frog" of Frisch et al.[66]. To use this scheme the values of the field at the first two time steps are required. Nevertheless, this scheme alone is unstable for the CGLE. This is not explicitly stated in the literature and probably a corrective algorithm is also applied. Obtaining such correction is straightforward: Following steps similar to the ones before one derives the auxiliary expression

$$A_q(n) = e^{-\alpha_q \delta t}A_q(n-1) + \frac{1-e^{-\alpha_q \delta t}}{\alpha_q}\Phi_q(n-1) + \mathcal{O}(\delta t^2) \,, \tag{A6}$$

The numerical method we use, which we will refer to as the two-step method, provides the time evolution of the field from a given initial condition by using Eqs. (A5) and (A6) as follows:

1. $\Phi_q(n-1)$ is calculated from $A_q(n-1)$ by going to real space.

2. Eq. (A6) is used to obtain an approximation to $A_q(n)$.

3. The non-linear term $\Phi_q(n)$ is now calculated from this $A_q(n)$ by going to real space.

4. The field at step $n+1$ is calculated from (A5) by using $A_q(n-1)$ and $\Phi_q(n)$.

At each iteration, we get $A_q(n+1)$ from $A_q(n-1)$, and the time advances by $2\delta t$. Note that the total error is $\mathcal{O}(\delta t^3)$, despite the error in the intermediate value obtained with Eq. (A6) is $\mathcal{O}(\delta t^2)$. The method can be easily made exact for plane waves (1.2) of wavenumber k (and then more precise for solutions close to this traveling wave) simply by replacing the nonlinear term Φ_q in (A1) by $\Phi_q + (1+ic_2)(1-k^2)A_q$, and subtracting the corresponding term from ω_q. We have not implemented this improvement because we were mostly interested in solutions changing its winding number, so that they are not close to the same traveling wave all the time.

The number of Fourier modes depends on the space discretization. We have used $dx = 1$ and usually $N = 512$. The time step was usually $dt = 2\delta t = 0.01$. The accuracy of the numerical method has been estimated by integrating plane-wave solutions. The amplitude and frequency of the field obtained numerically will differ slightly from the exact amplitude and frequency, not only due to round-off errors, but also due to the fact that the method is approximate. The method has been tested by using a stationary unstable traveling wave of wave number k as initial condition. The numerical errors will eventually move the solution away from the plane-wave unstable state. To be precise, in a typical run with $c_1 = -1.0$ and $c_2 = 2.4$, with $dt = 0.01$ and $k = 0.123$, the amplitude was kept constant to the fifth decimal digit during ~ 8000 iterations. In comparison, when a Gaussian noise with an amplitude as small as 10^{-7} is added to the traveling wave, the modulus is maintained equal to its steady value (up to the fifth decimal) during 1500 iterations. The frequency ω_q determined numerically by using $dt = 0.01$ fits the exact value up to the fourth decimal digit.

The integration method introduced here has also been applied succesfully to the case of two coupled equations, or equivalently a Vectorial CGLE [18, 67].

[1] M. Cross and P. Hohenberg, Rev. Mod. Phys. **65**, 851 (1993), and references therein.
[2] M. Cross and P. Hohenberg, Science **263**, 1569 (1994).
[3] M. Dennin, G. Ahlers, and D. S. Cannell, Science **272**, 388 (1996).
[4] D. Egolf and H. Greenside, Nature **369**, 129 (1994). chao-dyn/9307010.
[5] T. Bohr, E. Bosch, and W. van der Water, Nature **372**, 48 (1994).
[6] T. Bohr, M. H. Jensen, G. Paladin, and A. Vulpiani, *Dynamical systems approach to Turbulence* (Cambridge, Cambridge, 1996), to appear.
[7] B. Shraiman *et al.*, Physica D **57**, 241 (1992).
[8] P. C. Hohenberg and B. I. Shraiman, Physica D **37**, 109 (1989).
[9] M. Caponeri and S. Ciliberto, Physica D **58**, 365 (1992).
[10] R. Montagne, E. Hernández-García, and M. San Miguel, Phys. Rev. Lett. **77**, 267 (1996). chao-dyn/9604004.
[11] H. Chaté, Nonlinearity **7**, 185 (1994).
[12] H. Chaté, in *Spatiotemporal Patterns in Nonequilibrium Complex Systems*, Vol. XXI of *Santa Fe Institute in the Sciences of Complexity*, edited by P. Cladis and P. Palffy-Muhoray (Addison-Wesley, New York, 1995), pp. 5–49. patt-sol/9310001.
[13] B. Janiaud *et al.*, Physica D **55**, 269 (1992).
[14] W. van Saarloos and P. Hohenberg, Physica D **56**, 303 (1992), and (Errata) Physica D **69**, 209 (1993).
[15] H. Chaté and P. Manneville, in *A Tentative Dictionary of Turbulence*, edited by P. Tabeling and O. Cardoso (Plenum, New York, 1995).
[16] D. Egolf and H. Greenside, Phys. Rev. Lett. **74**, 1751 (1995). chao-dyn/9407007.
[17] R. Montagne, E. Hernández-García, and M. San Miguel, Physica D **96**, 47 (1996). cond-mat/9508115.
[18] A. Amengual, D. Walgraef, M. San Miguel, and E. Hernández-García, Phys. Rev. Lett. **76**, 1956 (1996). patt-sol/9602001.
[19] P. Kolodner, S. Slimani, N. Aubry, and R. Lima, Physica D **85**, 165 (1995).
[20] P. Coullet, L. Gil, and F. Roca, Opt. Comm. **73**, 403 (1989).
[21] M. San Miguel, Phys. Rev. Lett. **75**, 425 (1995).
[22] Y. Kuramoto and T. Tsuzuki, Progr. Theor. Phys. **52**, 356 (1974).
[23] Y. Kuramoto and S. Koga, Progr. Theor. Phys. Suppl. **66**, 1081 (1981).
[24] T. Leweke and M. Provansal, Phys. Rev. Lett. **72**, 3174 (1994).
[25] R. Schielen, A. Doelman, and H. de Swart, J. Fluid Mech. **252**, 325 (1993).
[26] R. Montagne and P. Colet, (1996), to be published.
[27] T.B.Benjamin and J. Feir, J. Fluid Mech. **27**, 417 (1967).
[28] A. Newell, Lect. Appl. Math. **15**, 157 (1974).
[29] H. Chaté and P. Manneville, Physica A **224**, 348 (1996).
[30] P. Manneville and H. Chaté, Physica D **96**, 30 (1996).

[31] A. Torcini, Phys. Rev. Lett. **77**, 1047 (1996). chao-dyn/9608006.
[32] A. Torcini, H. Frauenkron, and P. Grassberger, Phys. Rev. E (1996), to appear. chao-dyn/9608003.
[33] H. Sakaguchi, Prog. Theor. Phys. **84**, 792 (1990).
[34] R. Palmer, in *Lectures in the Sciences of Complexity*, Vol. I of *Santa Fe Institute in the Sciences of Complexity*, edited by D. Stein (Addison-Wesley, New York, 1989).
[35] M. N. Barber, in *Phase Transitions and Critical Phenomena*, edited by C. Domb and J. L. Lebowitz (Academic, London, 1983), Vol. 8, p. 146.
[36] J. Lega, Ph.D. thesis, Univ. Nice, 1989.
[37] E. Hernández-García, J. Viñals, R. Toral, and M. San Miguel, Phys. Rev. Lett. **70**, 3576 (1993). cond-mat/9302028.
[38] E. Hernández-García, M. San Miguel, R. Toral, and J. Viñals, Physica D **61**, 159 (1992).
[39] J. Viñals, E. Hernández-García, R. Toral, and M. San Miguel, Phys. Rev. A **44**, 1123 (1991).
[40] F. T. Arecchi, in *Noise and chaos in nonlinear dynamical systems*, edited by F. Moss, L. Lugiato, and W. Schleich (Cambridge University, New York, 1990), p. 261.
[41] D. Egolf, Ph.D. thesis, Duke University, 1994.
[42] H. Sakaguchi, Prog. Theor. Phys. **83**, 169 (1990).
[43] G. Grinstein, C. Jayaprakash, and R. Pandit, Physica D **90**, 96 (1996).
[44] Y. Kuramoto, Progr. Theor. Phys. Suppl. **64**, 346 (1978).
[45] G. Sivashinsky, Acta Astronautica **4**, 1177 (1977).
[46] Y. Kuramoto, Progr. Theor. Phys. **71**, 1182 (1984).
[47] D. E. Bar and A. A. Nepomnyashchy, Physica D **86**, 586 (1995).
[48] H.-C. Chang, E. Demekhin, and D. Kopelevich, Physica D **63**, 299 (1993).
[49] T. Kawahara, Phys. Rev. Lett. **51**, 381 (1983).
[50] T. Kawahara and S. Toh, Phys. Fluids **28**, 1636 (1985).
[51] T. Kawahara and S. Toh, Phys. Fluids **31**, 2103 (1988).
[52] A. Torcini, private communication.
[53] A related question that also needs further study is the appearance of singularities at finite time in the solutions of (4.2) [15, 13].
[54] H.-C. Chang, Annu. Rev. Fluid Mech. **26**, 103 (1994).
[55] C. V. Conrado and T. Bohr, Phys. Rev. Lett. **72**, 3522 (1994).
[56] I. H.-C. Chang, E. Demekhin, and D. Kopelevich, Phys. Rev. Lett. **75**, 1747 (1995), the instability of the isolated pulse has been shown to be not absolute but just of the convective type.
[57] A. Pumir, P. Manneville, and Y. Pomeau, J. Fluid Mech. **135**, 27 (1983).
[58] S. Wiggins, *Introduction to applied nonlinear dynamical systems and chaos* (Springer, New York, 1990).
[59] A. H. Nayfeh and B. Balachandran, *Applied nonlinear dynamics* (Wiley, New York, 1995).
[60] Y. A. Kuznetsov, *Elements of Applied Bifurcation Theory* (Springer, New York, 1995).
[61] Simply stated Shil'nikov theory establishes that in a three dimensional dynamical system with a fixed point being a saddle-focus (i.e. unstable in one direction and oscillatory stable in the other) and provided there exists, for a value of the parameters, a trajectory homoclinic to the fixed point, the eigenvalues obtained through a linearization around the fixed point determine the global behaviour for this value of the parameters and a neighbourhood of it. If these eigenvalues are $\lambda_{1,2} = -\rho \pm i\omega$ and $\lambda_3 = \lambda$ (ρ,$\lambda > 0$), then if $\rho > \lambda$ there is a countable infinity of chaotic trajectories near the homoclinic one. Proximity to the homoclinic trajectory implies that the shape of the chaotic trajectory is, as commented in the text, a sequence of irregularly spaced pulses. On the contrary, if $\rho < \lambda$ there are no chaotic trajectories. For a more precise statement of the theorems see [58, 59, 60].
[62] L. Pan and J. de Bruyn, Phys. Rev. E **49**, 2119 (1994).
[63] M. Mezard, G. Parisi, and M. A. Virasoro, *Spin glass theory and beyond* (World Scientific, Singapore, 1987).
[64] W. H. Press, *Numerical Recipes* (Cambridge University, Cambridge, 1989).
[65] D. Potter, *Computational Physics* (John Wiley & sons, New York, 1973).
[66] U. Frisch, Z. S. She, and O. Thual, J. Fluid Mech. **168**, 221 (1986).
[67] A. Amengual, E. Hernández-García, R. Montagne, and M. San Miguel, (1996), to be published. chao-dyn/9612011.

Phase Instabilities in the Laser Vector Complex Ginzburg-Landau Equation

Maxi San Miguel*

Department of Mathematics–Arizona Center for Mathematical Sciences, University of Arizona, Tucson, Arizona 85721
(Received 16 August 1994)

The interplay between the polarization state of light and transverse effects in lasers is analyzed through an amplitude equation description of an atomic transition between spin sublevels. Linearly polarized traveling waves are found, whose stability is restricted by a phase instability associated with the direction of polarization. The instability persists for polarization stabilized lasers. Novel states of laser light such as standing waves with a spatially periodic linear polarization or coexisting traveling waves with different wave numbers and circular polarizations are also found.

PACS numbers: 42.60.Mi, 42.65.-k, 47.20.Ky

The vector complex Ginzburg-Landau equation (VCGLE) [1,2] gives a generic description of spatiotemporal phenomena in systems described by a complex vector field. Lasers give very appealing opportunities for the study of such phenomena due to the vector nature of the complex amplitude of the electric field. The vector degrees of freedom are associated with the polarization of laser light. Polarization instabilities are currently studied in a variety of lasers [fiber, microchip Nd:YAG, and vertical cavity surface emitting lasers (VCSELs)] [3]. In particular, the lack of stability of transverse and polarization modes in VCSELs is known to produce a rich spatiotemporal phenomenology. In spite of the peculiarities of different lasers, a classification and understanding of possible states close to threshold is provided by a VCGLE. In this Letter I use such a framework to discuss pattern forming instabilities in wide aperture lasers [4,5]. The combination of spatial transverse dependence and polarization state is shown to lead to states of laser light so far unexplored. It is also shown that the stability of these states is determined by polarization phase instabilities.

The study of phase instabilities is linked to the concept of spontaneous symmetry breaking. Generally speaking, a neutral (zero energy) mode is associated with a state that breaks a continuous symmetry of the system. In equilibrium, thermal fluctuations excite nearby low energy modes and destroy long range order in low dimensional systems. On the other hand, the stability of nonequilibrium states is often restricted by phase instabilities in which the zero energy mode becomes unstable with respect to long-wavelength fluctuations. For example, in pattern forming systems such as Rayleigh-Bénard, the range of stable spatially periodic states is limited by an Eckhaus phase instability [6]. The consequences of rotational invariance for a vectorial order parameter are also well understood in equilibrium; for example, spin waves can destroy ferromagnetic order. However, phase instabilities associated with rotational symmetry have not yet been considered at length in nonequilibrium systems such as the laser. The complex vector field describing laser light has two neutral modes: a global phase θ and a rotational phase ψ. Spontaneous emission noise causes fluctuations of θ destroying frequency coherence and giving a finite linewidth. This is the relevant laser phase when the vector direction is fixed by external symmetry breaking such as Brewster windows (scalar case). Otherwise, the additional phase ψ, associated with the state of polarization of laser light, needs to be considered. For an isotropic laser cavity emitting linearly polarized light, ψ determines the orientation of the linearly polarized emission on the transverse plane. The selection of ψ breaks the rotational symmetry.

Laser transverse pattern formation has been associated with an instability of the global phase θ [7]: For a detuning $\Omega < 0$ between atomic and cavity frequencies, the amplitude equation description of the scalar laser instability features a CGLE [8,9]. The stability range of traveling wave solutions of the CGLE around the spatially homogeneous state is limited by a θ instability of the Eckhaus type. For $\Omega > 0$ [5,9] an amplitude equation description requires two coupled CGLE's and the spatially homogeneous lasing solution is θ unstable [10]. When the polarizarion degree of freedom is not frozen, ψ instabilities associated with polarization patterns occur. Polarization phase instabilities restrict the stability range of the laser states allowed in the scalar case.

A VCGLE can be written on symmetry grounds, but the determination of the parameters in the equation requires a specific physical model. The intrinsic polarization of laser light is of quantum nature, and it originates in the spin sublevels of the atomic lasing transition [11]. Purely temporal polarization instabilities have been studied using an homogeneously broadened $J = 1 \rightarrow J = 0$ atomic transition as a prototype situation [12]. I will consider here transverse effects in this same transition [13]. Specifically, I consider a wide aperture single longitudinal mode laser with transverse flat end reflectors. The upper $J = 1$ level is triply degenerate but, neglecting small longitudinal components of the electric field, dipole transitions are only allowed from the states $J_z = \pm 1$ to the lower $J = 0$ level. The complex slowly varying amplitude $\mathbf{E} = (E_x, E_y)$ of the vector electric field can

0031-9007/95/75(3)/425(4)$06.00

be decomposed into its right and left circularly polarized components,

$$E_\pm = \frac{1}{\sqrt{2}}(E_x \pm iE_y). \quad (1)$$

The components $E_\pm$ originate in the transitions from the states $J_z = \pm 1$, respectively. The Maxwell-Bloch equations for the system can be written as

$$\partial_t E_\pm = i\frac{c^2}{2\nu}\partial_x^2 E_\pm - (\kappa + i\nu)E_\pm - ig^* P_\pm, \quad (2)$$

$$\partial_t P_\pm = -(\gamma_\perp + i\omega_0)P_\pm + i\frac{g}{2}(D_1 \pm D_2)E_\pm + igC_\pm E_\mp, \quad (3)$$

$$\partial_t D_1 = -\gamma_\parallel(D_1 - 2\sigma) + 3i(g^* E_+^* P_+ - gE_- P_-^* - \text{c.c.}), \quad (4)$$

$$\partial_t D_2 = -\gamma_J D_2 + i(g^* E_+^* P_+ + gE_- P_-^* - \text{c.c.}), \quad (5)$$

$$\partial_t C_+ = -\gamma_c C_+ + i(g^* E_-^* P_+ - \text{c.c.}), \quad (6)$$

where $P_\pm$ are the complex dipole polarizations for each allowed transition, D_1 is the sum of the population differences between the upper $J_z = \pm 1$ levels and the lower $J = 0$ level, D_2 is the population difference between the two upper levels, C_+ is the density matrix coherence between the two $J_z = \pm 1$ levels, and $C_- = C_+^*$. The ν parameter is the cavity frequency, the detuning $\Omega = \omega_0 - \nu$, g is the coupling parameter, σ the pump parameter, and $\kappa, \gamma_\perp, \gamma_\parallel, \gamma_J, \gamma_c$ are relaxation constants. Possible different relaxation mechanisms lead in general to different states of polarization [14]. While in general $\gamma_J, \gamma_c > \gamma_\parallel$, only the case $\gamma_\parallel = \gamma_J$ was considered in Ref. [12]. The introduction of γ_J [14,15] allows for circularly or linearly polarized light depending on the ratio γ_J/γ_c.

Close to threshold, the set of equations (2)–(6) can be reduced, for $\Omega < 0$ [16], to two coupled equations for the amplitudes $A_\pm$ of the dominant $k = 0$ Fourier mode of $E_\pm$. In appropriate rescaled units one obtains

$$\partial_t A_\pm = \mu A_\pm + (1 + i\alpha)\partial_x^2 A_\pm - (1 + i\beta)(|A_\pm|^2 + \gamma|A_\mp|^2)A_\pm \quad (7)$$

These equations are equivalent to the following VCGLE for the vectorial amplitude $\mathbf{A}$:

$$\partial_t \mathbf{A} = \mu\mathbf{A} + (1 + i\alpha)\partial_x^2\mathbf{A} - (1 + i\beta) \times \{(\mathbf{A}\cdot\mathbf{A}^*)\mathbf{A} + [(\gamma - 1)/2](\mathbf{A}\cdot\mathbf{A})\mathbf{A}^*\}. \quad (8)$$

The parameters μ, α, β have exactly the same expression in terms of the original physical parameters as for a scalar two level model [9]: μ measures the distance to threshold, α originates in the diffraction, and β is associated with detuning. The coupling parameter γ between right and left circularly polarized components can be obtained by direct adiabatic elimination of material variables in the absence of transverse effects,

$$\gamma - 1 = \frac{2\gamma_\parallel}{3\gamma_J + \gamma_\parallel}\left(\frac{\gamma_J}{\gamma_c} - 1\right). \quad (9)$$

The novel features associated with a vectorial description of the laser instability originate in the last term in (8), which has no counterpart in a scalar description. The fact that γ is a real number, together with $1 + \alpha\beta > 0$ [9], are the two main peculiarities of the version of the VCGLE appropriate to describe laser systems.

A family of solutions of Eq. (7) is

$$A_\pm = Q_\pm \exp[-ik_\pm x + i\omega_\pm t + i(\theta_0 \pm \psi_0)], \quad (10)$$

where the real amplitudes $Q_\pm^2 = [\mu(1 - \gamma) + \gamma k_\pm^2 - k_\mp^2]/(1 - \gamma^2)$, the frequencies $\omega_\pm = -\alpha k_\pm^2 - \beta(Q_\pm^2 + \gamma Q_\mp^2)$, and θ_0 and ψ_0 are arbitrary phases. Solutions with either $Q_+ = 0$ or $Q_- = 0$ correspond to circularly polarized light. They are only stable for $\gamma > 1$ and will not be considered further in this paper where I will focus on the case $\gamma < 1$. The simplest particular case of (10) occurs for $k_\pm = 0$. It corresponds to linearly polarized light with $A_\pm$ having the same amplitude and frequency. The global phase θ_0 is the usual arbitrary field phase found in the scalar case and ψ_0 defines the arbitrary direction of linear polarization: $A_x \propto \cos\psi_0, A_y \propto \sin\psi_0$. For $k_\pm \neq 0$ and because of the pure intensity coupling in (7), in general $A_\pm$ do not have a common frequency and there is no well defined polarization (depolarized solutions). However, for wave numbers $k_- = \pm k_+$, $A_\pm$ have the same amplitudes $Q_\pm = Q$ and frequencies $\omega_\pm = \omega$, so that a linearly polarized state can be defined as explained in cases (a) and (b) below. A special case occurs in the limit $\gamma = 1$. For such marginal coupling, solutions of the family (10) only exist for $k_- = \pm k_+$. They correspond to elliptically polarized light with a common frequency for $A_\pm$ and a third arbitrary phase $\Sigma = \tan(Q_+/Q_-)$ associated with the ellipticity.

The linear stability analysis of the family of solutions (10) identifies two vanishing eigenvalues at zero wave number of the perturbation ($q = 0$). They are associated with the arbitrary phases θ_0 and ψ_0. The stability with respect to long-wavelength fluctuations is characterized by phase equations for slowly varying $\theta(x,t)$ and $\psi(x,t)$. Long-wavelength instabilities are characterized in the following for the different solutions mentioned above:

(a) Linearly polarized traveling waves (TW).—These solutions occur for $k_\pm = K$. They are linearly polarized with an arbitrary direction ψ_0. They are the natural generalization of the traveling waves previously considered in the scalar case [5,9]. The phase equations turn out to be decoupled:

$$\partial_t\theta = 2K(\alpha - \beta)\partial_x\theta + D_\theta\partial_x^2\theta, \quad (11)$$

$$\partial_t\psi = 2K(\alpha - \beta)\partial_x\psi + D_\psi\partial_x^2\psi, \quad (12)$$

$$D_\theta(K) = 1 + \alpha\beta - \frac{2(1+\beta^2)K^2}{\mu - K^2}, \quad (13)$$

$$D_\psi(K) = 1 + \alpha\beta - \frac{2(1+\gamma)(1+\beta^2)K^2}{(1-\gamma)(\mu - K^2)}. \quad (14)$$

The equation for the global phase θ is the same as the one obtained for the scalar case: The $K = 0$ solution is phase stable, and TW solutions are θ stable for wave numbers $K < K_t$, where K_t is independent of γ and determined by the Eckhaus instability: $D_\theta(K_t) = 0$. A new phase instability associated with the direction of polarization appears for $K > K_p$, where K_p is determined by $D_\psi(K_p) = 0$. Given that $K_p < K_t$ the stability range of TW solutions is determined by a polarization instability which shrinks the range of stable wave numbers obtained for the scalar case in the (μ, K) plane ("Busse balloon"). In the limit $\gamma \to 0$, $K_p \to K_t$, but (9) restricts γ to take values $\gamma > 1/2$. The smallest value of γ sets the limit of strongest possible linear polarization and broadest stability range. In the opposite limit $\gamma \to 1$, $K_p \to 0$, the phase polarization instability merges with an amplitude instability to circularly polarized light and all TW solutions of finite wave number K are unstable, with the $K = 0$ solution being marginally stable.

(b) Polarized standing waves (SW).—These solutions occur for $k_+ = -k_- = K$. They correspond to counterpropagating traveling waves of opposite circular polarization with a common amplitude, wave number, and frequency. Alternatively, they can be visualized as linearly polarized solutions in which the direction of polarization is periodic in space, with each Cartesian component of the field being a standing wave for the intensity of the electric field:

$$A_x \propto \cos(Kx + \psi_0), \qquad A_y \propto \sin(Kx + \psi_0). \quad (15)$$

For these solutions coupled phase equations are obtained,

$$\partial_t\theta = 2K(\alpha - \beta)\partial_x\psi + D_\psi\partial_x^2\theta, \quad (16)$$

$$\partial_t\psi = 2K(\alpha - \beta)\partial_x\theta + D_\theta\partial_x^2\psi, \quad (17)$$

where D_ψ and D_θ have now exchanged their role. These equations have a single complex eigenvalue,

$$\lambda_q = \pm 2i(\alpha - \beta)Kq - D_s q^2 + O(q^3), \quad (18)$$

where $D_s = (D_\theta + D_\psi)/2$. A single phase instability of the standing waves occurs when $D_s(K_s) = 0$,

$$K_s^2 = \frac{\mu(1-\gamma)(1+\alpha\beta)}{(1-\gamma)(1+\alpha\beta) + 2(1+\beta^2)}. \quad (19)$$

It is interesting to note that no stable SW are found when neglecting the polarization degree of freedom, and that the polarized SW have a broader range of stable wave numbers than the polarized TW waves. Indeed, the characteristic wave number K_s is such that $K_p < K_s < K_t$. In the unattainable limit $\gamma \to 0$, $K_s \to K_t$, while in the opposite limit $\gamma \to 1$, $K_s \to 0$, and the range of stable SW also shrinks to zero. It is also important to realize that the stability properties of the SW solutions depend critically on the nonvariational character of (7). The calculation of (18) is based on a long-wavelength limit which requires having a finite value of $\alpha - \beta$. This cannot be fulfilled in the variational limit [2] $\alpha = \beta = 0$. In such a limit the phase equations decouple, the eigenvalues become real, and the role of θ and ψ are just interchanged with respect to the case of polarized TW. Note also that the phase equation description breaks down for $\gamma \to 1^-$ since the eigenvalue associated with the amplitude difference between A_+ and A_- becomes positive at finite q, while it is negative at $q = 0$.

(c) Depolarized solutions.—The solution (10) for arbitrary $k_+ \neq k_-$ corresponds to spatiotemporal states of the laser field without a simple polarization description. These solutions can be parametrized by $K = (k_+ + k_-)/2$ and $d = k_+ - k_-$. The range of (K, d) values for which they are stable is limited by coupled phase equations which in general have two independent complex eigenvalues. A broad range of stable solutions exist in general. A very small value of d stabilizes a range of K values which are ψ unstable for $d = 0$ (Fig. 1). A TW or SW solution could naturally evolve, after becoming unstable, into a depolarized solution. More interesting is that when the laser is switched on a variety of these solutions can locally grow from spontaneous emission noise. By analogy with the spatiotemporal intermittency regime found in the Benjamin-Feir stable region of the CGLE [17] one can envisage rich disordered states of the laser VCGLE. In such states these local and linearly stable depolarized solutions are connected by localized objects.

Phase anisotropies.—It is interesting to consider the effect of small anisotropies of the laser cavity usually recognized by a detuning splitting. Such anisotropies can be modeled replacing μ in (8) by a general matrix Γ. The Hermitian part of Γ is associated with amplitude losses

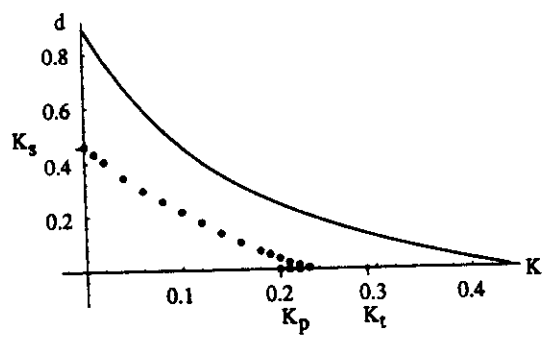

FIG. 1. Stability diagram for the family of solutions (10). Linearly polarized TW's are along the x axis. They are stable for $K < K_p$. Polarized SW are along the y axis. They are stable for $d < 2K_s$. Depolarized solutions exist below the continuous line. They are stable below the dotted line. $\mu = 0.2, \alpha = 2.6, \beta = 0.2, \gamma = 0.5$ ($K_t = 0.291, K_p = 0.198, K_s = 0.231$).

and the anti-Hermitian part with phase anisotropies. I consider here the case of a linear phase anisotropy, which amounts to add a term $i\gamma_p A_\pm$ to the right-hand side of (7). The parameter γ_p is arbitrarily taken such that $\beta\gamma_p > 0$. Solutions of the modified laser VCGLE with the form (10) only exist now for $k_+ = k_- = K$. The phase ψ_0 is no longer arbitrary but fixed by $\sin\{2\psi_0 = 0\}$, giving rise to states linearly polarized either in the x or y direction. These states have a common amplitude independent of γ_p, $Q^2 = (\mu - K^2)/(1 + \gamma)$, and different frequencies $\omega_{x,y} = -\alpha K^2 - \beta(1 + \gamma)Q^2 \pm \gamma_p$. The global phase θ is independent of γ_p and obeys the phase equation (11). The long-wavelength ψ stability of the x- and y-polarized solutions is described by a damped phase equation of the general form,

$$\partial_t\psi = l_0 + v\partial_x\psi + \tilde{D}_\psi\partial_x^2\psi . \qquad (20)$$

Simple particular cases of (20) illustrate well the effect of γ_p on the phase dynamics: When considering the stability of the $K = 0$ solutions, one finds $v = 0$ and $l_0^{x,y}$ is such that the x-polarized solution is always stable at $q = 0$, while the y-polarized solution is unstable for $\gamma_p < \gamma_p^c = \beta Q^2(1 - \gamma)$. In addition, $\tilde{D}_\psi^{x,y}$ is such that the x-polarized solution is further stabilized for $\alpha\gamma_p > 0$ by the phase anisotropy at finite q. From the point of view of polarization discrimination it is then convenient to take a value of $\gamma_p \ll \gamma_p^c$ for which only a stable solution exists at $q = 0$. In this limit the diffusion coefficient for the x-polarized solution of arbitrary K becomes

$$\tilde{D}_\psi^x = D_\psi + \gamma_p \frac{2(\beta^2 + 1)}{Q^2(1 - \gamma)}\left(\alpha - \frac{6K^2\beta}{Q^2(1 - \gamma)}\right). \qquad (21)$$

For finite K and q the damped phase equation describes a competition between the stabilizing effect of the phase anisotropy and the remanent of the ψ instability: $\tilde{D}_\psi^x$ in (21) vanishes at a modified $K_p(\gamma_p) > K_p(\gamma_p = 0)$, so that for $K > K_c$ an amplitude-type instability associated with ψ appears at finite q. The wave number $K_p(\gamma_p)$ sets a lower bound for K_c. A similar mechanism of stabilization of a modulational instability by external forcing has been invoked to explain pattern formation in passive optical systems [18]. In summary, small phase anisotropies fix a polarization direction of the spatially homogenous lasing solution, but the range of stability of polarized TW is still limited by a polarization instability at finite wave number q.

I thank N. B. Abraham for illuminating insights on polarization phenomena and to Q. Feng for helpful discussions. I have benefited from discussions with J. V. Moloney and A. Newell. I acknowledge financial support from the Direccion General de Investigacion Cientifica y Tecnica (DGICYT) and from the Arizona Center for Mathematical Sciences (ACMS). ACMS is sponsored by AFOSR Contract No. F49620-94-1-0144DEF.

*Permanent adress: Department de Física, Universitat de les Illes Balears, E-07071 Palma de Mallorca, Spain.

[1] L. Gil, Phys. Rev. Lett. **70**, 162 (1993).
[2] L. M. Pismen, Phys. Rev. Lett. **72**, 2557 (1994).
[3] R. Leners, R. L. Francois, and G. Stephan, Opt. Lett. **19**, 275 (1994); P. Besnard *et al.*, J. Opt. Soc. Am. B **10**, 1605 (1993); H. Li, T. Lucas, J. G. McInerney, and R. A. Morgan, Chaos, Solitons and Fractals **4**, 1619 (1994).
[4] J. R. Tredicce *et al.*, Phys. Rev. Lett. **62**, 1274 (1989); E. J. D'Angelo *et al.*, Phys. Rev. Lett. **68**, 3702 (1992); D. Dangoisse, D. Hennequin, C. Lepers, E. Louvergnaux, and P. Glorieux, Phys. Rev. A **46**, 5955 (1992); F. T. Arecchi, S. Bocaletti, and P. L. Ramazza, Phys. Rev. Lett. **70**, 2277 (1993); A. B. Coates *et al.*, Phys. Rev. A **49**, 1452 (1994).
[5] P. K. Jakobsen *et al.*, Phys. Rev. A **49**, 4189 (1994); J. Lega, P. K. Jakobsen, J. V. Moloney, and A. C. Newell, Phys. Rev. A **49**, 4201 (1994); Q. Feng, J. V. Moloney, and A. C. Newell, Phys. Rev. Lett. **71**, 1705 (1993).
[6] M. C. Cross and P. C. Hohenberg, Rev. Mod. Phys. **65**, 851 (1993).
[7] R. Lefever, L. A. Lugiato, W. Kaige, N. B. Abraham, and P. Mandel, Phys. Lett. A **135**, 254 (1989); W. Kaige, N. B. Abraham, and L. A. Lugiato, Phys. Rev. A **47**, 1263 (1993).
[8] P. Coullet, L. Gil, and F. Rocca, Opt. Commun. **73**, 403 (1989).
[9] A. C. Newell and J. V. Moloney, *Nonlinear Optics* (Addison Wesley, Redwood City, CA, 1992).
[10] For $\Omega \sim 0$ a complex Swift-Hohenberg equation has been proposed: P. Mandel, M. Georgiou, and T. Erneux, Phys. Rev. A **47**, 4277 (1993); J. Lega, J. V. Moloney, and A. C. Newell, Phys. Rev. Lett. **73**, 2078 (1994).
[11] Spin sublevels are not considered in Ref. [1], missing the specifics of polarization physics. However, the existence of a polarization phase instability is anticipated.
[12] G. P. Puccioni, M. V. Tratnik, J. E. Sipe, and G. L. Oppo, Opt. Lett. **12**, 242 (1987); M. Matlin, R. Gioggia, N. B. Abraham, P. Glorieux, and T. Crawford, Opt. Commun. (to be published).
[13] A similar derivation can be done for semiconductor lasers taking into account the spin dependence in the semiconductor band structure: M. San Miguel, Q. Feng, and J. V. Moloney Phys. Rev. A (to be published).
[14] N. B. Abraham, E. Arimondo, and M. San Miguel, Opt. Commun. **117**, 344 (1995).
[15] D. Lenstra, Phys. Rep. **59**, 300 (1980).
[16] The amplitude equation description for $\Omega > 0$ leads to two coupled VCGLE as in the case of semiconductors [13].
[17] H. Chate, Nonlinearity **7**, 185 (1994).
[18] P. Coullet and K. Emilsson, Physica (Amsterdam) **188A**, 190 (1992).

Wave-Unlocking Transition in Resonantly Coupled Complex Ginzburg-Landau Equations

A. Amengual,[1] D. Walgraef,[1,*] M. San Miguel,[1,2] and E. Hernández-García[1,2]
[1]*Departament de Física, Universitat de les Illes Balears, E-07071 Palma de Mallorca, Spain*
[2]*Instituto Mediterráneo de Estudios Avanzados, IMEDEA (CSIC-UIB), E-07071 Palma de Mallorca, Spain*
(Received 10 October 1995)

We study the effect of spatial frequency forcing on standing-wave solutions of coupled complex Ginzburg-Landau equations. The model considered describes several situations of nonlinear counterpropagating waves and also of the dynamics of polarized light waves. We show that forcing introduces spatial modulations on standing waves which remain frequency locked with a forcing-independent frequency. For forcing above a threshold the modulated standing waves unlock, bifurcating into a temporally periodic state. Below the threshold the system presents a kind of excitability.

PACS numbers: 82.20.–w, 42.65.Sf, 47.20.Ky

Different physicochemical systems driven out of equilibrium may undergo Hopf bifurcations leading to rich spatiotemporal behavior. When these bifurcations occur with broken spatial symmetries, they induce the formation of wave patterns described by order parameters of the form

$$\Psi = Ae^{ik_c x + i\omega_c t} + Be^{-ik_c x + i\omega_c t} + \text{c.c.}, \quad (1)$$

where the slow dynamics of the wave amplitudes A and B obey complex Ginzburg-Landau equations. This is the case, for example, for Rayleigh-Bénard convection in binary fluids, Taylor-Couette instabilities between corotating cylinders, electroconvection in nematic liquid crystals [1], or for the transverse field of high Fresnel number lasers [2]. Symmetry breaking transitions are usually very sensitive to small perturbations or external fields. For example, it has been shown that a spatial modulation of the static electrohydrodynamic instability of nematic liquid crystals modifies the selection and stability of the resulting roll patterns. In particular, the constraint imposed by a periodic modulation of the instability point may lead to a commensurate-incommensurate phase transition [3]. In the case of Hopf bifurcations, external fields inducing spatial or temporal modulations strongly affect the selection and stability of the resulting spatiotemporal patterns. For example, standing waves may be stabilized by purely temporal modulations at twice the critical frequency [4,5], or by purely spatial modulations at twice the critical wave number [6], in regimes where they are otherwise unstable, including domains where the bifurcation parameter is below the critical one.

External forcings that break space or time translational invariance, but not the space inversion symmetry of the wave amplitudes, induce linear resonant couplings between the complex Ginzburg-Landau equations (CGLE) which describe the dynamics of the amplitudes of left and right traveling waves. In the case of forcings that break the space translation invariance, the coupling coefficient ϵ is in general complex, and the corresponding coupled CGLE may be written, in one-dimensional geometries, as

$$\begin{aligned}\dot{A} + v_g\partial_x A &= \mu A + (1 + i\alpha)\partial_x^2 A \\ &\quad - (1 + i\beta)(|A|^2 + \gamma|B|^2)A + \epsilon B, \\ \dot{B} - v_g\partial_x B &= \mu B + (1 + i\alpha)\partial_x^2 B \\ &\quad - (1 + i\beta)(|B|^2 + \gamma|A|^2)B + \epsilon A. \quad (2)\end{aligned}$$

Due to the resonant coupling with coefficient ϵ, pure traveling waves are not solutions of these equations any more, and generic arguments of bifurcation theory allow a characterization of the possible uniform amplitude solutions depending on the various dynamical parameters of the system [6]. Here also, standing waves may be stabilized as the result of phase locking between the waves A and B. Predictions based on (2) in the x-independent case have been successfully tested for azimuthal waves in an annulus laser with imperfect $O(2)$ symmetry [7]. However, the combined effect of the complex coupling coefficient ϵ and the spatial degrees of freedom has not been explored.

In this Letter, we study Eqs. (2) with the following parameter restrictions: imaginary linear coupling coefficient ($\epsilon = i\gamma_P$), negligible group velocity v_g, and weak and real nonlinear cross-coupling term ($\gamma < 1$). We will, however, maintain the spatial derivative in the right-hand side of (2), and this will be crucial for the results below. We will show that the spatial forcing introduces spatial modulations of the standing wave solutions while A and B remain frequency locked with a forcing-independent frequency. By increasing the forcing, these stable modulated waves merge with unstable ones in saddle-node bifurcations with nontrivial global structure. This wave-unlocking transition results in a mixed state with limit cycle temporal behavior. The threshold value of the forcing and the limit cycle frequency are calculated analytically. Modulated standing waves can also be induced by strong enough temporal forcing [8].

The parameter regime explored here would be appropriate in physical situations where a spatial forcing modulates the frequency of the Hopf instability and induces a purely imaginary resonant forcing (a purely real ϵ would appear due to a spatial modulation of the distance to the instability point). Possible systems should have negligible group

 0031-9007/96/76(11)/1956(4)$10.00

velocities, as in some circumstances in binary fluid convection [9] or liquid crystals [10], and weak coupling such as in viscoelastic convection [11]. Up to now, the parameter range considered here best applies to several situations in laser physics. The first one corresponds to taking into account transverse effects in inhomogeneously broadened ($\gamma < 1$) bidirectional ring lasers [12]. The purely imaginary resonant coupling is a consequence of conservative (off-phase) backscattering [13], or, alternatively, a spatial modulation of the refraction index of the laser medium. In fact, a spatially periodic refractive index is the mechanism used for single frequency selection in index coupled distributed feedback lasers (DFB). A second situation is that of the transverse vector field in a laser near threshold [14]. The parameter γ_P corresponds to a detuning splitting between light linearly polarized in different orthogonal directions, produced, for example, by small cavity anisotropies. In this case, A and B are not the amplitudes of left or right traveling waves, but the amplitudes of the two independent circularly polarized components of light, that is, $A = (A_x + iA_y)/\sqrt{2}$ and $B = (A_x - iA_y)/\sqrt{2}$, where A_x and A_y are the linearly polarized complex amplitudes of the vector electric field with a spatially transverse dependence. Weak coupling ($\gamma < 1$) favors linear polarization ($|A| = |B|$). We will often use the light-polarization terminology, because it gives a clear physical insight into the states found for the general set of Eqs. (2) of broad applicability within the parameter restrictions above.

Two families of solutions of the coupled CGLE (2) can be distinguished. The first family corresponds to traveling waves for A and B with the same amplitude, frequency, and wave number

$$A = Q_0 e^{-ikx+i\omega t+i(\theta_0+\psi_0)},$$
$$B = Q_0 e^{-ikx+i\omega t+i(\theta_0-\psi_0)}. \quad (3)$$

Without forcing ($\gamma_P = 0$), the constant global and relative phases, θ_0 and ψ_0, are arbitrary, the amplitude is $Q_0^2 = (\mu - k^2)/(1+\gamma)$, and the frequency ω is $\omega_0 = -\alpha k^2 - \beta(1+\gamma)Q_0^2$. With forcing, the global phase and the amplitude remain unchanged, but the relative phase is fixed by $\sin 2\psi_0 = 0$; the two allowed values of ψ_0 give two solutions with frequencies $\omega = \omega_0 \pm \gamma_P$. The phase instabilities of these solutions were discussed in [14].

The second family of solutions can be searched in the form of two waves

$$A = e^{i\omega_0 t}\sum_n a_n e^{inkx}, \qquad B = e^{i\omega_0 t}\sum_n b_n e^{inkx}, \quad (4)$$

frequency locked to a frequency ω_0 independent of forcing. For $\gamma_P = 0$, the exact solutions of (2) in this form only have two terms, $|a_1| = |b_{-1}| = Q_0$. The effect of a small forcing in this solution is to generate higher harmonics, while keeping ω_0 fixed and the relative phase between a_1 and b_{-1} arbitrary. Now, the remaining coefficients a_n and b_n are not zero and can be calculated perturbatively in γ_P. Close enough to the threshold for a mode k ($\mu - k^2 \approx 0$), the amplitude of higher order harmonics is negligible and, to lowest order in $\mu - k^2$, an approximate solution takes the form

$$A = e^{i(\theta_0+\omega_0 t)}(Qe^{i(kx+i\psi_0)} + \mathrm{Re}^{-i(kx+\psi_0-\phi)}),$$
$$B = e^{i(\theta_0+\omega_0 t)}(Qe^{-i(kx+\psi_0)} + \mathrm{Re}^{i(kx+\psi_0+\phi)}), \quad (5)$$

with θ_0 and ψ_0 arbitrary, and ϕ fixed by the forcing. Q and R are real numbers (positive or negative) and, for small γ_P, $|R| \ll |Q|$ (an equivalent solution is found interchanging Q and R).

A visualization of these solutions can be given within the polarization interpretation of (2). Defining $C_\pm e^{i\zeta_\pm} \equiv Q \pm e^{i\phi}R$, the change of variables to the amplitudes of the x and y linearly polarized components gives

$$A_x = \sqrt{2}\,C_+ \cos(kx + \psi_0)e^{i(\omega_0 t+\theta_0+\zeta_+)},$$
$$A_y = \sqrt{2}\,C_- \sin(kx + \psi_0)e^{i(\omega_0 t+\theta_0+\zeta_-)}. \quad (6)$$

These equations describe at each point x the superposition of two dephased harmonic motions with different amplitudes and a frequency ω_0 independent of forcing. This identifies the solution (5) with an elliptically polarized standing wave pattern in which the orientation of the ellipse and its ellipticity vary periodically in the spatial coordinate x. In the limit of no forcing, $R = 0$, the ellipse degenerates in a linearly polarized standing wave with an angle of polarization $\psi = kx + \psi_0$. In this interpretation,

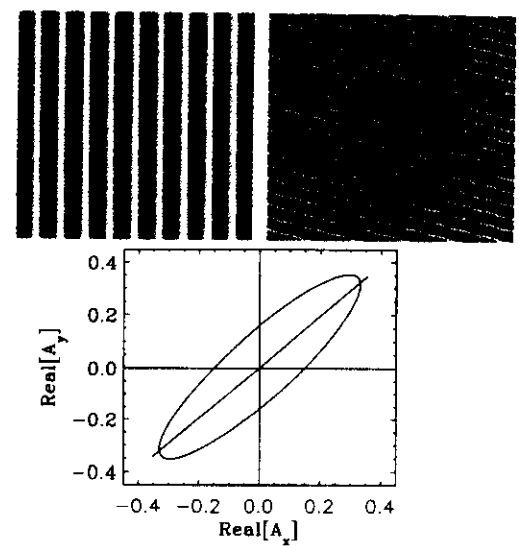

FIG. 1. Modulus (left) and phase (right) of A for $\gamma_P = 0.012 < \gamma_{P_c}$. The horizontal axis is space (256 units), and the vertical is time (1000 units). Gray levels range from black (0) to white (the maximum of the modulus or 2π for the phase). This numerical solution has been obtained from (2) with $\beta = 0.2$, $\gamma = 0.5$, $\mu = 0.2$, and $\alpha = 2.6$. The initial condition is a standing wave with $\omega = \omega_0$ and $k = 0.123$. Bottom: polarization representation of the solution at a given point x. For $\gamma_P = 0$ one has linear polarization (indicated by the straight line) which becomes elliptical for $\gamma_P \neq 0$. An equivalent solution has the major axis of the ellipse along the second and fourth quadrants.

the first family of solutions (3) would correspond to linearly polarized traveling waves with frequency ω and an angle of polarization ψ_0. In such a case, the forcing fixes the direction of polarization so that only x or y linearly polarized waves remain. On the contrary, forcing in (5) grows an ellipse from a linearly polarized standing wave keeping the frequency unchanged.

Elliptically polarized standing wave patterns are obtained from a direct numerical integration of the coupled CGLE as shown in Fig. 1. Increasing the forcing, these solutions become unstable through a bifurcation in which Q and R become time dependent. As shown in Fig. 2, the solution beyond this instability oscillates between the two equivalent elliptically polarized standing wave patterns found for small γ_P. In addition, from the numerical simulations, one finds that the period T of these oscillations decreases beyond the critical value γ_{Pc}. One has $T^{-2} \propto \gamma_P - \gamma_{Pc}$ (see Figs. 3 and 4).

A quantitative description of the instability, including the determination of the critical forcing γ_{Pc} and the period of the oscillations, can be performed by an amplitude analysis. Close to the threshold for the k modes, the equations for the slow time evolution of Q and R can be found by substitution of (5) into (2) and neglecting contributions from higher order harmonics. Defining $Xe^{i\Phi} \equiv Q + iR$, we find

$$\begin{aligned}
\dot{X} &= (\mu - k^2)X - (1 + \gamma)X^3 \\
&\quad - (1 + \gamma\cos 2\phi)\frac{X^3}{2}\sin^2 2\Phi , \\
\dot{\Phi} &= -(1 + \gamma\cos 2\phi)\frac{X^2}{2}\sin 2\Phi\cos 2\Phi \\
&\quad + \beta\gamma\sin 2\phi\,\frac{X^2}{2}\sin 2\Phi - \gamma_P\sin\phi , \\
\dot{\phi} &= \beta(1 + \gamma\cos 2\phi)X^2\cos 2\Phi + \gamma X^2\sin 2\phi \\
&\quad - 2\gamma_P\cos\phi\cot 2\Phi . \qquad (7)
\end{aligned}$$

The fixed points of (7) represent the polarized standing waves solutions (5). These points can be determined exactly in the limiting case of $\beta = 0$. The interesting solutions have two allowed values of ϕ: $\phi_0 = (2n + 1)\pi/2$, $n = 0, 1$; and for each value of ϕ, there are eight fixed points: Four are stable (+) and the other four are saddle points (−). The corresponding values of X and Φ are

$$\begin{aligned}
X_0(\pm)^2 &= \frac{\mu - k^2}{2(3 + \gamma)(1 + \gamma)} \\
&\quad \times \left[5 + 3\gamma \pm \sqrt{(1 - \gamma)^2 - \frac{8(1 + \gamma)(3 + \gamma)\gamma_P^2}{(\mu - k^2)^2}}\,\right], \qquad (8)
\end{aligned}$$

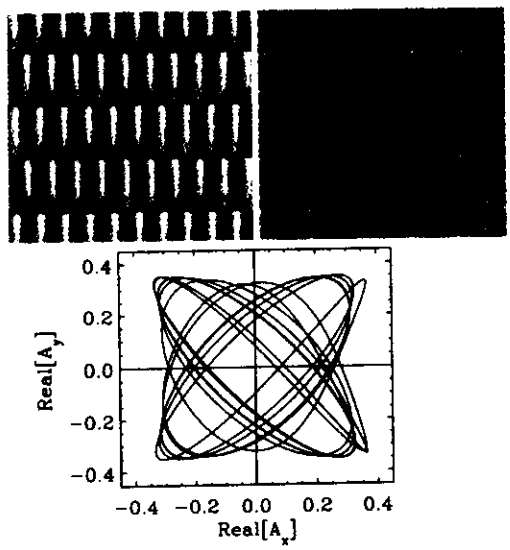

FIG. 2. Same as Fig. 1 but using $\gamma_P = 0.0145 > \gamma_{Pc}$.

$$\begin{aligned}
\Phi_0(+) &= \xi(+) + m\frac{\pi}{2}, \\
\Phi_0(-) &= \frac{\pi}{4} - \xi(-) + m\frac{\pi}{2}, \qquad (9)
\end{aligned}$$

where $m = 0, 1, 2, 3$, and

$$\xi(\pm) = \frac{(-1)^{n+1}}{4}\arcsin\frac{4\gamma_P}{(1 - \gamma)X_0(\pm)^2} . \qquad (10)$$

Heteroclinic orbits connect the saddles and the stable nodes with the same ϕ. When γ_P grows, saddles and nodes approach by pairs and at the critical value,

$$\gamma_{Pc} = \frac{(\mu - k^2)(1 - \gamma)}{\sqrt{8(1 + \gamma)(3 + \gamma)}}, \qquad (11)$$

they merge and disappear via inverse saddle-node bifurcations. The interesting point is the global structure of the bifurcation: The presence of the heteroclinic connections gives rise to the birth of limit cycles (one for each value of ϕ). This is similar to the Andronov–van der Pol bifurcation [15] that appears in several types of excitable systems [16]. The difference is that, due to symmetries, here we have several pairs of fixed points merging, instead of just one pair. The periodic behavior is illustrated in Fig. 2 by the periodic alternation of the trajectory between the "ghosts" of the disappeared elliptically polarized states corresponding to the fixed points. Below the bifurcation, small perturbations around the stable solutions decay, whereas perturbations above a threshold push the system along the heteroclinic trajectory toward another stable fixed point. Since the size of the perturbation required for such switches decreases by increasing γ_P, and vanishes at γ_{Pc}, the multistability of this system can be seen as a kind of excitability [17]. A different consequence of the multiplicity of stable states is their possible coexistence in space, leading to the formation of domains with different polarizations along the x axis.

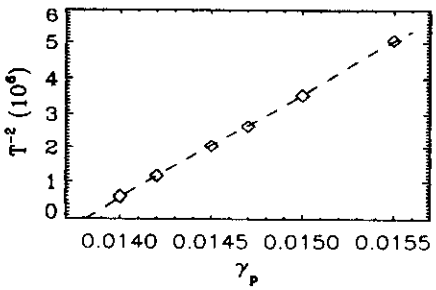

FIG. 3. Period of the oscillations (T) of Q and R, obtained from the numerical solution of the coupled CGLE using the parameters given in Fig. 1. The dashed line is a least squares fitting from which $\gamma_{Pc} = 0.0138$.

Close to the instability at γ_{Pc}, the time dependent behavior of the solution can be obtained reducing the problem to a phase dynamics by elimination of the variable X. We have (in the limit $\beta = 0$)

$$\dot{\Phi} = -\frac{(\mu - k^2)(1 - \gamma)\sin 4\Phi}{5 + 3\gamma - (1 - \gamma)\cos 4\Phi} + \gamma_P , \qquad (12)$$

which for $\gamma_P \geq \gamma_{Pc}$ yields the following time behavior:

$$\tan(2\Phi) = \tan(2\Phi_c)\left[1 + \sqrt{2(\gamma_P - \gamma_{Pc})/\gamma_{Pc}}\right.$$
$$\left.\times \tan\left((5 + 3\gamma)\sqrt{\gamma_{Pc}}\sqrt{\frac{\gamma_P - \gamma_{Pc}}{(1 + \gamma)(3 + \gamma)}}\, t\right)\right], \qquad (13)$$

where $\Phi_c = \Phi_0$, Eq. (9), for $\gamma_P = \gamma_{Pc}$.

An approximative analysis of Eqs. (7) for $\beta \neq 0$ indicates that this parameter appears squared in the expressions for γ_{Pc}, X, and Φ_c. Therefore, for small β, the previous analysis is still meaningful as explicitly seen in the numerical results of Figs. 3 and 4.

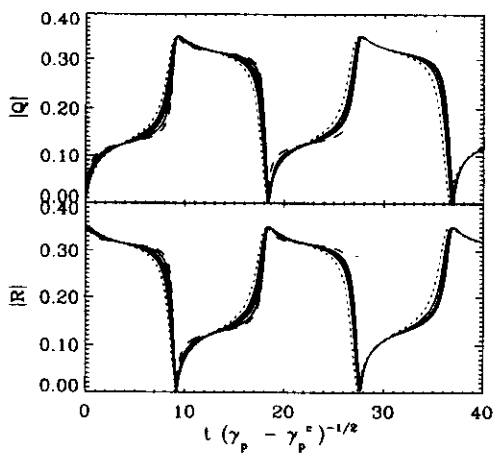

FIG. 4. The amplitudes of Q and R of the solution shown in Fig. 2 exhibit the periodic oscillations given by Eq. (13). The time has been scaled using the value of γ_{Pc} obtained from Fig. 3. The dotted line corresponds to $\gamma_p = 0.0155$, the dashed line to $\gamma_p = 0.0140$, and the lines in between to the other points of Fig. 3.

In summary, in the absence of forcing, and for the parameter regime considered here, there are solutions for the amplitudes A and B of the coupled CGLE which correspond to linearly polarized standing waves. We have shown that an imaginary coupling between them transforms these solutions into standing waves with spatially periodic elliptic polarization. Increasing the forcing, an instability of these solutions appears, via the unlocking of the underlying wave amplitudes, and the solutions acquire a time-periodic behavior. Locally, this bifurcation is of the saddle-node type, but the presence of heteroclinic connections between the fixed points gives rise to the appearance of a limit cycle when stable and unstable points merge.

Financial support from DGICYT Projects PB94-1167 and PB94-1172 is acknowledged.

*Also at the Belgian National Fund for Scientific Research, Center for Nonlinear Phenomena and Complex Systems, Université Libre de Bruxelles, Campus Plaine, Blv. du Triomphe B.P 231, 1050 Bruxelles, Belgium.

[1] M.C. Cross and P.C. Hohenberg, Rev. Mod. Phys. **65**, 854 (1993).
[2] A.C. Newell and J.V. Moloney, *Nonlinear Optics* (Addison-Wesley, Redwood City, 1992).
[3] M. Lowe and J.P. Gollub, Phys. Rev. A **31**, 3893 (1985).
[4] D. Walgraef, Europhys. Lett. **7**, 485 (1988).
[5] H. Riecke, J.D. Crawford, and E. Knobloch, Phys. Rev. Lett. **61**, 1942 (1988).
[6] G. Dangelmayr and E. Knobloch, Nonlinearity **4**, 399 (1991).
[7] E.J. D'Angelo, E. Izaguirre, G.B. Mindlin, G. Huyet, L. Gil, and J.R. Tredicce, Phys. Rev. Lett. **68**, 3702 (1992).
[8] S. Douady, S. Fauve, and O. Thual, Europhys. Lett. **10**, 309 (1989).
[9] P. Kolodner, Phys. Rev. A **44**, 6448 (1991); Phys. Rev. Lett. **66**, 1165 (1991).
[10] *Physics of Pattern Formation in Complex Dissipative Systems*, edited by S. Kai (World Scientific, Singapore, 1992).
[11] J. Martínez-Mardones, R. Tiemann, W. Zeller, and C. Pérez-García, Int. J. Bifurc. Chaos **4**, 5 (1994).
[12] S. Singh, Phys. Rep. **108**, 217 (1984).
[13] C. Etrich, P. Mandel, R. Neelen, R.J.C. Spreeuw, and J.P. Woerdman, Phys. Rev. A **46**, 525 (1992).
[14] M. San Miguel, Phys. Rev. Lett. **75**, 425 (1995).
[15] A.A. Andronov, A.A. Vitt, and S.E. Khaikin, *Theory of Oscillators* (Pergamon Press, Oxford, 1966).
[16] S.C. Mueller, P. Coullet, and D. Walgraef, Chaos **4**, 439 (1994).
[17] E. Meron, Phys. Rep. **218**, 1 (1992).

Synchronization of Spatiotemporal Chaos: The Regime of Coupled Spatiotemporal Intermittency

A. Amengual,[1] E. Hernández-García,[1,2,*] R. Montagne,[1,2,*,†] and M. San Miguel[1,2,*]
[1]*Departament de Física, Universitat de les Illes Balears, E-07071 Palma de Mallorca, Spain*
[2]*Instituto Mediterráneo de Estudios Avanzados, IMEDEA (CSIC-UIB), E-07071 Palma de Mallorca, Spain*
(Received 8 November 1996)

Synchronization of spatiotemporally chaotic extended systems is considered in the context of coupled one-dimensional complex Ginzburg-Landau equations (CGLE). A regime of coupled spatiotemporal intermittency (STI) is identified and described in terms of the space-time synchronized chaotic motion of localized structures. A quantitative measure of synchronization as a function of coupling parameter is given through distribution functions and information measures. The coupled STI regime is shown to disappear into regular dynamics for situations of strong coupling when localized structures become unstable, hence a description in terms of a single CGLE is not appropriate. [S0031-9007(97)03313-9]

PACS numbers: 05.45.+b, 47.20.Ky

Two issues of high current interest in the general field of nonlinear dynamics are the quantitative characterization of different regimes of spatiotemporal complex dynamics in extended systems [1] and the synchronization of chaotic oscillators [2]. The characterization of low-dimensional chaos is now a mature subject with well established techniques, including techniques of chaos control. In this context, the demonstration that the familiar phenomenon of synchronization of two regular oscillators [3] by a weak coupling can also be displayed by chaotic oscillators is an important new idea. This conceptual development has opened a new avenue of research with interesting practical implications. Chaos in extended systems is a much less mature subject, and many investigations are still at the level of classifying different types of behavior. Concepts and methods of statistical mechanics are commonly invoked in terms of "phase diagrams" and transitions among different "phases" of behavior [4–7]. Still, the possibility of a synchronized behavior of spatially extended systems in a spatiotemporal disordered phase is an appealing idea that we address in this Letter. More specifically, we will consider an extended one-dimensional system in a chaotic regime known as spatiotemporal intermittency (STI) [5], and we will characterize a coupled STI regime.

By synchronization of two chaotic oscillators O_1 and O_2, it is meant in a strict sense that plotting the time series $O_1(t_i)$ vs $O_2(t_i)$ one obtains a straight line of unit slope. For many practical applications, synchronization of chaotic oscillations calls for an expanded framework and the concept of "generalized synchronization" has been introduced [8,9] as the appearance of a functional dependence between the two time series. In this context, we understand here by synchronization the situation in which $O_1(t_i)$ becomes a given known function of $O_2(t_i)$. Transferring these concepts to spatially extended systems, we search for correlations between the space(x_i)-time(t_j) series of two variables $O_1(x_i, t_j)$ and $O_2(x_i, t_j)$. The synchronization of O_1 and O_2 occurs when these two space-time series become functionally dependent. This idea is different from the one much studied in the context of coupled map models in which the coupling and emerging correlations are among spatially coupled oscillators. Here we search for correlations of two variables at the same space-time point.

Our study has been carried out in the context of complex Ginzburg-Landau Equations (CGLE) which give a prototype example of chaotic behavior in extended systems [10,11]. Our results show that the coupling between two complex amplitudes A_1 and A_2 ($O_1 = |A_1|$ and $O_2 = |A_2|$), in a STI regime described below, establishes spatiotemporal correlations which preserve spatiotemporal chaos but lead to a synchronized behavior: Starting from the independent STI dynamics of A_1 and A_2, coupling between them leads to a STI regime dominated by the synchronized chaotic motion of localized structures in space and time for A_1 and A_2. An additional effect observed in our model is that the coupled STI regime is destroyed for coupling larger than a given threshold. At this threshold, maximal mutual information and anticorrelation of $|A_1|$ and $|A_2|$ are approached.

The CGLE is the amplitude equation for a Hopf bifurcation for which the system starts to oscillate with frequency ω_c in a spatially homogeneous mode. When, in addition, the Hopf bifurcation breaks the spatial translation symmetry it identifies a preferred wave number K_c and traveling waves appear. In one-dimensional systems the amplitudes A_1 and A_2 of the two counterpropagating traveling waves satisfy coupled CGLE of the form

$$\partial_t A_{1,2} = \mu A_{1,2} + (1 + i\alpha)\partial_x^2 A_{1,2} - (1 + i\beta)(|A_{1,2}|^2 + \gamma|A_{2,1}|^2)A_{1,2}. \quad (1)$$

Equation (1) is written here in the limit of negligible group velocity. In particular, this limit is of interest to describe the coupled motion of the two complex components of a vector CGLE. In this context, (1) is used to describe vectorial transverse pattern formation in nonlinear optical systems, $A_{1,2}$ stand for the two independent circularly polarized components of a vectorial electric field amplitude

0031-9007/97/78(23)/4379(4)$10.00

[12,13], and the coupling parameter γ is taken to be a real number.

Homogeneous solutions of Eq. (1) are of the form

$$A_{1,2}(x,t) = Q_{1,2}e^{i\omega_{1,2}t}, \quad (2)$$

with $Q_{1,2}$ real and $\omega_{1,2} = -\beta(Q_{1,2}^2 + \gamma Q_{2,1}^2)$. For $\gamma = 0$, $Q_{1,2}^2 = \mu$, and the two amplitudes satisfy the independent CGLE whose phase diagram has been studied in much detail in terms of the parameters α and β [7,14]. For $\gamma = 0$, solutions of type (2) and other plane waves of different periodicities are known to be linearly stable below the Benjamin-Feir (BF) line ($1 + \alpha\beta > 0$). Above this line, regimes of phase and defect chaos occur. However, for a range of parameters below the BF line there is an additional attractor, coexisting with the one of plane waves, in which the system displays a form of spatiotemporal chaos known as STI. In this attractor the solution is intermittent in space and time. Space-time plots of $|A_1|$ or $|A_2|$ in the STI regime for $\gamma = 0$ are qualitatively similar to the ones shown in Fig. 1 (top). The question we address here is how the STI regimes of A_1 and A_2 change when the coupling γ is introduced. We first recall that for a weak coupling situation ($\gamma < 1$) the solution (2) with $Q_{1,2}^2 = \mu/(1 + \gamma)$ is linearly stable below the same BF line $1 + \alpha\beta > 0$ [12], whereas the solutions with $Q_1 = 0$ or $Q_2 = 0$ are unstable. For large coupling, $\gamma > 1$, the competition between the two amplitudes is such that only one of them survives, so that linearly stable solutions are either $Q_1 = \sqrt{\mu}$, $Q_2 = 0$ or $Q_2 = \sqrt{\mu}$, $Q_1 = 0$. In addition to these ordered states we also find a STI attractor for coupled CGLE and values of α and β which are in the STI region of a single CGLE. Changes of such STI behavior with varying γ are shown in Fig. 1 [15].

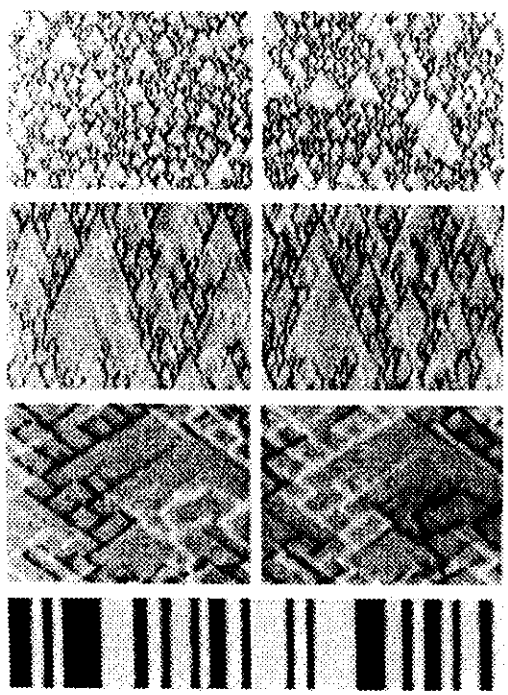

FIG. 1. Space-time plot of the modulus $|A_1|$ (left) and $|A_2|$ (right). From top to bottom, $\gamma = 0.1$, 0.5, 0.95, and 1.05. The horizontal axis represents space and the vertical axis represents time (2000 time units for $\gamma = 0.95$, 100 for $\gamma = 1.05$, and 200 in the other two plots). The grey levels change linearly from the minimum (black) to the maximum (white) of the modulus. The parameters are $\mu = 1$, $\alpha = 0.2$, and $\beta = -2.0$.

For small coupling ($\gamma \ll 1$) we observe that $|A_1|$ and $|A_2|$ follow nearly independent dynamics, with the flat gray regions in the space-time plot being laminar regions separated by localized structures that appear, travel, and annihilate. In the laminar regions, configurations close to (2) with $Q_1 = Q_2$ occur. Disorder occurs via the contamination by localized structures. These structures have a rather irregular behavior and, in a first approach, they can be classified as holelike or pulselike [11]. In Fig. 1 these holelike and pulselike structures are associated with black and white localized structures, respectively. As γ increases we observe two facts: First, both $|A_1|$ and $|A_2|$ continue to display STI dynamics, although in larger and slower space-time scales. Second, and more interesting, is that the dynamics of $|A_1|$ and $|A_2|$ become increasingly correlated. This is easily recognized by focusing in the localized structures: A black traveling structure in the space-time plot of $|A_1|$ has its corresponding white traveling structure in the space-time plot of $|A_2|$ and vice versa. This results in laminar states occurring in the same region of space-time for $|A_1|$ and $|A_2|$. The coupled STI dynamical regime is dominated by localized structures in which maxima of $|A_1|$ occur, always together with minima of $|A_2|$ and vice versa (bounded pulse-hole). In the vicinity of the localized structures, and emerging from them, there appear traveling wave solutions of (1) but with a different wave number for $|A_1|$ and $|A_2|$ so that $|A_1| \neq |A_2|$. Eventually (going beyond the marginal coupling $\gamma = 1$), the STI dynamics is destroyed and $|A_1|$ and $|A_2|$ display only laminar regions, in which either $|A_1|$ or $|A_2|$ vanish, separated by domain walls.

In the optical interpretation of (1), the laminar regions with $|A_1| = |A_2|$ correspond to transverse domains of linearly polarized light, although with a random direction of linear polarization. The localized structures are essentially circularly polarized objects since one of the two amplitudes dominates over the other. Around these structures the plane wave solutions with $|A_1| \neq |A_2|$ have different frequencies, so that they correspond to depolarized solutions of (1) [12]. As $\gamma > 1$, localized traveling structures disappear, and one is left with circularly polarized domains separated by polarization walls.

It is usually argued that for $\gamma > 1$ the dynamics of the coupled CGLE (1) is well represented by a single CGLE since only one of the two waves survives. This is certainly not true in the STI domain of parameters considered here since single CGLE would give rise to STI dynamics, whereas the coupled set (1) does not for $\gamma > 1$. In general, a description in terms of a single CGLE would not be reliable for parameter values at which the single amplitude dynamics produces amplitude values close to

zero. We next show that the correlations observed for increasing γ in Fig. 1 are, in fact, a kind of spatiotemporal synchronization, in the generalized sense defined in [8,9]. To this end, a characterization of the synchronizing process can be given by analyzing the joint distribution of the two variables. This distribution and values of $|A_1|$ vs $|A_2|$ are plotted in Fig. 2. The cloud of points correspond to the different space-time points of Fig. 1. For $\gamma \ll 1$ we obtain a diffuse cloud of points indicating essentially independent dynamics. The concentration of points around $|A_1|^2 = |A_2|^2 = \mu/(1+\gamma)$ corresponds to the laminar regions, but excursions away from that solution are independent. As the coupling is increased with $\gamma < 1$, the cloud of points approaches the curve given by $|A_1|^2 + |A_2|^2 = \mu$. This indicates synchronization of the dynamics of structures departing from the laminar regions. The relationship between $|A_1|$ and $|A_2|$ can be thought of as a kind of antiphase dynamics [17]. The points with larger values of $|A_1|$ and smaller values of $|A_2|$ (and vice versa) correspond to the localized traveling structures. Intermediate points among these, and those around $|A_1| = |A_2|$, correspond to the regular solutions of a nonzero wave number that surround the localized structures. The special case of marginal coupling is discussed below, but as we enter into the strong coupling situation ($\gamma > 1$) the cloud of points concentrates in the regions $|A_1|^2 = \mu$, $|A_2| = 0$ and $|A_2|^2 = \mu$, $|A_1| = 0$ corresponding to the stable nonchaotic solutions. Intermediate points correspond to the domain walls separating these ordered regions. It should be pointed out that we are considering just the modulus of the complex fields $A_{1,2}$. The coupled phase dynamics does not show any obvious form of synchronization. Therefore we find a case of partial synchronization of the dynamical variables. A different type of partial synchronization of chaotic oscillators has been described in [18].

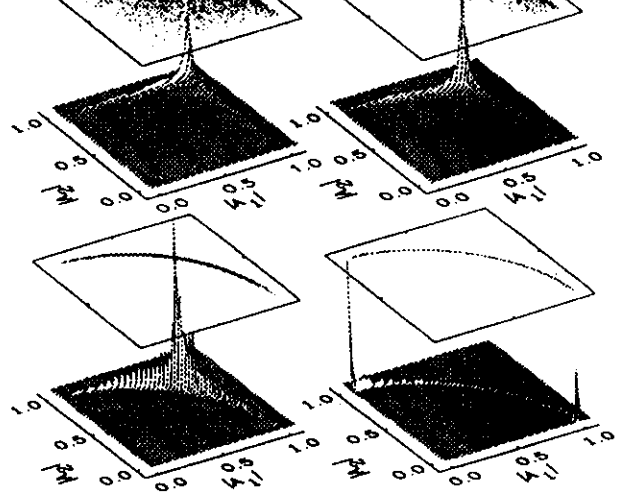

FIG. 2. Asymptotic states for (from left to right, and from top to bottom) $\gamma = 0.1$, 0.5, 0.95, and 1.05. The joint probability distribution $p(|A_2|, |A_1|)$ is shown as a 3D surface. On top of each surface, $|A_1(x,t)|$ vs $|A_2(x,t)|$ are shown in the form of a dotted plot obtained from the values of $|A_1|$ and $|A_2|$ at space-time points during a time interval of 50 units.

A quantitative measure of the synchronizing process can be given in terms of information measures [19]. The entropy $H(X) = -\sum_x p(x) \ln p(x)$, where $p(x)$ is the probability that X takes the value x, measures the randomness of a discrete random variable X. For two random discrete variables X and Y, with a joint probability distribution $p(x,y)$, the mutual information $I(X,Y) = -\sum_{x,y} p(x,y) \ln[p(x)p(y)/p(x,y)]$ gives a measure of the statistical dependence between both variables; the mutual information being 0 if and only if X and Y are independent. Considering the discretized values of $|A_1|$ and $|A_2|$ at space-time points as random variables $X = |A_1|$, $Y = |A_2|$, their mutual information is a measure of their synchronization. In Fig. 3 (left) we have plotted the mutual information and the entropy of $|A_1|$ and $|A_2|$ as a function of γ [20]. This graph shows that the entropy of $|A_1|$ and $|A_2|$ remains constant for increasing values of γ, so that increasing γ does not reduce the uncertainty associated with the single-point distributions of $A_{1,2}$. This indicates here that synchronization is not the result of reduced randomness due to the increase of time and length scales observed in Fig. 1. However, when γ is larger, the mutual information becomes larger, approaching its maximum possible value [$I = H(|A_1|) = H(|A_2|)$] as $\gamma \to 1$. An additional quantitative measurement of synchronization is given by the linear correlation coefficient $\rho = (\langle |A_1||A_2| \rangle - \langle |A_1| \rangle \langle |A_2| \rangle)[\mathrm{var}(|A_1|)\mathrm{var}(|A_2|)]^{-1/2}$ with $\mathrm{var}(x)$ being the variance of x. This coefficient, plotted as a function of γ in Fig. 3 (right), is negative, indicating that when $|A_1|$ increases, $|A_2|$ decreases and vice versa.

Our quantitative indicators of synchronization, I and ρ, approach their maximum absolute values as $\gamma \to 1$. We also observe that the regime of coupled STI disappears for $\gamma > 1$. This can be explained by considering the stability of the localized structures responsible for STI. We have examined the stability of localized structures, isolating an individual pulse-hole structure from a STI configuration at $\gamma < 1$ and letting it evolve in time. For $\gamma < 1$ it recreates STI while for $\gamma \geq 1$ it is unstable, becoming

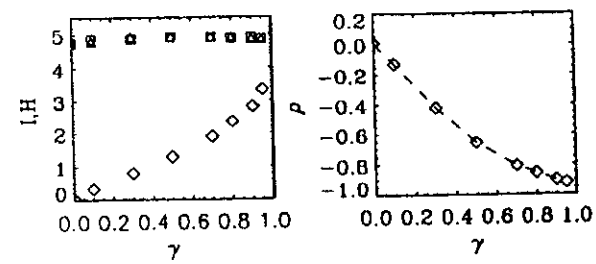

FIG. 3. Left: Entropy of $|A_1|$ (□) and $|A_2|$ (△) and their mutual information I (◇) as a function of γ. Right: Correlation coefficient ρ of $|A_1|$ vs $|A_2|$ as a function of γ.

wider and evolving into laminar states. It has been argued that the domain of parameters (α, β) in which STI exists for $\gamma = 0$ is given by the stability of localized structures [21]. In the same way, we find here that coupled STI disappears in the limit of stability $\gamma = 1$ of coupled pulse-hole structures. The change in behavior at $\gamma = 1$ can be alternatively understood from the emergence of $|A_1|^2 + |A_2|^2 = \mu$ as an attracting manifold. Writing (1) in terms of $R^2 \equiv |A_1|^2 + |A_2|^2$ and $\chi \equiv \arctan(|A_1|/|A_2|)$, one can see immediately that homogeneous solutions for $\gamma = 1$ are $R^2 = \mu$ and χ arbitrary. The transient dynamics starting from random initial conditions at $\gamma = 1$ consists of a very fast evolution of $R(x, t)$ towards $\sqrt{\mu}$, with no regime of STI existing at any time, with $\chi(x, t)$ covering almost completely the range of its possible values. In the late dynamical stages, $\chi(x, t)$ reaches an arbitrary value χ_0 through spatial diffusion. An explanation for this behavior is that, while for $\gamma \neq 1$ the zero-wave-number components $\hat{R}(k = 0)$ and $\hat{\chi}(k = 0)$ have a nonzero driving force, at $\gamma = 1$, $\hat{\chi}(k = 0)$ is a marginal variable while $\hat{R}(k = 0)$ is strongly driven. Once R becomes space homogeneous, the homogeneous state is asymptotically approached because the different wave-number components of $A_{1,2}$ become decoupled:

$$|\hat{A}_{1,2}(k, t)|^2 = e^{2(\mu - k^2)t - 2\int_0^t R(s)ds} |\hat{A}_{1,2}(k, t = 0)|^2. \quad (3)$$

Requiring bound solutions for $t \to \infty$, (3) implies that all Fourier components of A decay to zero, except the one with the smallest wave number. Since a homogeneous component is usually present in the initial condition, the system will evolve into a homogeneous state, as observed numerically. In some of our simulations the STI regime has been observed to disappear for a coupling smaller than $\gamma = 1$, but this seems to be a consequence of finite-size effects: The size of the laminar portions of Fig. 1 increases with the coupling γ. When this size becomes similar to system size, one of the stable plane waves can occupy the whole system, thus preventing any further appearance of defects and STI. For a given initial condition, with parameters $\alpha = 0.2$ and $\beta = -1.4$, and a system size $L = 512$, the STI regime was seen to disappear at $\gamma = 0.85$. As soon as the system size was doubled the STI regime reappeared again. By reducing the system size to $L = 256$ the STI regime disappeared for smaller γ. The conclusion from this and other numerical experiments is that STI exists for all $\gamma < 1$ in the same range of parameters as it exists in the single CGLE, with time and length scales diverging as γ approaches 1, where STI disappears.

In summary we have described a regime of synchronized STI dominated by the space-time synchronization of localized structures. Synchronization is measured by mutual information and a correlation parameter that take their absolute maximum value at the boundary between weak and strong coupling $\gamma = 1$. Beyond this boundary $(\gamma > 1)$, STI disappears, but the strong, coupled system dynamics cannot be described in terms of a single dominant amplitude.

Financial support from DGICYT Project PB94-1167 (Spain) and European Union QSTRUCT (FMRX-CT96-0077) are acknowledged. R.M. acknowledges support from PEDECIBA and CONICYT (Uruguay).

*Electronic address: http://www.imedea.uib.es/Nonlinear
†On leave from Universidad de la República (Uruguay).

[1] M. Cross and P. Hohenberg, Science **263**, 1569 (1994); M. Dennin, G. Ahlers, and D. S. Cannell, Science **272**, 388 (1996); R. Ecke, Y. Hu, R. Mainieri, and G. Ahlers, Science **269**, 1704 (1995).
[2] L. M. Pecora and T. L. Carrol, Phys. Rev. Lett. **64**, 821 (1990); P. Colet and R. Roy, Opt. Lett. **19**, 2056 (1994).
[3] C. Huygens and J. des Scavans (1665); K. Wiesenfeld, P. Colet, and S. H. Strogatz, Phys. Rev. Lett. **76**, 404 (1996).
[4] B. Shraiman *et al.*, Physica (Amsterdam) **57D**, 241 (1992).
[5] H. Chaté, Nonlinearity 7, 185 (1994).
[6] M. Caponeri and S. Ciliberto, Physica (Amsterdam) **58D**, 365 (1992).
[7] R. Montagne, E. Hernández-García, and M. San Miguel, Phys. Rev. Lett. **77**, 267 (1996); Physica (Amsterdam) **96D**, 47 (1996).
[8] N. F. Rulkov, M. M. Sushchik, L. S. Tsimring, and H. D. I. Abarbanel, Phys. Rev. E **51**, 980 (1995).
[9] L. Kocarev and U. Parlitz, Phys. Rev. Lett. **76**, 1816 (1996).
[10] M. Cross and P. Hohenberg, Rev. Mod. Phys. **65**, 851 (1993).
[11] W. van Saarloos and P. Hohenberg, Physica (Amsterdam) **56D**, 303 (1992).
[12] M. San Miguel, Phys. Rev. Lett. **75**, 425 (1995).
[13] A. Amengual, D. Walgraef, M. San Miguel, and E. Hernández-García, Phys. Rev. Lett. **76**, 1956 (1996).
[14] H. Chaté, in *Spatiotemporal Patterns in Nonequilibrium Complex Systems*, edited by P. Cladis and P. Palffy-Muhoray, Santa Fe Institute in the Sciences of Complexity Vol. XXI (Addison-Wesley, New York, 1995), pp. 5–49.
[15] Our numerical integration is performed by a second order pseudospectral method described elsewhere [16]. Except when indicated explicitly, we use $L = 512$. Without loss of generality, $\mu = 1$. The initial condition is white Gaussian noise with a mean squared amplitude at each point of 0.002.
[16] R. Montagne, E. Hernández-García, A. Amengual, and M. San Miguel, Phys. Rev. E (to be published).
[17] K. Wisenfeld, C. Bracikowski, G. James, and R. Roy, Phys. Rev. Lett. **65**, 1749 (1990).
[18] M. G. Rosenblum, A. S. Pikovsky, and J. Kurths, Phys. Rev. Lett. **76**, 1804 (1996).
[19] R. J. McEliece, *The theory of Information and Coding: a Mathematical Framework for Communication*, Encyclopedia of Mathematics and its Applications (Addison-Wesley, New York, 1977), Vol. III.
[20] To calculate H and I we have discretized the range of possible values $0 < |A_i| < 1.1$ in $N = 200$ bins. Therefore, the maximum possible entropy is $\ln 200 = 5.3$.
[21] S. Popp *et al.*, Phys. Rev. Lett. **70**, 3880 (1993).

Noise-sustained structures in coupled complex Ginzburg-Landau equations for a convectively unstable system

M. Neufeld,[1] D. Walgraef,[1,2] and M. San Miguel[1,3]
[1]*Departament de Física, Universitat de les Illes Balears, E-07071 Palma de Mallorca, Spain*
[2]*Center for Nonlinear Phenomena and Complex Systems, Université Libre de Bruxelles, CP 231, B-1050 Brussels, Belgium*
[3]*Instituto Mediterraneo de Estudios Avanzados, IMEDEA (CSIC-UIB), E-07071 Palma de Mallorca, Spain*[1]*
(Received 15 April 1996)

We investigate a pattern-forming system close to a Hopf bifurcation with broken translational symmetry. In one-dimensional geometries, its evolution is governed by two coupled complex Ginzburg-Landau equations which describe the amplitude of the counterpropagating traveling waves that develop beyond the instability. The convective and absolute instabilities of the possible steady states are analyzed. In the regime of strong cross coupling, where traveling waves are favored by the dynamics, the results of previous analysis are recovered. In the weak cross-coupling regime, where standing waves are favored by the dynamics, traveling waves nevertheless appear, in the absence of noise, between the uniform steady state and the standing-wave patterns. In this regime, standing waves are sustained by spatially distributed external noise for all values of the bifurcation parameter beyond the Hopf bifurcation. Hence, the noise is not only able to sustain spatiotemporal patterns, but also to modify pattern selection processes in regimes of convective instability. In this weak coupling regime we also give a quantitative statistical characterization of the transition between deterministic and noise-sustained standing waves when varying the bifurcation parameter. We show that this transition occurs at a noise-shifted point and it is identified by an apparent divergence of a correlation time and the saturation of a correlation length to a value given by the system size. [S1063-651X(96)10412-8]

PACS number(s): 47.20.Ky, 02.50.Ey, 05.40.+j, 43.50.+y

I. INTRODUCTION

A series of physicochemical systems driven out of equilibrium undergo Hopf bifurcations with broken translational symmetries, which lead to the development of traveling or standing wave patterns. This is, for example, the case in Rayleigh-Bénard convection in binary or viscoelastic fluids [1], for spiral vortex flow in the Taylor-Couette system with counterrotating cylinders [2], or in electrohydrodynamic convection in liquid crystals [3]. Traveling rolls may also be obtained by the application of a through flow on hydrodynamic instabilities of the Rayleigh-Bénard or Taylor-Couette type [4–6]. As a result of the generic behavior of these systems in the vicinity of Hopf bifurcations, they may be described by coupled complex Ginzburg-Landau equations (CCGLE).

Effectively, it is now well known that, close to an instability, the spatiotemporal behavior of a system far from thermal equilibrium can be described by order-parameter-like equations [7–9]. The mathematical structure of these equations is rather universal and independent of the underlying physical system. The derivation of the order parameter equation from the basic evolution equations is made possible by the space-time separation between unstable and stable modes, and can be performed by different methods, such as adiabatic elimination of the stable, or "slaved" modes [8], or multiple scale analysis [9], for example.

In one-dimensional systems which undergo a Hopf bifurcation with broken spatial inversion symmetry, the order parameter field $\sigma(x,t)$ can be represented by two slowly varying envelope functions $A(x,t)$ and $B(x,t)$ for left and right traveling waves:

$$\sigma(x,t)=A(x,t)e^{i(k_c x+\omega_c t)}+B(x,t)e^{-i(k_c x-\omega_c t)}. \quad (1.1)$$

The evolution of the amplitude A and B is governed by CCGLE [7,10–14]. The nonlinear cross coupling between both amplitudes that determines if the stable patterns correspond to traveling (strong cross coupling) or standing (weak cross coupling) waves. The effect of the group velocity may usually not be discarded in the determination of the stability domain of the wave patterns. One has to distinguish between convective and absloute instability, and it is now well known that, sufficiently close to the Hopf bifurcation, the unpatterned state is convectively unstable but absolutely stable [5,13–17]. In this regime, localized perturbations are convected with the mean flow in such a way that they grow only in a moving reference frame but decay at any fixed location. On increasing the bifurcation parameter, one reaches a well defined threshold determined by the group velocity, and above which the reference state becomes absolutely unstable. In this regime, perturbations grow locally at fixed locations. As a result, the behavior of the system is qualitatively very different in both regimes. In the convectively unstable regime, a deterministic system cannot develop the expected wave patterns, except in special geometries, while in a stochastic system, noise is spatially amplified and gives rise to noise-sustained structures [15]. On the contrary, in the absolutely unstable regime, waves are intrinsically sustained by the deterministic dynamics.

Convectively unstable systems have been widely studied, both numerically and experimentally, but mostly in the case

[1]*URL: http://formentor.uib.es/Nonlinear/

of single traveling waves. This situation is modeled by a single CGLE which emerges in the strong cross-coupling regime. In this case Deissler [15] obtained numerically noise sustained structures in the convectively unstable regime. Babcock *et al.* [5] and Tsamaret *et al.* [6] analyzed in detail the corresponding experimental situation in the case of a Taylor-Couette system with through flow. Both groups observed the transition from convective to absolute instability and were able to generate noise-sustained structures. They also showed that structures sustained by dynamics or by noise have different statistical properties. This is, in particular, reflected by the behavior of their power spectrum which is essentially noise-free in the absolutely unstable regime and presents broadening in the convectively unstable regime. This broadening results from the phase wandering induced by noise amplification. The onset of spectral broadening corresponds to the absolute instability boundary, which may be slightly shifted, according to the noise intensity. As shown by Babcock *et al.* [5] the experimental results fit nicely with the numerical analysis of the corresponding amplitude equation which is of the complex Ginzburg-Landau type.

The problem of interacting noise-sustained counterpropagating waves was first studied by Deissler and Brand [13]. However, the lack of a detailed stability analysis of individual traveling waves did not allow a complete analysis of the problem. In particular, the distinction these authors make for positive and negative cross couplings between left and right traveling waves does not determine the stability of a traveling wave solution. Nevertheless, they presented qualitatively new results consisting in the possibility of obtaining transitions from convective to absolute instability and vice versa for a given set of parameters. Such transitions can easily be interpreted in the framework of the stability analysis of the uniform and traveling waves states.

It is the aim of this paper to study the effect of spatially distributed noise on convectively unstable systems, either for weak and strong cross couplings between counterpropagating waves, in the presence of group velocity. In Sec. II we introduce the CCGLE and study the linear stability of the uniform reference state and homogeneous traveling wave. We find five different regions with different stability properties in our parameter space. In particular we find that for weak cross coupling there is an intermediate regime between the uniform steady state and the standing wave patterns where traveling waves are convectively unstable. In Sec. III we present our stochastic numerical analysis in the five regions previously identified. We show that, in the weak cross-coupling regime, noise sustained standing waves appear for all values of the bifurcation parameter beyond the Hopf bifurcation. Finally, Sec. IV reports a statistical characterization of the transition between deterministic and noise-sustained standing waves in terms of the behavior of an average amplitude, correlation time, and correlation length. An appendix contains details of our numerical procedures.

II. COUPLED COMPLEX GINZBURG-LANDAU EQUATIONS. STABILITY ANALYSIS OF HOMOGENEOUS STATES

We consider the CCGLE which describe the dynamics of the amplitudes of two counterpropagating traveling waves with spatial variations in one direction:

$$\begin{aligned}
&\partial_t A(x,t) - v\,\partial_x A(x,t) \\
&\quad = \mu A(x,t) + (1+i\alpha)\partial_x^2 A(x,t) \\
&\quad - (1+i\beta)|A(x,t)|^2 A(x,t) - (\gamma + i\delta)|B(x,t)|^2 A(x,t) \\
&\quad + \sqrt{\varepsilon}\,\xi_A(x,t); \\
&\partial_t B(x,t) + v\,\partial_x B(x,t) \\
&\quad = \mu B(x,t) + (1+i\alpha)\partial_x^2 B(x,t) \\
&\quad - (1+i\beta)|B(x,t)|^2 B(x,t) - (\gamma + i\delta)|A(x,t)|^2 B(x,t) \\
&\quad + \sqrt{\varepsilon}\,\xi_B(x,t),
\end{aligned} \tag{2.1}$$

where $A(x,t)$ and $B(x,t)$ are the complex amplitudes of the right and left traveling waves. The control parameter μ measures the distance to the onset of the instability, v is the group velocity. The coefficients α, β, γ, and δ can be determined from the basic equations of the underlying physical system. A Gaussian, delta correlated, complex white noise of strength level denoted by ε, $\xi_j(x,t)$, $j=A,B$ is assumed to be present in the system. This noise can be spatially distributed or localized (for example, at the inlet of a Taylor-Couette system with through flow). We will consider in this paper a spatially distributed noise with vanishing correlation length (white noise in space and time).

Next we analyze, from a deterministic point of view ($\varepsilon=0$) the linear stability of homogeneous solutions of Eqs. (2.1).

A. Stability of the uniform reference state

Linearizing the equations (2.1) around the trivial solution $A(x,t) = B(x,t) = 0$, the complex dispersion relation ω for a disturbance of wave number K, that thus behaves as $e^{\omega t + Kx}$, becomes:

$$\omega = \mu + Kv + (1+i\alpha)K^2, \quad K = k + iq, \tag{2.2}$$

and the growth rate of such a perturbation is given by $\mathrm{Re}\,\omega(K)$. Using the method of steepest descent, the long-time behavior of the system along a ray defined by fixed x/t, i.e. in a frame moving with a velocity $v_0 = x/t$, is governed by the saddle point defined by:

$$\mathrm{Re}\left(\frac{d\omega}{dK}\right) = v_0, \quad \mathrm{Im}\left(\frac{d\omega}{dK}\right). \tag{2.3}$$

Since absolute instability occurs when perturbations grow at fixed locations, one has to consider the growth rate of modes evolving with zero group velocity, which are defined by:

$$\mathrm{Re}\left(\frac{d\omega}{dK}\right) = \mathrm{Im}\left(\frac{d\omega}{dK}\right) = 0. \tag{2.4}$$

These conditions define the following wave number:

$$q=-\alpha k,$$

$$k=-\frac{v}{2(1+\alpha^2)}. \tag{2.5}$$

The real part of ω, which determines the growth rate λ of these modes is then:

$$\lambda=\mathrm{Re}(\omega)=\mu-\frac{v^2}{4(1+\alpha^2)}. \tag{2.6}$$

Therefore, the uniform reference state is absolutely unstable if $\lambda>0$. As already shown in [15], this condition determines a critical line in the parameter space which can be expressed for the group velocity v or the control parameter μ as

$$v_c=2\sqrt{\mu(1+\alpha^2)} \quad \text{or} \quad \mu_c=\frac{v^2}{4(1+\alpha^2)}. \tag{2.7}$$

Hence, for $0<\mu<\mu_c$, the uniform reference state is convectively unstable, and wave patterns are convected away in the absence of noise. For $\mu>\mu_c$, wave patterns may grow and are sustained by the dynamics, even in the absence of noise [15].

B. Stability of the uniform traveling wave

The CGLE (2.1) admits two families of solutions corresponding to traveling waves, $A=\sqrt{\mu-k^2}\exp i[kx-(\beta\mu+\alpha k^2)t]$, $B(x,t)=0$, and $B=\sqrt{\mu-k^2}\exp i[kx-(\beta\mu+\alpha k^2)t]$, $A(x,t)=0$. For the sake of simplicity, we first consider uniform solutions ($k=0$). Without loss of generality, one may study the first family, and, in order to analyze its linear stability, one has to look for solutions in the form $A=(\sqrt{\mu}+a)\exp -i\beta\mu t$, $B(x,t)=b$, and compute the eigenvalues of the linearized evolution equations for a, b, and their complex conjugate. The real parts of the eigenvalues of the Fourier transform of a are well known (see, for example, [7] and [18]) and read:

$$\mathrm{Re}\omega_{|a|}=-2\mu-(1-\alpha\beta)q^2+\cdots,$$

$$\mathrm{Re}\omega_{\phi}=-(1+\alpha\beta)q^2-\frac{\alpha^2(1+\beta^2)}{2\mu}q^4+\cdots. \tag{2.8}$$

The first one, associated with amplitude, is always negative, but the second one, associated with phase, may become positive and the system may experience a Benjamin-Feir instability when $1+\alpha\beta$ is negative [19,20]. In the following, we will consider systems where α and β are small and positive, such that $1+\alpha\beta>0$.

The only remaining instability mechanism may then result from the growth of B. Effectively, the linearized evolution equations for b give the following growth rate:

$$\omega_B=\mu(1-\gamma)-Kv+(1+i\alpha)K^2. \tag{2.9}$$

Hence, in the absence of group velocity, single traveling waves are always stable for $\gamma>1$, while they are unstable for $\gamma<1$ leading to standing wave solutions with $|A|=|B|\neq 0$. The condition $\gamma=1$ thus separates the strong cross-coupling regime ($\gamma>1$) from the weak cross-coupling regime ($\gamma<1$). Note that the point $\gamma=0$ does not play any particular role in the stability of traveling waves.

In the presence of a nonvanishing group velocity, traveling waves remain stable for $\gamma>1$, while for $\gamma<1$, they are convectively unstable for $\mu<\mu_c'$, where μ_c' is determined similarly to the preceeding case. Effectively, the conditions

$$\mathrm{Re}\left(\frac{d\omega_B}{dK}\right)=\mathrm{Im}\left(\frac{d\omega_B}{dK}\right)=0 \tag{2.10}$$

define the same wave number

$$q=-\alpha k,$$

$$k=-\frac{v}{2(1+\alpha^2)}. \tag{2.11}$$

However, the real part of ω_B, which determines the growth rate of the corresponding modes, is now:

$$\lambda_B=\mathrm{Re}(\omega_B)=\mu(1-\gamma)-\frac{v^2}{4(1+\alpha^2)} \tag{2.12}$$

and

$$\mu_c'=\frac{v^2}{4(1-\gamma)(1+\alpha^2)}<\mu_c. \tag{2.13}$$

The corresponding critical group velocity is $v_c'=v_c\sqrt{1-\gamma}$ or

$$\gamma_c=1-\frac{v^2}{4\mu(1+\alpha^2)}. \tag{2.14}$$

As a result, on increasing the bifurcation parameter in deterministic systems at fixed v and with $\gamma<1$, traveling waves should be expected between the trivial uniform state and standing waves, as shown on the phase diagram displayed in Fig. 1.

The above deterministic linear stability analysis divides, for v fixed, the μ-γ parameter space in five regions of different spatiotemporal behavior which we label as follows (cf. Fig. 1):

$$\left.\begin{array}{lll} 1: & \mu<\mu_c & O \\ 2: & \mu_c<\mu & \mathrm{TW} \end{array}\right\}\ \gamma>1,$$

$$\left.\begin{array}{lll} 3: & \mu<\mu_c & O \\ 4: & \mu_c<\mu<\dfrac{\mu_c}{1-\gamma} & \mathrm{TW} \\ 5: & \dfrac{\mu_c}{1-\gamma}<\mu & \mathrm{SW} \end{array}\right\}\ \gamma<1. \tag{2.15}$$

In the strong cross-coupling regime ($\gamma>1$) we distinguish two regions. In region 1 the uniform reference state (O) is convectively unstable and it becomes absolute unstable in region 2 where a traveling wave (TW) is absolutely stable. In the weak cross-coupling regime ($\gamma<1$) we find three regions. In region 3 the uniform reference state (O) is convectively

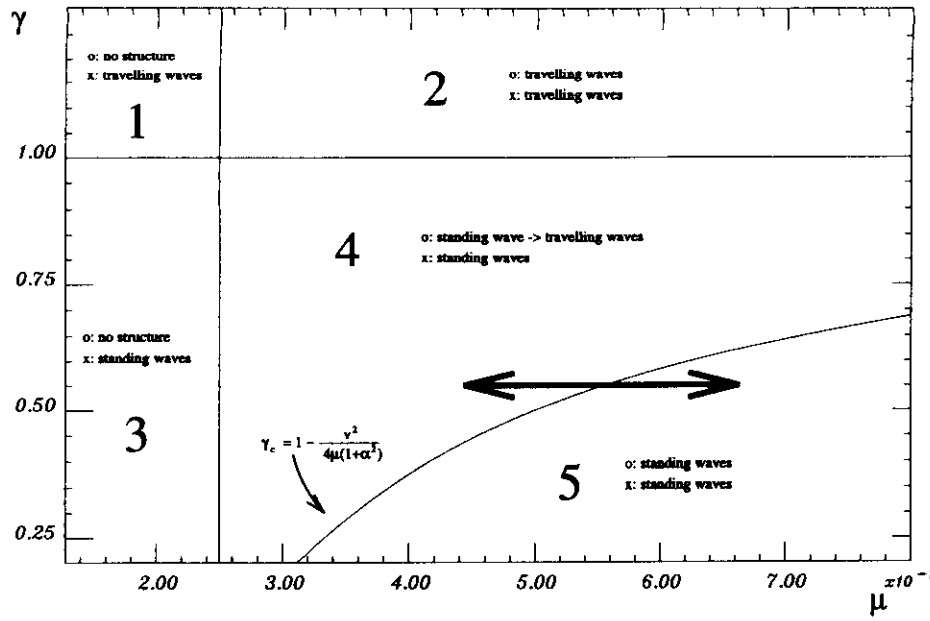

FIG. 1. Stability diagram for homogeneous solutions of Eqs. (2.1). The numbers 1–5 denote regions of different spatiotemporal behavior, as discussed in the text. o stands for the deterministic case ($\varepsilon=0$), x stands for the stochastic case ($\varepsilon\neq 0$). Parameter values are $\alpha=0.02$, $\beta=0.04$, $\delta=0.05$, and $v=1$.

unstable, while in region 4 the traveling wave is the convectively unstable solution. This latter solution becomes absolutely unstable in region 5 where the standing wave (SW) solution is absolutely stable, since we are considering values of α, β, and δ sufficiently small to satisfy the standing waves phase stability condition $1+\alpha(\beta-\gamma\delta)/(1-\gamma^2)$ [10,21].

These results can easily be generalized to traveling waves solutions with nonzero wave numbers ($k\neq 0$). In this case, a perturbations decay if the Benjamin-Feir-Eckhaus criterion $1+\alpha\beta-(2k^2/\mu-k^2)>0$ is satisfied, while b perturbations grow locally when $\mu(1-\gamma)+\gamma k^2-v^2/4(1+\alpha^2)$ is positive.

We finally note that the absolute instability criteria derived in this section are a direct consequence of the criterion derived in Sec. II A and Ref. [15], where the linear growth rate of the 0 state, μ, is replaced by its effective linear growth rate $\mu-\gamma|A|^2$. This replacement was noted in [13] and it can be interpreted (depending on the sign of γ) as a stabilizing or destabilizing effect of the wave A on the wave B. However, as shown above, the sign of γ does not determine stability boundaries of the traveling wave solution $A=\sqrt{\mu-k^2}\exp i[kx-(\beta\mu+\alpha k^2)t]$, $B(x,t)=0$.

III. NOISE-SUSTAINED STRUCTURES

In this section we analyze numerically the effect of spatially distributed noise on the homogeneous solutions of the CCGLE (2.1). We will explore the parameter space by varying the cross-coupling parameter γ and the reduced distance to threshold μ while keeping the group velocity v set to 1. We note that this is equivalent to the variation of γ and v with μ fixed, thanks to the scaling

$$A=\mu^{1/2}A',\quad B=\mu^{1/2}B',\quad T=\mu^{-1}t,$$

$$X=\mu^{-1/2}x\rightarrow v'=\frac{v}{\sqrt{\mu}}. \tag{3.1}$$

In addition we will fix the noise level to $\varepsilon=0.0001$ and we assign fixed values to the other parameters of (2.1): $\alpha=0.02$, $\beta=0.04$, and $\delta=0.05$. These values belong to the domain of parameters in which the CGLE does not show phase instabilities of the homogenous solutions leading to chaotic behavior.

Noise is expected to be amplified by the convective terms leading to noise-sustained structures in regions where the reference state is deterministically convectively unstable. Therefore, we anticipate that noise effects will result in TW states in the strong coupling regime (regions 1 and 2 of Fig. 1), being noise sustained in region 1. Likewise we anticipate finding SW states in regions 3, 4, and 5 of Fig. 1 corresponding to weak cross coupling. This implies that noise transforms a O state into a noise-sustained SW in region 3 and a TW state into a noise-sustained SW in region 4.

In order to check these predictions the stochastic CCGLE (2.1) have been solved numerically with a Heun method (cf. Appendix), random initial conditions around the $A=B=0$ solution, and the following boundary conditions: at the upstream end of each amplitude we use a rigid boundary condition

$$A(L,t)=0,\quad B(0,t)=0. \tag{3.2}$$

It turned out to be unimportant for the downstream part of the system whether the inlet is fixed or is fluctuating with the noise level [5]. We also checked boundary conditions with a subcritical part ($\mu<0$) in front of the inlet ($x<0$, $x>L$). This influenced only a very small portion of the system near $x=0$ and $x=L$. Different boundary conditions on the outstream end have also a very small influence on the bulk of the system [5,22]. We furthermore used a vanishing derivative at the outstream end of each amplitude:

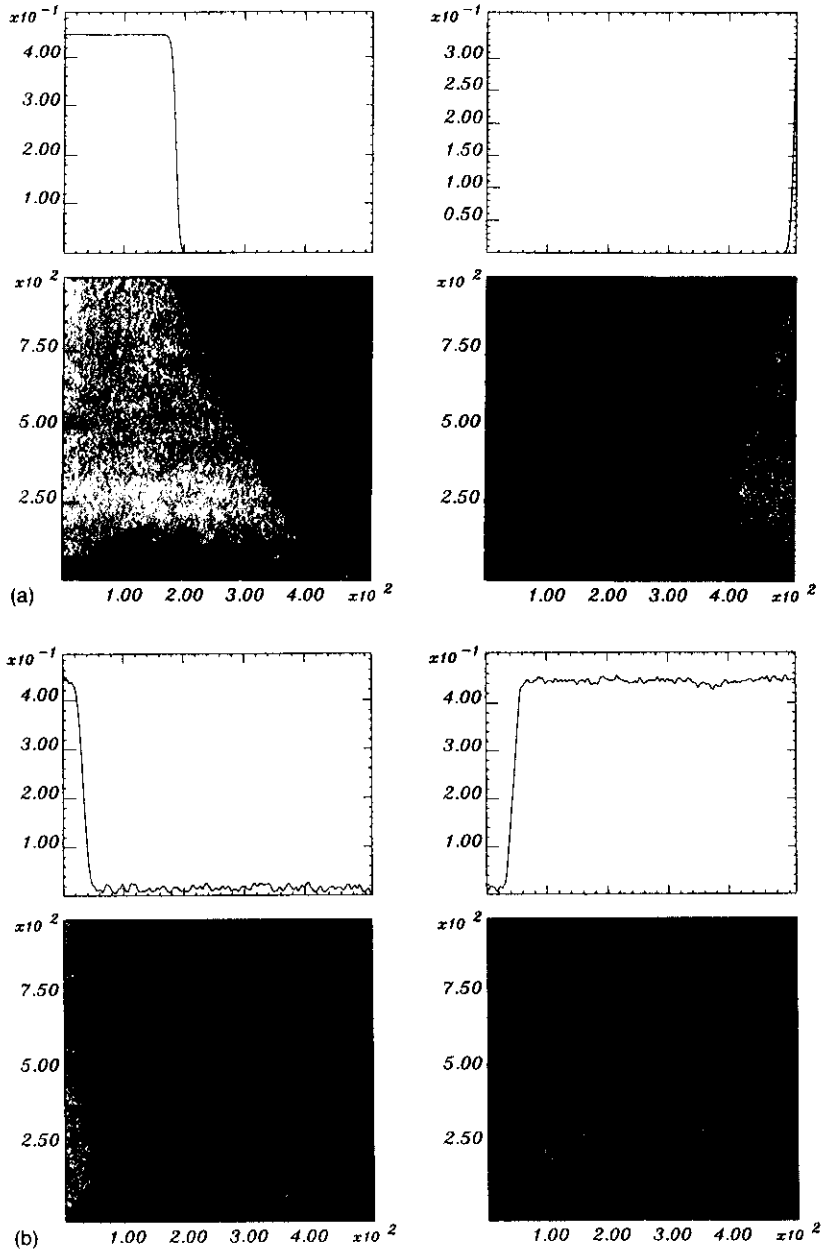

FIG. 2. Space (horizontal axis)-time (vertical axis) plot of the moduli of the amplitudes $A(x,t)$ (left) and $B(x,t)$ (right), in arbitrary units, in the region 1 of Fig. 1 ($\gamma=1.2$, $\mu=0.165$, $v=1$). The upper diagrams show the spatial dependence of A and B at the end of the space-time plots. In this region the trivial state $[A(x,t)=B(x,t)=0]$ is convectively unstable. (a) Deterministic case ($\varepsilon=0$). The disturbances of the initial random pattern are convected out of the system. (b) Same as (a) but for the stochastic case ($\varepsilon=0.0001$). Due to the strong cross-coupling ($\gamma>1$), only a traveling wave structure can survive. The spatially distributed noise effectively sustains the traveling wave structure.

$$\partial_x A(0,t)=0, \quad \partial_x B(L,t)=0. \tag{3.3}$$

These boundary conditions mimic extended systems with no reflection of the individual traveling waves at the ends of the system. As such, they rule out the possibility of standing waves maintained by end effects, as it occurs for example in binary fluid convection, even in the absence of noise [23]. In this case, even in the convectively unstable regime, counterpropagating waves, emitted at the boundaries are not entirely convected out of the system since they are partially reflected at each opposite boundary and may thus build an effective but artificial standing wave pattern in the bulk. With the boundary condition used here this effect is absent and no boundary effect should thus interfere with the stochastic effects that we analyze.

A. Strong cross-coupling, $\gamma>1$

Due to the fact that the real part of the cross coupling parameter ($\gamma>1$) between the two fields is larger than the real part of the self coupling ($1+i\beta$), traveling waves should be the selected pattern in this domain. Due to the symmetry between A and B, a competition between these two traveling waves may be observed.

In region 1, where the group velocity is larger than the critical one ($\mu<\mu_c$ or $v_c<v$) all structures are convected out of the system in the deterministic case ($\varepsilon=0$), which leads to a stable trivial state with no structure [cf. Fig. 2(a)]. Noise-sustained traveling waves can, however, be observed [cf. Fig. 2(b)]. In the stochastic case one of the traveling waves reaches its saturation value in the bulk and suppresses the other one. There exists a layer at the inlet with a width depending on the distance to the instability μ and the noise

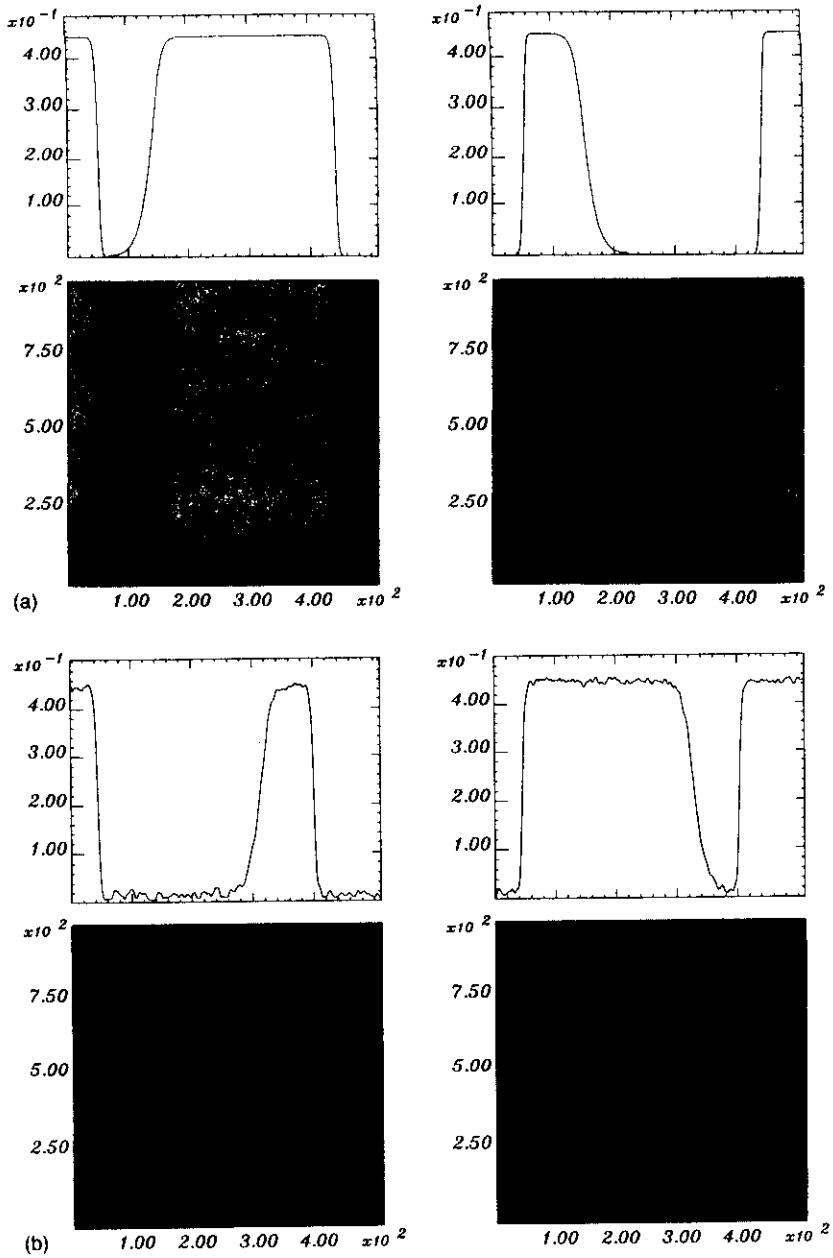

FIG. 3. Same as Fig. 2 in region 2 of Fig. 1 ($\gamma=1.2$, $\mu=0.8$, $v=1$). In this region the trivial state $[A(x,t)=B(x,t)=0]$ is absolutely unstable. The disturbances of the initial random pattern create a traveling wave pattern. The locations of the sources and sinks (fronts between right and left traveling waves) depend on the initial condition as well as on the noise. There is no qualitative difference between the deterministic case (a) ($\varepsilon=0$) and the stochastic case (b) ($\varepsilon=0.0001$).

level ε. The noise-sustained structure is thus created due to the convectively unstable amplification of the noise as already discussed in [5,15].

In region 2 ($\mu_c<\mu$ or $v<v_c$) the final states are traveling waves for both cases (deterministic, stochastic). Depending on the initial conditions the system exhibits regions where one of the two traveling waves survives [cf. Figs. 3(a), 3(b)]. Between the right and left traveling wave regions emerge sharp fronts which are called sources and sinks. The motion of these fronts has a very large time scale compared to the emergence of the patterns and have not been studied in this work.

B. Weak cross-coupling, $\gamma<1$

When the cross-coupling ($\gamma<1$) is small, the selected patterns should correspond to standing waves. Coexistence of the two traveling waves can be observed. The modulus of the two amplitudes can reach the same value which is the condition for standing waves.

If the group velocity is smaller than the critical value for the absolute instability of the traveling wave state [(region 5) $v<v_c'$ or $\mu_c'<\mu$] there is no qualitative difference between the final states, which consist in a standing wave structure [cf. Figs. 4(a), 4(b)].

In the region 4 where the traveling wave state is absolutely stable and the velocity is smaller than the critical velocity for stability of the trivial state ($v_c'<v<v_c$ or $\mu_c<\mu<\mu_c'$) one observes different spatiotemporal behavior in the deterministic and the stochastic case [cf. Figs. 5(a), 5(b)]. In absence of noise ($\varepsilon=0$), the first transition, during the time evolution, is from a random initial condition to a standing wave structure. Due to front propagation this state

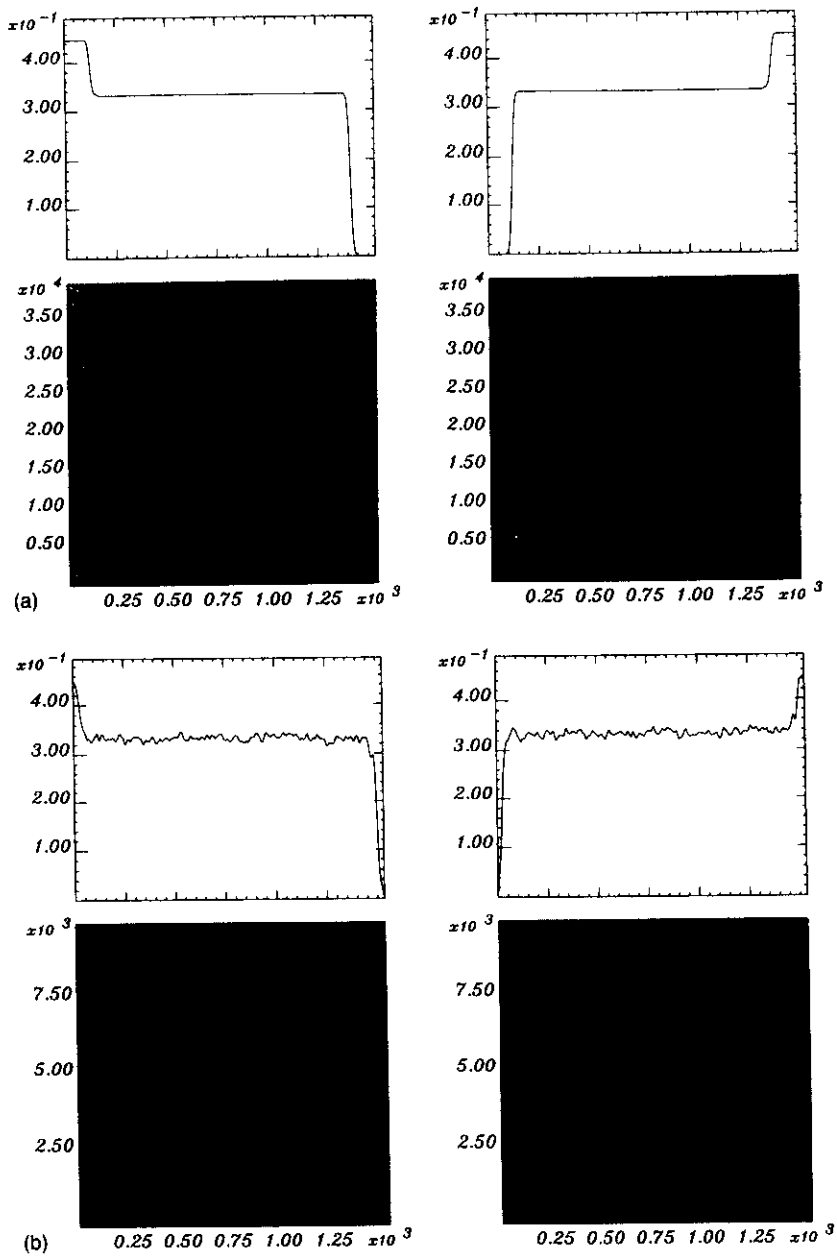

FIG. 4. Same as Fig. 2 in region 5 of Fig. 1 ($\gamma=0.8$, $\mu=1.385$, $v=1$). The disturbances of the initial random pattern create a standing wave pattern. There is no qualitative difference between the deterministic (a) ($\varepsilon=0$) and the stochastic case (b) ($\varepsilon=0.0001$).

is replaced by an exactly symmetric traveling wave structure due to the symmetric boundary conditions [cf. Fig. 5(a)]. If noise effects are included ($\varepsilon\neq 0$) a standing wave structure is sustained [cf. Fig. 5(b)]. It is important to note that in this case noise changes the nature of the observed spatial structure: In region 1, noise sustains a pattern where there is no pattern with no noise [5,15], but here noise transforms a deterministic TW structure into a noise sustained SW structure.

When the group velocity overcomes the critical value for stability of the trivial state [(region 3) $\mu<\mu_c$ or $v_c<v$] a complicated noise-sustained structure arises. This structure has the main features of a standing wave structure sustained by spatially distributed noise, with a bulk region which fluctuates around the deterministic values for the standing wave solution. From time to time one observes holes (peaks) which are convected through the structure (cf. Fig. 6). Note that the results presented in Fig. 1 of the numerical study performed by Deissler and Brand [13] also correspond to this region of the parameter space where both uniform and traveling wave states are convectively unstable but absolutely stable. Different to us, these authors consider only localized noise at the boundaries. Such a noise source is able to sustain two traveling waves, each of which only fills the half of the system which includes the boundary where it originates. These TWs are convected out of the system when the noise is suppressed. On the contrary, Fig. 2 of [13] presents a situation where, according to our stability analysis, the uniform state is convectively unstable while the traveling wave state is absolutely unstable ($\mu_c'<\mu<\mu_c$ with $\mu_c'<\mu_c$ since $\gamma<0$). In this case, localized noise generates traveling waves which, as the result of their absolute instability, should be

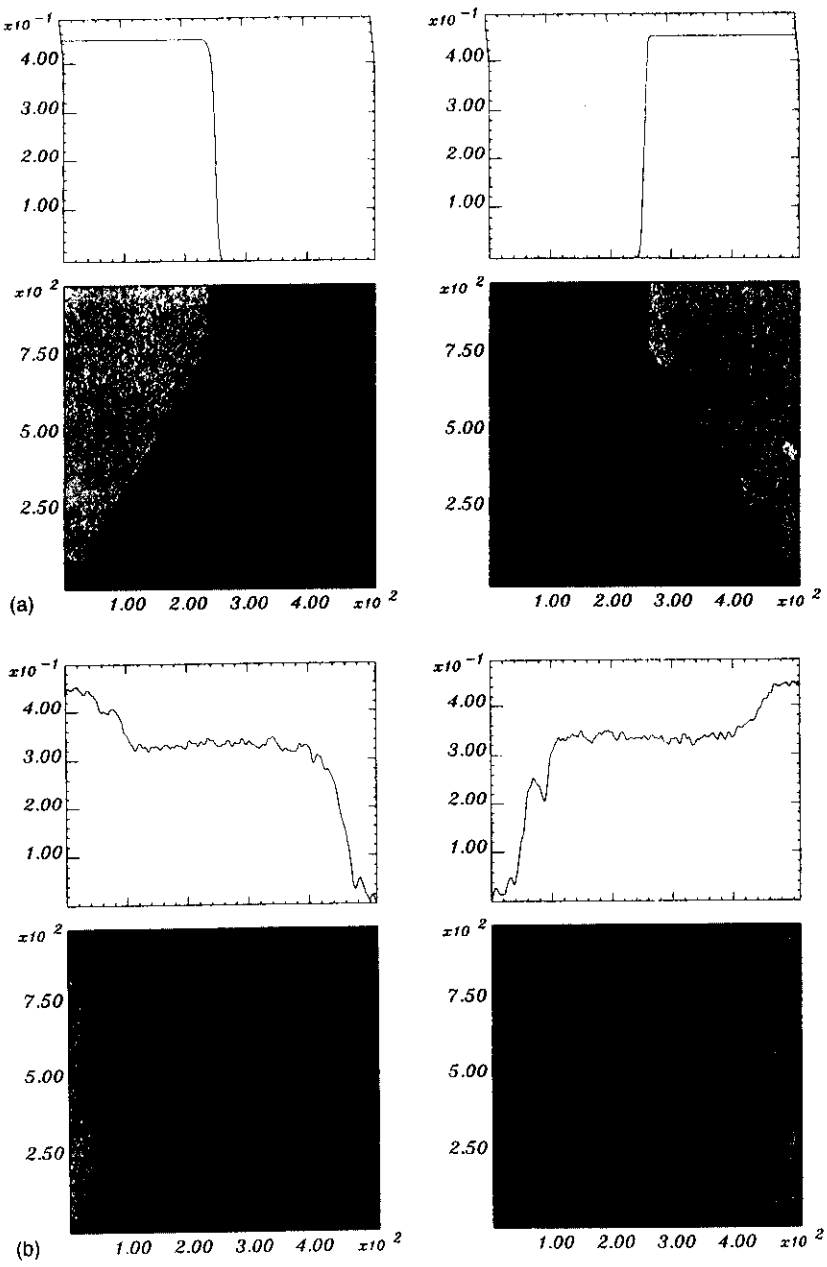

FIG. 5. Same as Fig. 2 in region 4 of Fig. 1 ($\gamma=0.8$, $\mu=0.408$, $v=1$). (a) Deterministic case ($\varepsilon=0$): the disturbances of the initial random pattern create initially a standing wave pattern which is replaced, due to front propagation, by a symmetric traveling wave pattern. (b) Stochastic case ($\varepsilon=0.0001$): the spatially distributed noise gives rise, in the bulk of the system, to a noise-sustained standing wave structure fluctuating around the deterministic value.

transformed into standing waves which persist after noise removal, in complete agreement with the numerical results of [13].

IV. CHARACTERIZATION OF THE TRANSITION FROM SW TO NOISE-SUSTAINED SW

The boundary between regions 4 and 5 of Fig. 1 identifies a transition between convective and absolute instability of the traveling wave state (cf. arrow in Fig. 1). When noise is taken into account this transition is transformed into one between a deterministic SW structure and a noise-sustained SW. In this section we give a quantitative statistical characterization of this new type of transition investigating the behavior through the transition of different quantities such as amplitudes, correlation time, and correlation length. Our analysis has similarities with the analysis in [5] of the transition between deterministic TW structures and noise-sustained TW (boundary between regions 1 and 2 of Fig. 1).

A. Modulus of the amplitude

The time average value of the amplitude A at a fixed space point, calculated with no noise ($\varepsilon=0$), exhibits the deterministic transition between traveling and standing waves at the critical value μ_c'. In the region of stable standing waves ($\mu>\mu_c'$), the amplitude has its stationary standing wave value $\langle|A(x,t)|^2\rangle=\mu/(1+\gamma)$, which bifurcates to the stationary value of the traveling wave $\langle|A(x,t)|^2\rangle=\mu$ at the critical value $\mu=\mu_c'$ (cf. Fig. 7). However, the same calculation taking noise into acount shows no trace of the transition: the amplitude has the same averaged value for a deterministic or a noise-sustained standing wave. In order to

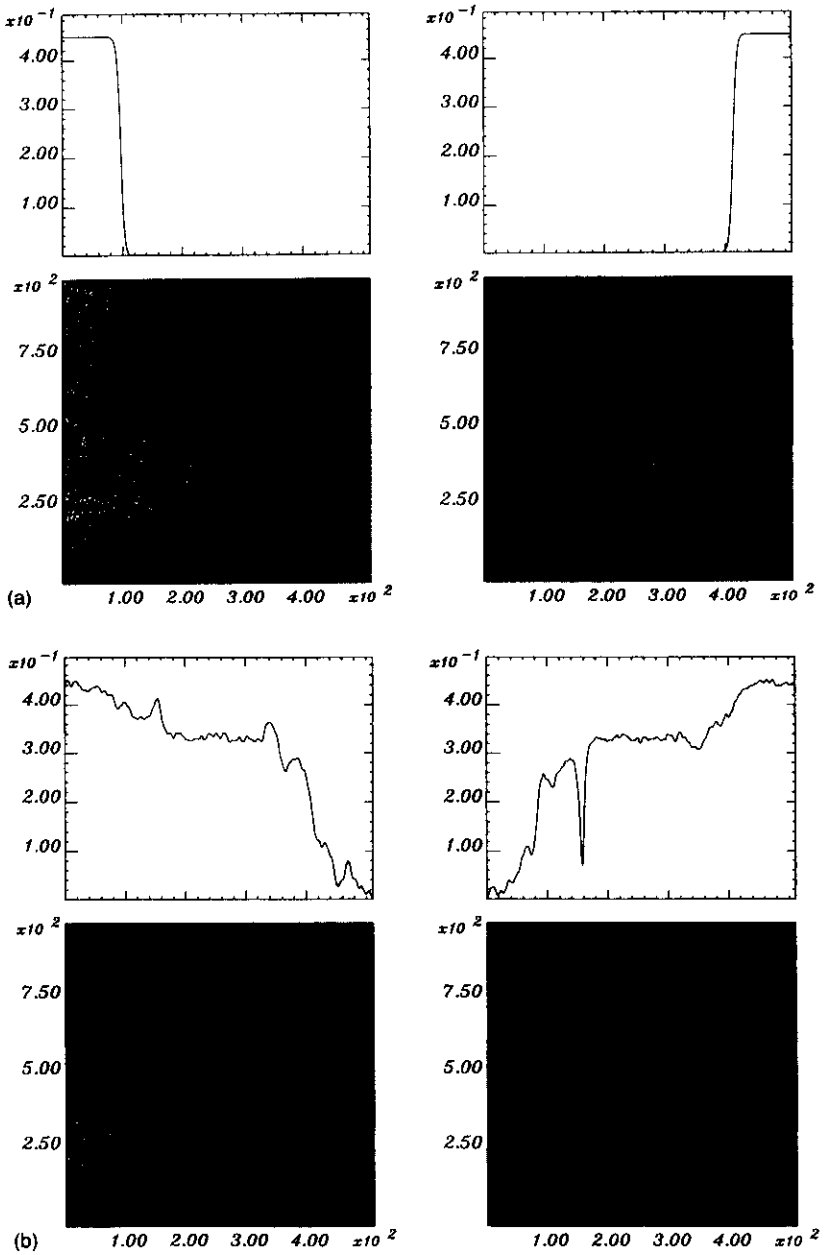

FIG. 6. Same as Fig. 2 in region 3 of Fig. 1 (γ=0.8, μ=0.165, v=1). (a) In the deterministic case the structure is convected out of the system which goes back to the trivial solution. (b) Stochastic case (ε=0.0001): a complicated spatiotemporal structure can be observed. The bulk fluctuates around the deterministic value of the standing wave pattern but from time to time a hole (peak) is convected through the pattern.

characterize the transition between deterministic and noise-sustained standing waves we need to consider quantities giving some information on the degree of temporal or spatial order, as we do next.

B. Correlation time

We can calculate a correlation time by considering the width of the power spectrum $A(x_0,w)$ of a time series $A(x_0,t)$ at a fixed location x_0 in the bulk. Since we deal with spatially distributed noise and symmetric boundary conditions, $A(x_0,w)$ is statistically independent of x_0. We then consider an averaged correlation time σ_t^{-1} defined in terms of the spatially averaged second moment of the power spectrum:

$$\bar{\omega}=\left\langle \frac{\int d\omega |A(x_0,\omega)|^2 \omega}{\int d\omega |A(x_0,\omega)|^2} \right\rangle ,$$

$$\sigma_t^2=\left\langle \frac{\int d\omega |A(x_0,\omega)|^2 (\omega-\bar{\omega})^2}{\int d\omega |A(x_0,\omega)|^2} \right\rangle , \qquad (4.1)$$

where $\langle\cdots\rangle$ stands for the spatial average in the interval $0<x<L$.

In Fig. 8 we plot the inverse correlation time σ_t as a function of μ. The vertical line marks the critical value μ_c'

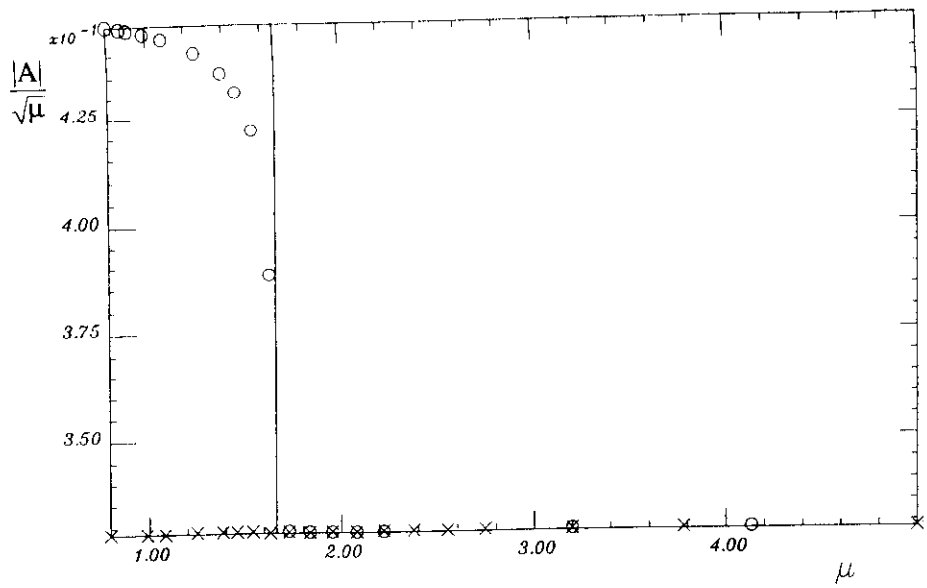

FIG. 7. The time averaged value of $|A|/\sqrt{\mu}$ at a fixed spatial point plotted as a function of the bifurcation parameter for the stochastic (x) and deterministic cases (o). The vertical scale is normalized to the value of $|A|$ for $\mu=0.2$, and the cross-coupling parameter is $\gamma=0.85$. The vertical line denotes the critical control parameter μ_c' given by Eq. (2.10).

for the instability of the traveling wave solution. We see that no change of behavior is observed in the deterministic case ($\varepsilon=0$): a narrow power spectrum exists either for deterministic traveling waves $\mu<\mu_c'$ or for deterministic standing waves $\mu>\mu_c'$. However, when noise is taken into account a rather sharp transition is observed between a narrow power spectrum for deterministic standing waves and a wide power spectrum associated with a noise-sustained standing wave. The transition is identified by an apparent divergence of the correlation time σ_t^{-1}. Such divergence occurs for a value of μ which is shifted with respect to the one identified in a deterministic analysis as the limit for convective instability of traveling waves ($\mu=\mu_c'$). Noise induced shifts of instability boundaries is a rather well known phenomena, and the numerical and experimental results reported in [5] for a transition between regions 1 and 2 of Fig. 1 do not seem to be inconsistent with the possibility of such shift.

C. Correlation length

As an alternative characterization we now consider a correlation length σ_x^{-1} which gives a quantitative characterization of the spatial fluctuations. It is defined in terms of the width σ_x of the time averaged Fourier spectrum $A(k,t)$ of the amplitude $A(x,t)$:

$$\sigma_x^2=\left\langle \frac{\int dk|A(k,t)|^2(k-\bar{k})^2}{\int dk|A(k,t)|^2} \right\rangle , \tag{4.2}$$

where $\langle\cdots\rangle$ stands now for the time average in a large time window $t_0<t<t_0+T$.

Figure 9 shows the correlation length σ_x^{-1} under variation of the bifurcation parameter μ. A transition is clearly identi-

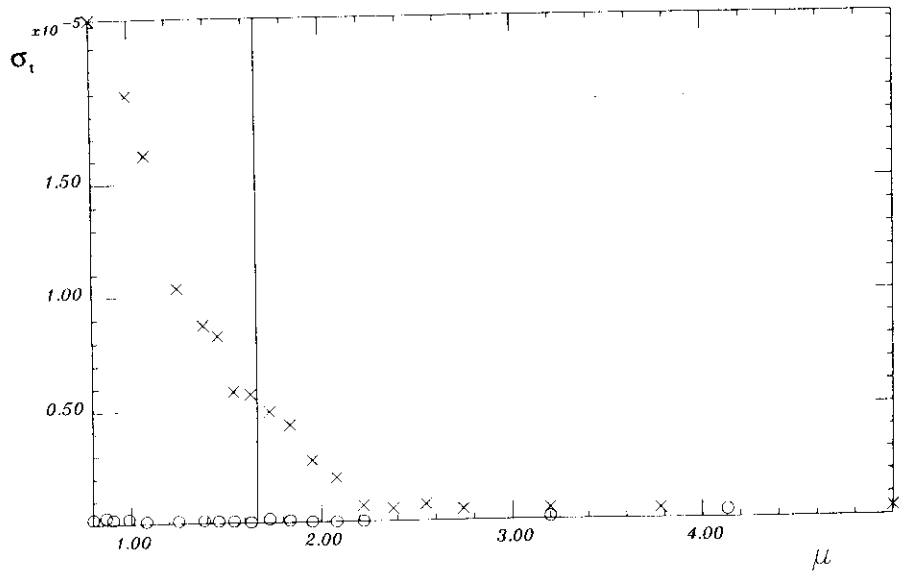

FIG. 8. Width of the power spectrum, in arbitrary units, as given by Eq. (4.1) as a function of the bifurcation parameter for the stochastic (x) and deterministic cases (o). Vertical line as in Fig. 7 and $\gamma=0.85$.

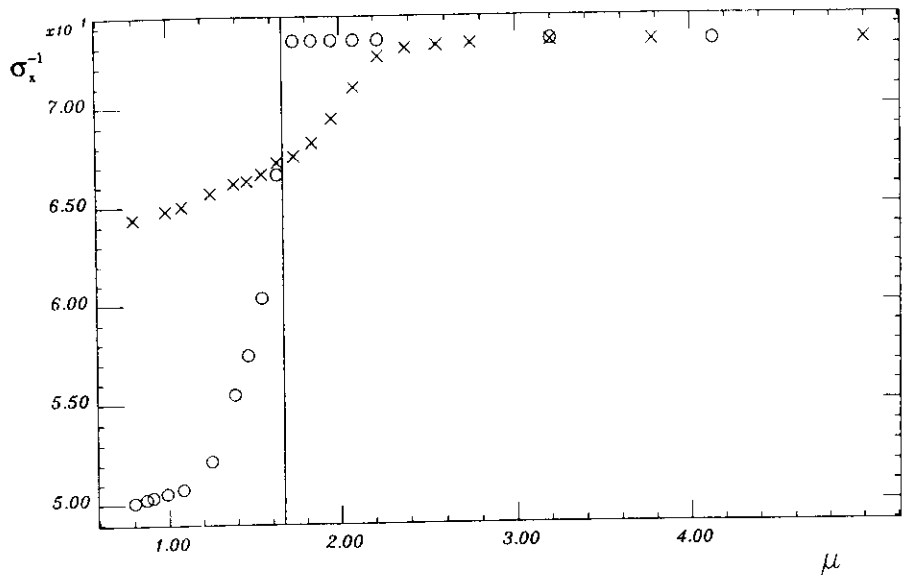

FIG. 9. Correlation length, in arbitrary units, as given by Eq. (4.2) as a function of the bifurcation parameter for the stochastic (x) and deterministic cases (o). Vertical line as in Fig. 7 and $\gamma=0.85$.

fied at the same shifted instability point at which the correlation time diverges. At this value of μ the correlation length saturates here to the system size, while for smaller values of μ we obtain a smaller correlation length indicating absence of long range order associated with a noise-sustained structure. On the other hand, the deterministic equation ($\varepsilon=0$) shows a transition exactly at the value μ_c' which is predicted in the linear stability analysis (Sec. II). For $\mu>\mu_c'$ the correlation length also saturates to the system size, while for $\mu<\mu_c'$ it goes to a value which is a factor $1/\sqrt{2}$ smaller. This factor is a matter of the definition used for the correlation length of the amplitude A. It can be easily understood by noting that for $\mu>\mu_c'$ the wave with amplitude A fills the whole system in a standing wave state, while for $\mu<\mu_c'$ it only fills half of the system in the traveling wave state [compare Figs. 4(a) and 5(a)].

V. CONCLUSION

In this paper, we have studied the effect of noise on coupled complex Ginzburg-Landau equations on varying not only control parameters such as the distance to threshold μ or the group velocity v, but also the cross coupling γ between individual counter-propagating traveling waves. In the strong coupling regime ($\gamma>1$), we recover the results obtained by other authors, namely, the development of noise-sustained traveling waves. In the small coupling regime ($\gamma<1$), we show that there is an intermediate region between the trivial uniform state and the standing wave domain where traveling waves are convectively unstable. Our deterministic numerical analysis confirms this result since one observes, on increasing the bifurcation parameter (or decreasing the group velocity), transitions from the trivial state to traveling waves, and finally to standing waves. In the presence of spatially distributed noise our stochastic numerical analyis shows that sustained standing waves are obtained in all the domain beyond the Hopf bifurcation. Therefore, in the intermediate region mentioned above, noise amplification by the convective terms transforms a traveling wave structure into a noise-sustained standing wave structure. Hence, we conclude that noise is not only able to sustain spatiotemporal patterns, but also to modify pattern selection processes in regimes of convective instability. In addition, we have given a quantitative statistical characterization of the transition between deterministic and noise-sustained standing waves. We have shown that this transition occurs at a noise-shifted point with respect to the one at which traveling waves become absolutely unstable. The transition is identified by an apparent divergence of a correlation time and the saturation of a correlation length to a value given by the system size.

ACKNOWLEDGMENTS

M.N. was supported by a grant from the Direccion General de Investigacion Cientifica y Tecnica (DGICYT, Spain). D.W. also benefited from the support of the DGICYT, through a grant for a sabbatical stay. We acknowledge financial support from the DGICYT grant PB94-1167. We would also like to thank Raúl Toral for making available a library to create Gaussian distributed random numbers on our computer cluster as well as for his discussions and help during the creation and testing of the numerical integrator. We also acknowledge helpful discussions with H. Brand.

APPENDIX: NUMERICAL METHOD

The discretized time integration of the CCGLE (2.1) was performed with a second order Runge-Kutta algorithm (Heun method in vector form) [24]

$$\partial_t \mathbf{A}(x,t)=\mathbf{F}(\mathbf{A}(x,t))+\sqrt{\varepsilon}\,\boldsymbol{\xi}(x,t). \tag{A1}$$

The Heun recursion relation prescribes

$$\mathbf{g}_1(x,t)=\mathbf{F}(\mathbf{A}(x,t)),$$

$$\mathbf{g}_2(x,t)=\mathbf{F}\left(\mathbf{A}(x,t)+\Delta t\,\mathbf{g}_1(x,t)+\sqrt{\frac{\varepsilon\Delta t}{(\Delta x)^n}}\mathbf{u}(x,t)\right),$$

$$\mathbf{A}(x,t+\Delta t)=\mathbf{A}(x,t)+\frac{\Delta t}{2}[\mathbf{g}_1(x,t)+\mathbf{g}_2(x,t)]+\sqrt{\frac{\varepsilon\Delta t}{(\Delta x)^n}}\mathbf{u}(x,t), \tag{A2}$$

where $u_i(x,t)$ are independent random variables with unit variance and vanishing mean value, and n denotes the dimension of the spatial coordinates. The correlation of the noise variables have the form

$$\langle\xi_\alpha^a,\xi_\beta^b\rangle=\varepsilon\,\delta_{\alpha,\beta}\delta_{a,b}\delta(x-x',t-t'), \tag{A3}$$

with $a,b=\mathrm{Re,Im}$ and $\alpha,\beta=A,B$.

[1] J.J. Niemela, G. Ahlers, and D.S. Cannell, Phys. Rev. Lett. **64**, 1365 (1990); K.E. Anderson and R.P. Behringer, Phys. Lett. **A145**, 323 (1990); P. Kolodner, Phys. Rev. Lett. **66**, 1165 (1991).

[2] S. Snyder, Phys. Fluids **11**, 728 (1968); C.D. Andereck, S.S. Liu, and H.L. Swinney, J. Fluid. Mech. **164**, 155 (1986).

[3] A. Joets and R. Ribotta, in *Propagation in Systems far from Thermal Equilibrium*, edited by J.E. Wesfreid, H.R. Brand, P. Manneville, G. Albinet, and N. Boccara (Springer, Berlin, 1988).

[4] K.L. Babcock, D.D. Cannell, and G. Ahlers, Phys. Rev. Lett. **67**, 3388 (1991); Physica D **61**, 40 (1992).

[5] K.L. Babcock, G. Ahlers, and D.S. Cannell, Phys. Rev. E **50**, 3670 (1994).

[6] A. Tsameret and V. Steinberg, Europhys. Lett. **14**, 331 (1991); Phys. Rev. E **49**, 1291 (1994); A. Tsameret, G. Galdner, and V. Steinberg, *ibid.* **49**, 1309 (1994).

[7] M.C. Cross and P.C. Hohenberg, Rev. Mod. Phys. **65**, 851 (1993).

[8] H. Haken, *Synergetics. An Introduction*, 3rd ed. (Springer, Berlin, 1983); *Advanced Synergetics*, 2nd ed. (Springer, Berlin, 1987).

[9] A.C. Newell, T. Passot, and J. Lega, Annu. Rev. Fluid Mech. **25**, 399 (1993).

[10] P. Coullet, S. Fauve, and E. Tirapegui, J. Phys. Lett. **46**, L787 (1985).

[11] S. Fauve, in *Instabilities and Nonequilibrium Structures*, edited by E. Tirapegui (Reidel, Dordrecht, 1987), pp. 69–88.

[12] M. Bestehorn, R. Friedrich, and H. Haken, Z. Phys. **72B**, 265 (1988).

[13] R.J. Deissler and H. Brand, Phys. Lett. A **130**, 293 (1988).

[14] P. Coullet, T. Frisch, and F. Plaza, Physica D **62**, 75 (1993).

[15] R.J. Deissler, J. Stat. Phys. **40**, 376 (1985); **54**, 1459 (1989); Physica D **25**, 233 (1987).

[16] R.J. Deissler, Phys. Rev. E **49**, R31 (1994).

[17] J.M. Chomaz, Phys. Rev. Lett. **69**, 1931 (1992).

[18] W. van Saarloos and P. C. Hohenberg, Physica D **56**, 303 (1992).

[19] T.B. Benjamin and J.E. Feir, J. Fluid Mech. **27**, 417 (1967).

[20] A.C. Newell, in *Lectures in Applied Mathematics* (Am. Math. Society, Providence, 1974), Vol. 15, p. 157.

[21] M. San Miguel, Phys. Rev. Lett. **75**, 425 (1995).

[22] M.C. Cross, Phys. Rev. A **38**, 3593 (1988).

[23] P. Kolodner, C.M. Surko, and H. Williams, Physica D **37**, 319 (1989).

[24] T.C. Gard, *Introduction to Stochastic Differential Equations* (Marcel Dekker, New York, 1987).